

## Adsorption on Metals

H.-J. FREUND and H. KUHLENBECK

*Abteilung Chemische Physik  
Fritz-Haber-Institut der  
Max-Planck-Gesellschaft*

## Contents

10.1. Introduction . . . . .	671
10.2. Alkali adsorption . . . . .	677
10.3. Chalcogenide adsorption . . . . .	679
10.4. Hydrogen adsorption . . . . .	689
10.5. Carbon monoxide adsorption . . . . .	693
10.6. Nitrogen adsorption . . . . .	715
10.7. Carbondioxide adsorption . . . . .	718
10.8. Ethylene adsorbates . . . . .	722
10.8.1. Symmetry considerations and ethylene–substrate interaction . . . . .	722
10.8.2. Ordered ethylene overlayers . . . . .	725
10.9. Benzene adsorbates . . . . .	728
10.9.1. Symmetry considerations on the molecule–substrate interaction in a dilute disordered layer of $C_6H_6/Ni(111)$ . . . . .	729
10.9.2. Ordered layers: $C_6H_6/Ni(111)$ and $C_6H_6/Os(0001)$ . . . . .	733
10.9.3. Symmetry considerations on molecule–substrate interaction in a dilute disordered layer of $C_6H_6$ of $Ni(110)$ . . . . .	735
10.9.4. Ordered overlayer: $C_6H_6/Ni(110)$ . . . . .	736
10.10. Co-adsorbates . . . . .	738
References . . . . .	742

### 10.1. Introduction

Irving Langmuir (1881–1957) may be looked at as one of the founders and promoters of modern surface science and its applications, and in particular he is one of the pioneers in adsorption studies on solid surfaces (Langmuir, 1918; Kingdom and Langmuir, 1923; Villars and Langmuir, 1931; Taylor and Langmuir, 1933). Adsorption on transition metal substrates has been interesting in Langmuir's days and it remains to be an interesting topic at present (Ertl and Küppers, 1985; Zangwill, 1988; Henzler and Göpel, 1991). The question is: How does an atom bind to a transition metal surface and what are the consequences for the electronic levels of the combined systems? Answer: It depends! Some limiting cases are depicted in Fig. 10.1, where we consider one electron levels. In Fig. 10.1a the atomic level is sharp as long as the atom is far away from the surface. The metal is represented by a potential well. This particular situation may for example represent an alkali metal atom on a free electron metal surface. As the atom approaches the metal we observe two effects (Lang, 1971; Muscat and Newns, 1978). The level changes its energy position and it increases its width considerably. Generally, the level changes its position because it feels the additional potential of the metal. The second effect, i.e., the increase in width is due to the reduced residence time of the electron on the atomic level as soon as hopping or hybridization with the metal levels becomes possible. Obviously, we have placed the atomic level in an energetic position so that it lies within the region of the metal band. The atomic level which was occupied in the free atom case, is energetically placed upon interaction with the metal completely or partly – depending on its width – above the Fermi level of the metal. Then, the electron density on the atom changes. In the present case a larger fraction of the electronic charge on the atom is transferred towards the metal. The adsorbate substrate bond is formed including a pronounced dipole pointing from the positively charged adsorbate towards the negatively charged metal surface. For alkali metal atoms bonding to transition metal, this discussion goes back to R.W. Gurney in 1935 (Gurney, 1935) and it has very recently been revisited with modern *ab initio* computer methods by Scheffler and his group (see Chapter 5). If the resonance ends up fully below the Fermi level (Fig. 10.1b), the charge transfer contribution is reduced.

So far we have assumed that the coupling between adsorbate and metal is only rather weak. If we increase the coupling we eventually form a “surface molecule” characterized by two features split off from the metal band. The two features shown in Fig. 10.1c may be looked at as a bonding and an antibonding combination of the wave functions of adsorbate and metal level. Depending on the relative position of the adsorbate level with respect to the metal both or only one of the two split off resonances is occupied.

In summary, bonding of an atom to a metal surface leads either to a shift of the atomic level and a considerable increase in width, or to the split off of a bonding and an antibonding level. The wide level may overlap the Fermi level so that the position of the Fermi level within the level determines the electronic density on the adsorbate. This model of

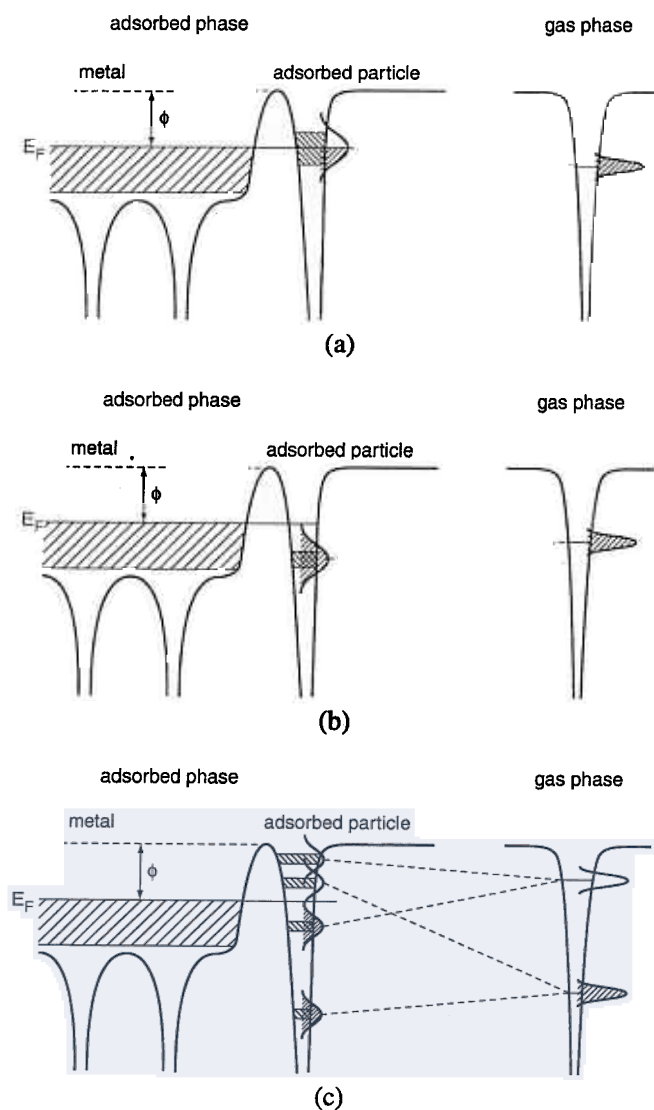


Fig. 10.1. Energy levels of free atoms (right) and atoms adsorbed on a metallic surface (left). (a) Partly occupied adsorbate level, (b) fully occupied adsorbate level, (c) interaction of an atom having an occupied and an unoccupied orbital with the valence band and the conduction band of the metal.

the adsorbate bonding is based on the so called Anderson–Grimley–Newns Hamiltonian (Anderson, 1961; Grimley, 1967; Newns, 1969; Spanjaard and Desjouqueres, 1990).

Another model describing the interaction of an isolated adsorbate and a clean surface which has been mainly developed for molecular, in particular for CO adsorption is called the Blyholder model (Blyholder, 1964, 1974) and is based primarily on molecular orbital



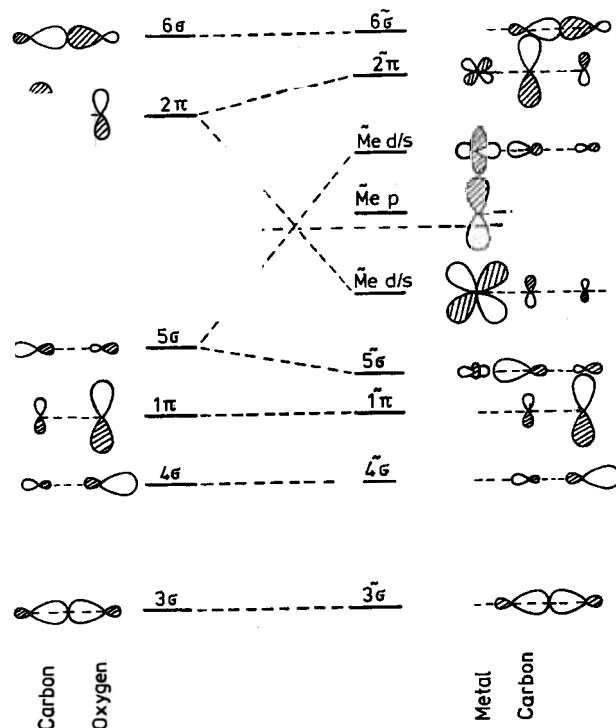


Fig. 10.2. The Blyholder model for the interaction of a CO molecule with a transition metal surface (Blyholder, 1964, 1974).

theory. It carries much of the essentials of the "surface molecule" aspect of the Anderson–Grimley–Newns Hamiltonian (Anderson, 1961; Grimley, 1967; Newns, 1969). In fact it is the "surface molecule" model. The essentials of the Blyholder model are summarized in Fig. 10.2. Assume an atom or a molecule has a doubly occupied non degenerate ( $\sigma$ -symmetry) and an empty degenerate ( $\pi$ -symmetry) orbital. The molecule interacts with its occupied orbital with the occupied and unoccupied orbitals of the metal. The interaction between occupied orbitals leads to a non-bonding Pauli repulsion. The interaction between occupied and unoccupied orbitals on the other hand leads to a bonding interaction. The interaction of the molecule's unoccupied orbital with the occupied metal orbitals belongs to the latter category and is important to understand the rather strong CO-metal bond. Since the occupied and the unoccupied orbital of the metal belong to different irreducible representations the coupling with the metal involves two independent subsets of metal orbitals, occupied and unoccupied. The synergetic interaction of substrate and adsorbate levels in the case of CO involves the  $5\sigma$  and  $2\pi$  levels and has been termed  $\sigma$ -donation and  $\pi$ -back-donation. This notation was introduced into surface science by Blyholder in 1965 and has been named after him although it has great similarities to the so called Dewar–Chatt–Duncanson model (Dewar, 1951; Chatt and Duncanson, 1953) well known in the discussion of the electronic structure of transition metal complexes since the early fifties.

Several modifications to the model have been proposed concerning in particular the relative importance of the donation and backdonation contributions to the metal molecule bond. It appears in several cases the  $\pi$ -backdonation channel dominates. Once again, the Blyholder model and its modifications may be mapped onto the surface molecule solution of the Anderson–Grimley–Newns–Hamiltonian in spite of the controversial discussion that has taken place in the literature in the past (Gumhalter et al., 1988).

The notion so far has assumed the interaction of a single adsorbate species with a bare metal surface. However, in general we have to deal with a finite coverage of the surface. In Langmuir's picture of adsorption (Langmuir, 1918; Kingdom and Langmuir, 1923; Villars and Langmuir, 1931; Taylor and Langmuir, 1933) the adsorbed particles occupy the lattice points of a two-dimensional substrate with equal probability and with hard wall potentials between the adsorbed particles, preventing double or multiple occupancy of any particular site and a well defined adsorption energy typical of the site. As a result saturation would be characterized by  $\Theta = 1$  and the formation of a true  $1 \times 1$  adsorbate layer. Obviously, the formation of ordered layers with coverages far below  $\Theta = 1$  are more the exception than the rule and are a direct consequence of the existence of rather long reaching "softer" interaction potentials (Somorjai and Van Hove, 1979). Intermolecular interaction potentials may be either attractive or repulsive and may be classified into direct and indirect interactions. Direct interactions involve dipole–dipole (multipole–multipole) and orbital overlap interactions, and are often repulsive. On the other hand, indirect interactions mediated through the metal surface may be either attractive or repulsive depending on distance and surface sites, i.e., the kind of charge modification of the electronic structure of the substrate by the adsorbate (Koutecky, 1958; Grimley, 1960, 1971; Einstein and Schieffer, 1973). The interplay of the interadsorbate interaction potential and the adsorption energy of the isolated adsorbate with the clean substrate finally determines the observed structure of an ordered layer. In other words, the structure of the ordered layer depends on the heat of adsorption and the coverage.

A way to understand bonding in adsorbates on metals is to study their geometric and electronic structure experimentally and theoretically. Figure 10.3 shows a schematic representation of the electronic structure of an adsorbate as it develops from an isolated adsorbed atom into a two-dimensionally ordered adsorbate. Briefly, we have chosen the example representing a chalcogen atom like oxygen in a fourfold site on a (100) surface. The three fully occupied 2p-orbitals are situated well below the Fermi energy. They are split into a degenerate ( $p_x$ ,  $p_y$ ) set of orbitals and a non degenerate  $p_z$  orbital as shown on the right hand side of Fig. 10.3. The relative position of the two levels is determined by the strengths of interaction with the substrate. If we, on the contrary, assume that there is no interaction between adsorbate and substrate but consider exclusively interadsorbate interaction we arrive at a situation depicted on the left hand side of Fig. 10.3: An adsorbate band structure develops. The last step in the formation of the full adsorbate–substrate band structure is to interact the adsorbate band structure with the metal, which is depicted in the central panel of Fig. 10.3. Order is particularly important because in the case of two-dimensionally well ordered overlayers the wave vector parallel to the surface ( $k_{\parallel}$ ) is a good quantum number, and therefore energy dispersions as a function of  $k_{\parallel}$  may be observed experimentally. Consequently, it is possible to carry out angle dependent inelastic electron spectroscopic measurements to determine the  $k_{\parallel}$  dependence of the particular elementary excitation. If

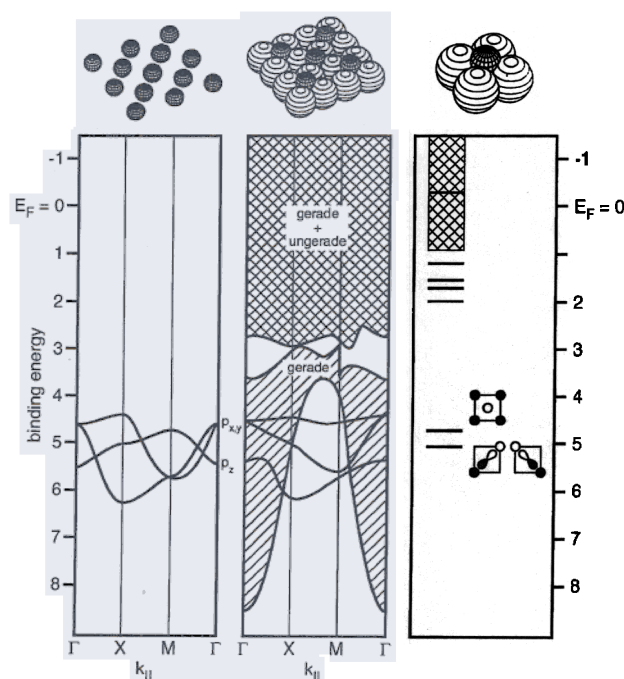


Fig. 10.3. Schematic one-electron diagrams of the valence electrons of a small chalcogen/metal cluster (right), an unsupported chalcogen  $c(2 \times 2)$  adlayer (left), and a chalcogen  $c(2 \times 2)$  adlayer on the surface of a transition metal (center).

we use, for example, electron energy loss spectroscopy we get the photon dispersion relations (Szeftel et al., 1983; Toennies, 1991) or the plasmon dispersion relations, etc. (Fink, 1992). If we perform angle resolved photoelectron spectroscopic (ARUPS) measurements we get the “band structure” of the ordered layer, or better the dispersion relations of the ion states of the system (Kevan, 1992). The experimentally determined band structure can be connected with the intermolecular interaction potential through theoretical modeling. Briefly, in the simplest form of the band structure formulation, the tight-binding approximation, the bandwidth is determined by the strength of the intermolecular interaction as probed by the particular molecular orbital (ion state) under consideration (Jones, 1975). If it is possible to identify a particular ion state of a molecule in ordered layers of different coverage densities, i.e., varying intermolecular distances, then we are in a position to determine ion state specific intermolecular interaction parameters as a function of intermolecular distance (Freund and Neumann, 1988). The last point is particularly interesting: Take diatomic molecules with localized orbitals. Assume the molecules interact on one end only with the surface and form an ordered layer. Ionization of an orbital localized on the far end of the molecules away from the surface most likely will lead to a dispersion relation predominantly determined by the direct, or “through space”, interaction (Greuter et al., 1983). If on the other hand we choose to ionize an orbital localized on the near end of the molecules close to the surface, we are going to measure a dispersion relation determined

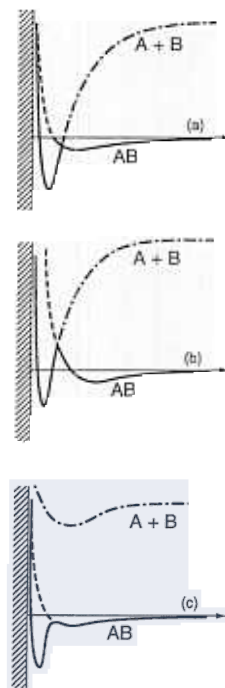


Fig. 10.4. Schematic diagrams of the potential energy of an adsorbate/substrate complex appropriate to three different state configurations: (a) dissociative chemisorption, (b) dissociative chemisorption with a physisorbed precursor, (c) molecular chemisorption (Lennard-Jones, 1932).

by direct as well as indirect, “through bond”, interaction of the molecules (Heskett et al., 1985a). It is therefore possible to use measured ion state specific dispersion relations to study intermolecular interaction mechanisms. It must be understood, however, that experimentally determined band dispersions are excited state properties and intermolecular potentials are usually considered to be ground state properties. Up to this point we have assumed that the adsorbate has been formed somehow. However, the question of how an atomic adsorbate layer forms is important.

Atomic adsorption often occurs through binding a molecule from the gas phase which subsequently dissociates to form the adsorbate. This means that there is the question of molecular precursors for atomic adsorption. This energetic scenario has been discussed early by Lennard-Jones and others (Lennard-Jones, 1932), and a schematic representation is shown in Fig. 10.4. A molecule AB approaches a surface along the  $z$ -axis. In Fig. 10.4a the situation characteristic for dissociative adsorption is shown. The potential well for the adsorbed atoms is considerably deeper than that for the adsorbed molecules and there is no or a very small activation energy between the associative and the dissociative well. In Fig. 10.4b the activation energy is larger so that the molecular adsorbate is a real precursor for dissociative adsorption. Figure 10.4c represents the potential energy well for molecular chemisorption. Dissociative adsorption is unfavorable in this case. In principle these exam-

ples already represent the simplest cases of a reactive system and it is quite obvious that the potential energy hypersurface is the key ingredient in understanding chemical reaction on solid surfaces. The question of chemical reactivity is intimately connected with adsorption dynamics which is a topic finding increasing attention in recent years (Ertl, 1982).

We have organized the present chapter in such a way that we have chosen several well studied examples that represent the limiting cases of our present state of understanding surface-adsorbate bonding. Alkali-metal adsorption is meant to be an example for a system where a resonance near the Fermi energy of the substrate is formed. Chalcogen adsorption leads to a resonance below or at the lower end of the metal valence bands. An intermediate case is the adsorption of atomic hydrogen. Although the simplest of all adsorbates it leads to rather complicated changes in the energy distribution of metal levels and a qualitative discussion is often difficult. From the discussion of atomic adsorbates we shall turn to the study of molecular adsorbates. The largest data set on electronic structure exists for CO adsorption and some aspects, in particular the Blyholder model, shall be exemplified on the basis of this. After a few comments on the electronic structure of other di- and tri-atomic adsorbates we discuss more complex molecular adsorbates, the largest being aromatic ring compounds. Finally we shall comment on coadsorbate systems.

## 10.2. Alkali adsorption

In 1935 Gurney (1935) proposed the quantum mechanical model which has been shortly referred to in the introduction. According to this model the valence  $s$  level of a free alkali atom broadens and shifts while the atom approaches a free electron like metal, becoming partially emptied when the surface is reached. Thus the adsorbed alkali atom is positively charged, which may be traced back to the electropositive nature of alkali metals. This charge introduces a negative image charge in the substrate and the resulting dipole reduces the workfunction of the system considerably. When the coverage of alkali atoms on the surface is increased, the repulsive interaction of the dipoles comes into play, inducing a partial depolarization of the alkali ions; i.e., part of the charge flows back from the metal substrate to the alkali ions. This mechanism leads to a dependence of the workfunction on coverage as displayed in Fig. 10.5: a steeply decreasing workfunction at low coverages, a minimum at intermediate coverage and, due to depolarization, an increasing workfunction at higher coverage. Workfunction curves of this type have been found experimentally for many alkali/metal systems (Bonzel et al., 1989; Horn et al., 1988). For a long time the Gurney model has been considered to be valid. Later theoretical and experimental studies suggested that there was practically no charge transfer from the adsorbate to the substrate, but instead a polarization of the adsorbate and the adsorbate/substrate bond should be responsible for the experimentally observed workfunction decrease upon alkali deposition (Ishida, 1988, 1990; Riffe et al., 1990).

More recent studies (Stampfl and Scheffler, 1995; Stampfl, 1996; Burchhardt et al., 1995) indicate that the Gurney model is valid at low alkali coverage, but needs to be modified at higher coverage since it does not take into account the formation of ordered overlayers, phase transitions within the overlayers, and alloy formation. Model systems which have been theoretically and experimentally extensively studied (Stampfl and Scheffler, 1995; Stampfl, 1996; Burchhardt et al., 1995) are alkali atoms on Al(111). Some results

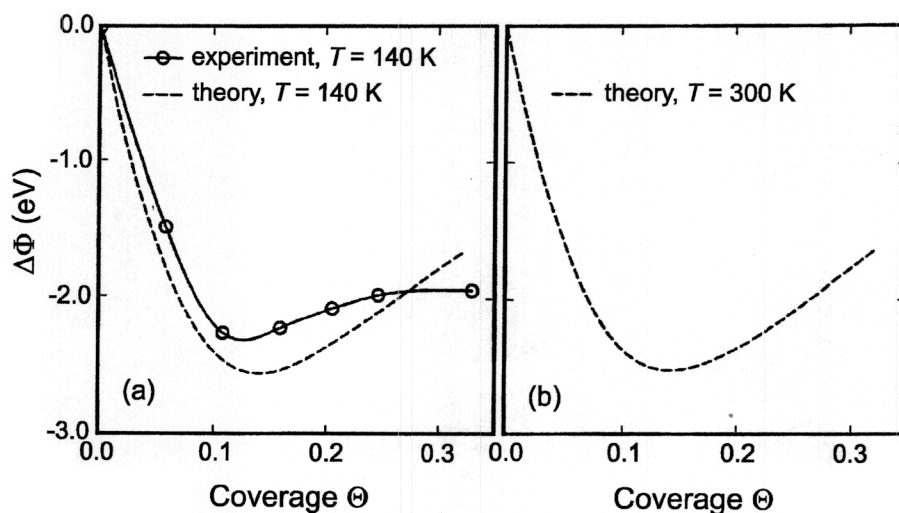


Fig. 10.5. Calculated (dashed line) (Stampfl and Scheffler, 1995) and measured (full line with open circles) (Horn et al., 1988) workfunction change with coverage for K on Al(111).

shall be repeated here. For these systems the Gurney model is valid at coverages below about  $\Theta = 0.1$  (Stampfl and Scheffler, 1995). In this coverage regime the overlayer consists of randomly distributed atoms with negligible interaction. For K on Al(111) at low temperature (below 220 K) and coverages above  $\Theta = 0.15$  ( $\sqrt{3} \times \sqrt{3}$ )R30° islands form on the surface (Stampfl and Scheffler, 1995). The lateral bonding in these island is mainly metallic and the ionicity of the adatoms is considerably reduced as compared to the low coverage regime. Neither the formation of a metallic bond nor the formation of the ordered adlayer is explained by the Gurney model (Gurney, 1935), although the reduced ionicity is in line with this model. When the same adsorption experiment is performed at temperatures above 220 K, a different process occurs. At such temperatures the thermal energy is high enough to overcome the activation barrier for replacement of aluminum atoms in the first layer by potassium atoms. This means that aluminum atoms are kicked out of the surface layer and the remaining holes are filled with alkali atoms, again forming a ( $\sqrt{3} \times \sqrt{3}$ )R30° structure (Stampfl et al., 1992). According to calculations (Stampfl and Scheffler, 1995) the potassium atoms are charged in this configuration. However, due to the embedding of the alkali atoms into the surface the length of the resulting dipole is small, so that the net dipole moment is not much different from the one observed for the ( $\sqrt{3} \times \sqrt{3}$ )R30° layer formed at lower temperature, giving rise to similar workfunction vs. coverage curves. Views of the ( $\sqrt{3} \times \sqrt{3}$ )R30° structures formed below and above 220 K are displayed in Fig. 10.6. Substitutive adsorption is not unique for potassium; similar observations have also been made for sodium (Stampfl et al., 1992) and rubidium atoms (Nielsen et al., 1994). According to calculations silver and copper are also candidates for substitutive adsorption of alkalis (Polatoglu et al., 1993), making this process a candidate for a rather general phenomenon.

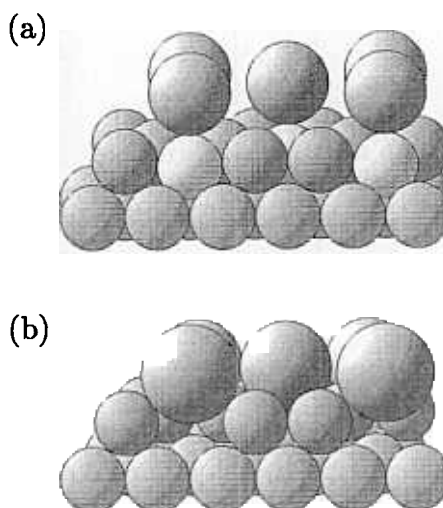


Fig. 10.6. Perspective view of the atomic structure of  $(\sqrt{3} \times \sqrt{3})R30^\circ$  K/Al(111) (Stampfl and Scheffler, 1995). (a) K atoms are in ontop sites on the surface (low temperature adsorption). The first Al layer is slightly buckled due to interaction with the adatoms. (b) Substitutional geometry where the Al atoms which were beneath the K atoms in (a) have been kicked out.

### 10.3. Chalcogenide adsorption

Oxygen adsorption has been studied for a long time. One of the most frequently studied systems is  $c(2 \times 2)\text{O}/\text{Ni}(100)$  (Starke et al., 1988; Chubb et al., 1990). Nevertheless oxygen adsorbate systems are complicated in the sense that often different ordered structures coexist. Even oxide formation starts at rather low oxygen coverages (Brundle and Broughton, 1990). Therefore we shall discuss the bonding of chalcogens to metal surfaces by using sulphur adsorbates as examples. Atomic chalcogenides are characterized by the valence configuration  $ns^2np^4$  and exhibit due to their electronegativity, the tendency to withdraw electrons from more electropositive bonding partners (Plummer and Eberhardt, 1982). These electrons then fill the chalcogenide valence shell. This is true in particular for oxygen but in a reduced form also in the case for the heavier chalcogenides. The first ionization potential for oxygen is 13.6 eV (Radzig and Smirnov, 1985), for sulphur it is 10.4 eV (Radzig and Smirnov, 1985). Taking into account a work function of approximately 5 eV we expect oxygen emission at about 8 eV below and at about 5 eV below the Fermi energy sulphur emission. For transition metals this is an energy range of small density of states. Mixing between adsorbate levels and substrate levels is comparably small. The wave functions conserve to a large extent their atomic character and interpretation is thus straight forward. Consider sulphur chemisorption on a Ni(100) surface. From structural studies it is well known that chalcogen atoms in general reside in four fold hollow sites on Ni(100) surfaces (Demuth et al., 1973). This is a situation very similar to the schematic diagram shown

in Fig. 10.3. As briefly alluded to in the introduction the threefold degenerate 2p orbitals of the chalcogenide atoms split due to the influence of the substrate potential. Let us choose a coordinate system with the  $z$ -axis parallel to the surface normal. The  $p_z$ -orbitals then feel a different potential as compared with the  $p_x/p_y$ -orbitals oriented parallel to the surface. The  $p_x/p_y$  orbitals on the other hand remain degenerate due to the four fold symmetry of the site. The splitting of the 3p orbitals in a level with  $a_1$ -symmetry ( $p_z$ ) and a level with  $e$ -symmetry ( $p_x/p_y$ ) may be evaluated experimentally because the angular distribution of the photocurrent in an ARUPS experiment is sensitive to the symmetry of the involved states. The question, that may be addressed experimentally is which atomic level interacts more strongly with the substrate. This follows directly from the relative energetic position of the two levels if we assume simultaneously that the effect of many particle contributions and final state screening is the same for both levels. Experimental results are shown in Fig. 10.7 (Plummer et al., 1980). Clearly, the feature associated with the  $e$ -level is situated at higher binding energy as compared with the  $a_1$ -level, indicating that the  $p_x/p_y$  orbitals do interact more strongly with the substrate. The spectra are recorded for a  $p(2 \times 2)\text{S}/\text{Ni}(100)$  layer. Its structure is schematically shown in Fig. 10.8. The distance of the individual sulphur atoms is large enough to suppress strong direct lateral interactions. Therefore the result can be taken as characteristic for an individual sulphur atom. It is immediately obvious that this line of reasoning cannot be completely correct because in the absence of lateral interaction there were no ordered layer formation. On the other hand the lateral interaction leads to identical adsorption sites which is very useful for the following symmetry analysis: Briefly, the photoionization cross-section is proportional to the square of the dipole matrix element between the initial and the final state of the ionization process (Freund and Neumann, 1988; Plummer and Eberhardt, 1982; Hermanson, 1977)

$$I \propto |A_0 \langle \varphi_f | A p | \varphi_i \rangle|^2 \quad (10.1)$$

Firstly, it has to be remembered that  $\varphi_f$  is the final state after electron excitation consisting of the ion state  $^{N-1}\psi_{e,E}$  and the emitted electron  $\Phi_e(n)$ , and that  $\varphi_i$  represents the neutral ground state of the system.  $A_0$  is the constant vector potential. Since  $p$  is a one electron operator the matrix element can be rewritten as (Cederbaum and Domcke, 1977)

$$I \propto |\sum \langle \Phi_e(n) | p_n | \Phi_k(n) \rangle \langle ^{N-1}\psi_{e,E} | a_k \varphi_i \rangle|^2, \quad (10.2)$$

where  $a_k$  and  $\Phi_k(n)$  are the annihilation operator and the one electron wave function of the electron that is being emitted, respectively. These  $\Phi_k(n)$  are called initial states in the following.

The first matrix element determines the angular distribution pattern, the second matrix element defines the absolute value and contains the internal degrees of freedom of the system, e.g., the line widths (Cederbaum and Domcke, 1977). The sum takes all possible ion states  $^{N-1}\psi_{e,E}$  into account and explains the existence of satellite structure (Cederbaum and Domcke, 1977). Since we are interested in ARUPS, much of the discussion will concentrate on the first matrix element. Secondly, in order to evaluate whether this matrix element is nonzero, and thus leads us to expect a finite photoelectron current into a specific direction in space, symmetry arguments can be used (Hermanson, 1977). In principle the



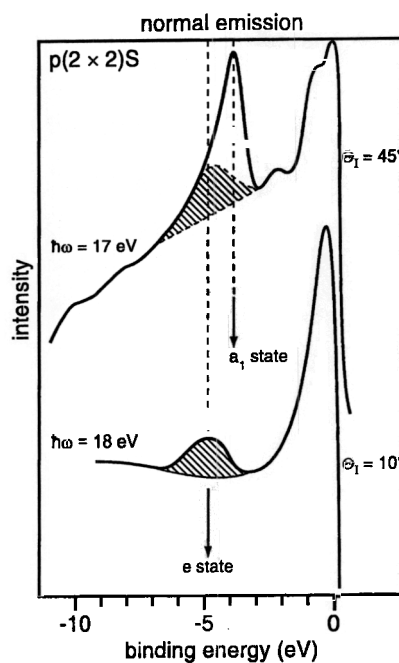


Fig. 10.7. Photoelectron spectra of  $p(2 \times 2)S/Ni(100)$  recorded in normal emission for two different light incidence angles ( $\Theta_i$ ) (Plummer et al., 1980).

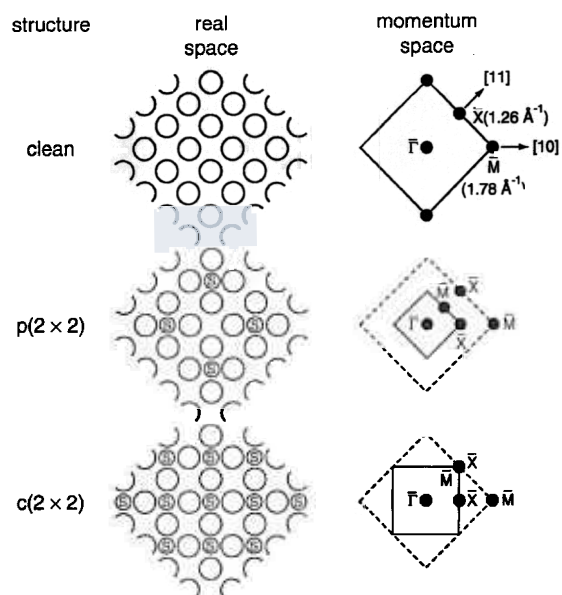


Fig. 10.8. Real space and  $k$ -space lattices of  $Ni(100)$ ,  $p(2 \times 2)S/Ni(100)$ , and  $c(2 \times 2)S/Ni(100)$  (Plummer et al., 1980).

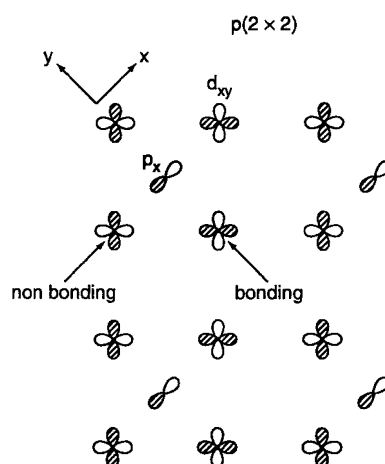


Fig. 10.9. Schematic orbital diagram of a possible S3p–Ni3d interaction for p(2 × 2)/S/Ni(100).

space group of the adsorbate under consideration has to be chosen, and then we have to classify the wave functions according to its irreducible representations. Often, it is sufficient to consider one specific symmetry operation belonging to the point group, instead of all possible symmetry operations, in order to predict the angular variations of electron emission.

In the present case the layer has p(2 × 2) structure, i.e., the system has fourfold symmetry with four symmetry planes at 45° angles (Demuth et al., 1973). If we place the electron detector perpendicular to the surface, final states that lead to an observable signal must be even with respect to reflection at the mirror plane. In other words they have a<sub>1</sub> symmetry. If we chose the photon incidence for polarized light such that the electric field vector is either parallel (e-symmetry) or perpendicular (a<sub>1</sub>-symmetry) to the surface plane, then initial states with e-symmetry emit in the former, initial states with a<sub>1</sub>-symmetry emit in the latter case into the direction of the detector. This is the typical approach for the analysis of photoemission spectra.

We now come back to our specific example. In our case the p<sub>x</sub>/p<sub>y</sub> are more strongly bound than the p<sub>z</sub> state. This is not a trivial result, because naively we might assume that the p<sub>z</sub> level is the more strongly bound level because it is oriented towards the substrate. A detailed analysis shows, however, that the fourfold hollow site is the reason for the level sequence. The chalcogen atom in the hollow site is above a Ni atom in the second layer and thus relatively close to the first layer. This leads to a strong interaction parallel to the surface as schematically shown in Fig. 10.9. In this diagram the overlap between a chalcogen p<sub>x</sub>-orbital and the metal d<sub>xy</sub> orbitals is indicated. Please note that the presence of the adsorbate leads to a reduction of the size of the Brillouin zone. The Brillouin zone boundary of the clean substrate is folded back onto the Γ point of the new reduced Brillouin zone. Consequently, not in all wave functions the metal orbitals are in phase at Γ.

Let us consider next another S/Ni(100) system where at a higher sulphur coverage interadsorbate interactions become more important (Plummer et al., 1980). At a coverage

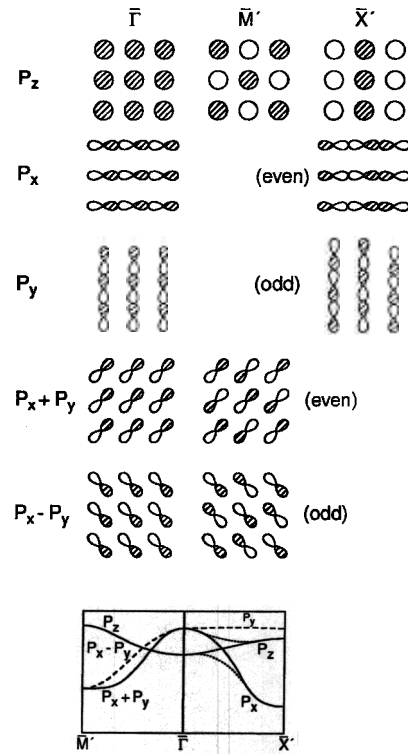


Fig. 10.10. Two-dimensional representation of  $p_x$ ,  $p_y$  and  $p_z$  derived wave functions at different high symmetry points in  $k$ -space (Plummer and Eberhardt, 1982).

of  $\Theta \sim 0.5$  sulphur forms a  $c(2 \times 2)$ S/Ni(100) overlayer. If the intermolecular interaction potential is large enough to demand consideration of the two-dimensional crystal periodicity, the overlap of adsorbate wave functions is sufficient to produce two-dimensional Bloch states  $\Psi_k$  and to make a band description of the electronic structure more appropriate (Horn et al., 1978a). Then the one-electron wave function at a lattice site  $\mathbf{R}_1$  is related to the wave function at site  $\mathbf{R}_2$  by:

$$\Psi_k(\mathbf{R}_1) = \Psi_k(\mathbf{R}_2) \exp[i\mathbf{k}_{\parallel}(\mathbf{R}_1 - \mathbf{R}_2)] \quad (10.3)$$

where  $\exp[i\mathbf{k}_{\parallel}(\mathbf{R}_1 - \mathbf{R}_2)]$  gives the phase difference between the two sites for a state specified by the two-dimensional wave vector  $\mathbf{k}_{\parallel}$ . A schematic representation of this system is shown in Fig. 10.10. Let us consider first the free unsupported sulphur layer. We only consider the 3p niveous of sulphur. We can qualitatively estimate the band structure expected on the basis of nearest neighbour interactions only. The schematic wave functions of the  $c(2 \times 2)$  layer are shows at three critical points  $\Gamma$ , X, M of the Brillouin zone (Plummer et al., 1980). The  $p_z$  orbital transforms at  $\Gamma$  according to  $a_1$ , the  $p_x/p_y$  orbitals belong to the irreducible representation  $e$ . The two-dimensional wave function that may be formed

through combinations of  $p_z$  orbitals is strongly bonding at  $\Gamma$ . The two-dimensional wave functions based on the  $p_x$  and  $p_y$  orbitals indicate strongly antibonding character at  $\Gamma$ . Note that due to the orbital degeneracy we may either consider the pure  $p_x/p_y$  components or linear combinations  $p_x + p_y$  and  $p_x - p_y$ . On the way from  $\Gamma \rightarrow M$  the phase relation between the atomic orbitals change. At  $M$  the two-dimensional wave functions derived from  $p_z$  are antibonding. This is the reason why the  $p_z$  derived band disperses from higher to lower binding energies. Due to the lower symmetry the  $p_x$  and  $p_y$  bands are no longer degenerate along  $\Gamma-M$ . They disperse towards higher binding energies on the way to  $M$ . The dispersion of the  $p_x/p_y$  bands are considerably larger than the one of the  $p_z$  derived bands. This is caused by the weaker interaction of the  $p_z$  orbitals as compared with the  $p_x/p_y$  orbitals which are directed towards each other. In the direction  $\Gamma \rightarrow X$  the situation is quite analogous for the  $p_z$  orbitals, i.e., the antibonding character of the two-dimensional wave function increases. On the contrary the  $p_x$  and  $p_y$  bands have considerably different energies because the  $p_x$  band at  $X$  is strongly bonding while the  $p_y$  band remains antibonding at  $X$ . Coming back to the  $\Gamma$  point we realize from Fig. 10.3 that in the present situation the  $p_z$  orbital is situated at higher binding energies than the  $e$  orbital derived from  $p_x/p_y$ . This is reversed with respect to the  $p(2 \times 2)$  structure. While in the case of the  $p(2 \times 2)$  structure coupling between adsorbate and substrate determines the sequence, the relative position of  $a_1$  and  $e$  levels at  $\Gamma$  is dominated by the interadsorbate interactions. The symmetry of the unsupported layer is  $D_{4h}$ . If we now bring this layer in contact with the substrate we destroy the symmetry of the layer in the sense that the system has no longer  $D_{4h}$  but rather  $C_{4v}$  symmetry. This induces hybridization between the  $p_z$  and the  $p_x$  derived bands along  $\Gamma \rightarrow X$  and  $\Gamma \rightarrow M$ . A hybridization gap is formed as indicated. At the same time the adsorbate levels mix with the levels of the substrate and a diagram as indicated in the middle panel of Fig. 10.3 results schematically. The same experiments that were shown in Fig. 10.7 for the  $p(2 \times 2)$  structure are depicted in Fig. 10.11 for the  $c(2 \times 2)/S/Ni(100)$  structure (Plummer et al., 1980). The spectra taken in normal emission indicate that the sequence deduced from the unsupported layer survives when interaction with the substrate is switched on. In order to judge this statement in more detail, the band structure has to be determined via an angle resolved measurement. In our example we can try to probe the bands of various symmetries by choosing different measurement geometries. In order to detect the dispersion of odd bands within a mirror plane perpendicular to the surface we orient the electric field vector of the exciting radiation perpendicularly towards this mirror plane and place the detector within the plane. In this geometry only odd initial states are detected and their dispersion can be determined experimentally. If on the other hand, we place the electric field vector within the mirror plane we may record the dispersion of the even bands. In Fig. 10.11 the results of such measurements along the  $\Gamma \rightarrow M$  direction are included. We find that in the present case not only the qualitative behaviour is correctly predicted but even the size of the dispersions is described semiquantitatively by the above predictions. One may conclude that the intermolecular interactions in sulphur adsorbates are dominated by direct sulphur-sulphur contacts.

The systems discussed so far involved chalcogenide adsorption without massive restructuring of the substrate. If we turn from the close packed (100) surface towards the more open (110) surfaces and choose as an adsorbate the more reactive oxygen we find examples where adsorption is accompanied by a pronounced reconstruction of the substrate (Bader

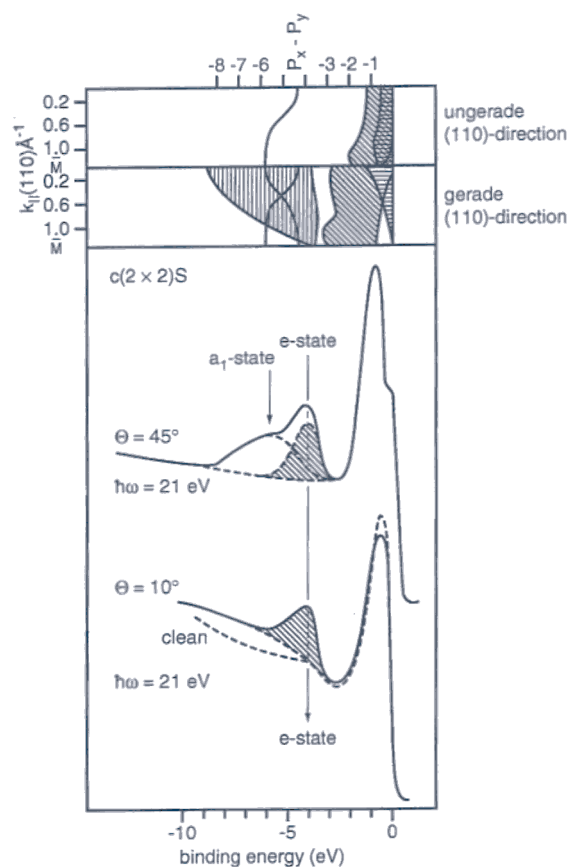


Fig. 10.11. Photoelectron spectra of  $c(2 \times 2)S/Ni(100)$  recorded in normal emission for two different light incidence angles ( $\Theta_i$ ) (Plummer et al., 1980).

et al., 1987; Coulman et al., 1990; Wintterlin et al., 1991). Oxygen adsorption on Cu(110) is a rather well studied adsorption system which has recently gained even more attention as it is to a certain extent a model system to study the electronic structure of high temperature superconductors. Upon exposure of oxygen to a Cu(110) surface a  $p(2 \times 1)$  LEED pattern is observed which is caused by the so called “missing row” reconstruction, schematically shown in Fig. 10.12 in comparison with the unreconstructed surface. The (110) surface is characterized by two different bridging sites, namely the “short” bridge along  $(1\bar{1}0)$  and the “long” bridge along (001). Oxygen occupies the long bridge sites of every second row. Then the row of Cu atoms between the oxygen containing rows is missing. Another way of looking at this situation is to take the unreconstructed surface and add O–Cu–O–Cu rows at the appropriate periodicity along the substrate (100) direction. This “added” row description (Coulman et al., 1990; Wintterlin et al., 1991) may even be the more appropriate description if we consider the mechanism of formation and growth of this structure

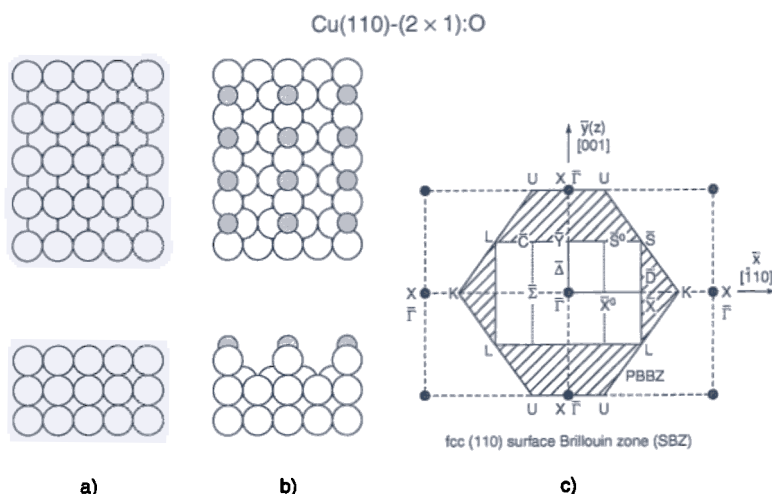


Fig. 10.12. Geometric structure of the clean Cu(110) surface (a), of O(2  $\times$  1)/Cu(110) (b), and the Brillouin zone of O(2  $\times$  1)/Cu(110) (c).

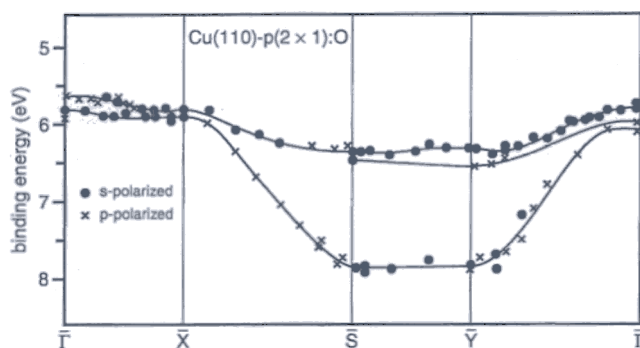


Fig. 10.13. Dispersion of oxygen 2p-derived bonding bands for several Brillouin zone directions of the reconstructed surface. Data from (Didio et al., 1984; Courths et al., 1986, 1987; Jacob et al., 1986; Courths, private communication; Goldmann, 1992).  $\Gamma Y$  is oriented along [001], i.e., along the oxygen chains, while  $\Gamma X$  is oriented along [110].  $S$  bisects  $X\text{--}X$  and  $Y\text{--}Y$ , respectively, in the extended zone scheme.

as revealed through scanning tunneling microscopy. It is clear from what has been said that the electronic structure of the system has a certain degree of one dimensionality. The Brillouin zone of the system is shown in Fig. 10.12 and it is indicated how the Brillouin zone of the adsorbate is connected with the one of the unreconstructed surface. The electronic structure, i.e., the measured dispersions in the occupied energy region, is shown in Fig. 10.13 (Didio et al., 1984; Courths et al., 1987; Jacob et al., 1986). The one dimensionality is clearly evident from the experimental dispersions: there are unusually large (1.85 eV) dispersions measured along  $\Gamma Y$  and  $X S$ . These are directions (see Fig. 10.12) along the (001) azimuth. The very large dispersions are hard to explain just on the basis

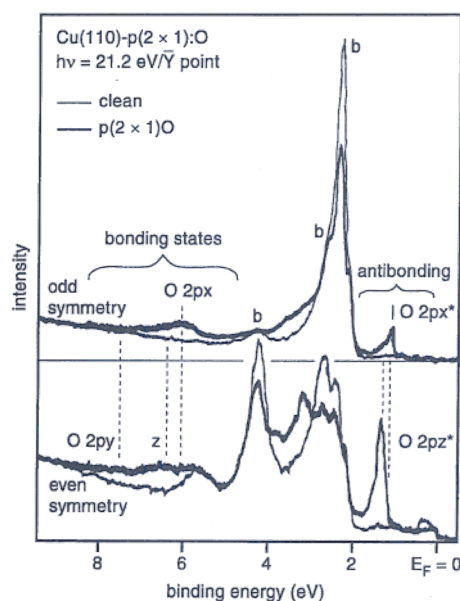


Fig. 10.14. ARUPS spectra taken with linearly polarized HeI radiation at the Y point of the surface Brillouin zone. For definition of coordinates see text. From Courths et al., 1986; Courths, private communication; Goldmann, 1992.

of pure oxygen-oxygen interactions because the distance is 3.5 Å. Probably quite strong Cu–O–Cu–O interactions must be considered. In contrast to this there is very little dispersion ( $< 0.3$  eV) along  $\Gamma X$  and  $SY$ . The dispersions shown in Fig. 10.13 represent the three oxygen 2p derived resonances situated below the Cu d-band and they are related to the features discussed for the sulphur adsorbates in the last section. Due to the particular electronic structure of the coin metals there is a range of about 2 eV between the Fermi energy and the onset of the d-band density which is dominated by s-band density. Due to the relatively low intensity of the s-band features it is possible to detect adsorbate induced states that are the antibonding analogs to the features below the d-band. Typical spectra recorded for even and odd symmetry states at Y are shown in Fig. 10.14 (Courths et al., 1986; Courths, private communication; Goldmann, 1992).

The surface coordinates  $y$  ( $x$ ) are oriented along (perpendicular to) the Cu–O chains, while  $z$  is defined along the surface normal. Using linearly polarized light and the appropriate nonrelativistic dipole selection rules, the orbital symmetry of all five occupied bands could be uniquely determined. In the upper part of Fig. 10.14 s-polarized light (vector potential  $A_0$  along  $X$ ) was used to project out the odd states. The lower part reveals the even orbitals since p-polarized radiation ( $A$  in  $yz$ -plane) was incident. A summary of all experimental dispersion curves along  $\Gamma Y$  is shown in Fig. 10.15 (Didio et al., 1984; Courths et al., 1987; Jacob et al., 1986). The orbital symmetry at Y from bottom ( $-7.8$  eV) to  $E_F$  is  $y, z, x, z$  and  $x$ . Also included is an empty band observed by inverse photoemission spectroscopy (Jacob et al., 1986). Note that these dispersion curves exhibit the periodicity of the

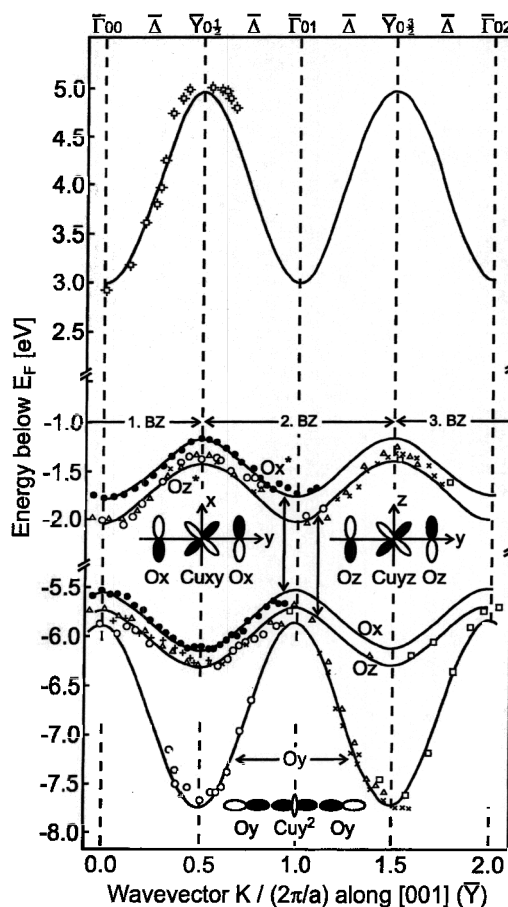


Fig. 10.15. Experimentally determined band structure of the adsorbate induced bands of the  $O(2 \times 1)/Cu(110)$  adsorbate system (Didio et al., 1984; Courths et al., 1986, 1987; Jacob et al., 1986; Courths, private communication; Goldmann, 1992).

substrate lattice constant along Y, in agreement with the proposed structure model. The adsorption site is reflected in the number of bands: the  $C_{2v}$  point group symmetry of the long-bridge site dictates a splitting of the  $2p_x$  and  $2p_y$  levels at  $\Gamma$ , which is clearly observed. Figure 10.15 immediately shows that the observed dispersion curves represent an oxygen-copper bond: in case of an exclusive linear O—O bond all three oxygen derived bonding (or antibonding) bands would not run in parallel. Courths et al. (Courths et al., 1986, 1987; Courths, private communication; Goldmann, 1992) have shown that all six dispersion curves may be modelled assuming  $O2p$  and  $Cu3d/4s$  orbitals to form Cu—O bonds in a linear O—Cu chain along y. Figure 10.16 shows a schematic molecular orbital diagram for the formation of Cu—O bonds from five degenerate  $3d$  and a non degenerate  $4s$  orbital of Cu and three degenerate  $2p$  orbitals of O. Due to the  $C_{\infty v}$  symmetry of the system the



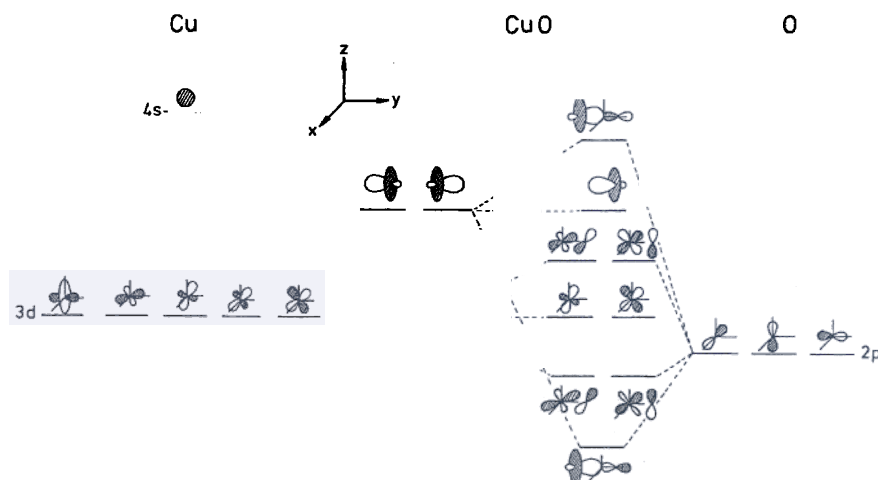


Fig. 10.16. Schematic molecular orbital diagram for a Cu–O bond on the basis of 5 Cu3d, 1 Cu4s, and 3 O2p orbitals. The energy scale is arbitrary.

4s and the 3d<sub>y<sup>2</sup></sub> orbitals hybridize. Upon interaction bonding and antibonding combinations are formed. The energy split is large for the one  $\sigma$ -type interaction due to the large overlap of the atomic orbitals. The  $\pi$ -type interactions are smaller and thus the splitting of the doubly degenerate d<sub>yz</sub>–p<sub>z</sub> and d<sub>yx</sub>–p<sub>x</sub> combinations is considerably smaller. The two d<sub>z<sup>2</sup>–x<sup>2</sup></sub> and d<sub>xz</sub> orbitals transform according to  $\sigma$ -symmetry and have no oxygen counterparts. They are thus nonbonding with respect to the Cu–O interaction. The same is true for the second  $\sigma$ -interaction of the 3d<sub>y<sup>2</sup></sub>/4s hybrids and caused by the very small overlap with respect to the Cu–O bond. If we fill this schematic diagram in Fig. 10.16 with 15 electrons (Cu:11 + O:4) the antibonding  $\sigma$ -combination is empty, and the non-bonding 3d<sub>y<sup>2</sup></sub>/4s combination is the highest molecular orbital. This diagram is the starting point for the qualitative discussion of the band structure: The strong bonding and antibonding  $\sigma$ -orbitals lead to pronounced dispersions along  $\Gamma Y$  and  $XS$  with opposite signs. These dispersions are about three times as larger as those of the  $\pi$ -bands. The parallel dispersions are explained by the phase relations. In other words, the observed dispersions are compatible with the electronic structure of linear chains, which are only weakly altered by interaction with the substrate.

Summarizing, the experiments indicate that the electronic structure of the O(2 × 1)/Cu(110) adsorbate system may be interpreted on the basis of linear Cu–O chains weakly interacting with the substrate.

#### 10.4. Hydrogen adsorption

The adsorption of hydrogen has been discussed in great detail on various substrates in the past (Christmann, 1988). One of the main issues has been the dissociation mechanism. On most surfaces hydrogen adsorbs dissociatively at room temperature. However, the sticking



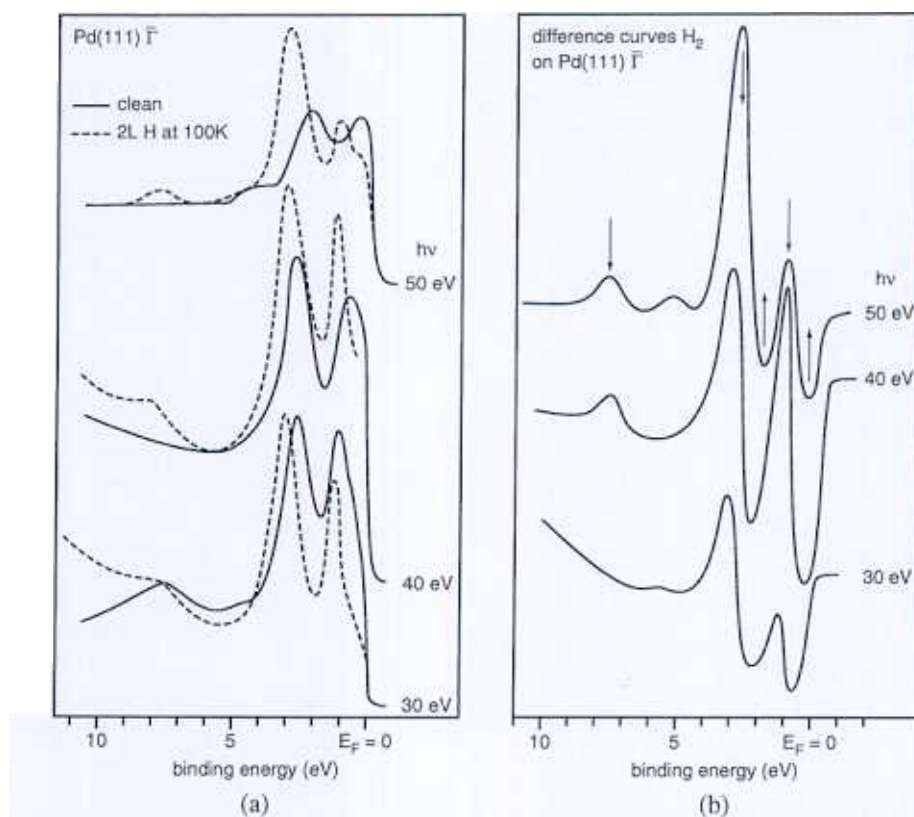


Fig. 10.18. (a) Energy distribution curves of clean Pd(111) (solid line) and H/Pd(111) (dashed line). (b) Difference spectra (Eberhardt et al., 1981).

results will emerge from these studies. It may be stated, however, that the adsorption behaviour of hydrogen on simple metals also follows the scheme outlined in Fig. 10.17. The activation for dissociation seems to be high and the important parameter controlling the adsorption mode of atomic hydrogen appears to be the conduction electron density ( $r_s$ ). As a function of this parameter it is found that atomic hydrogen is adsorbed on high density metal, such as Be and Al, but for low density metals, such as Na, the hydrogen is absorbed into the bulk forming a hydride. Intermediate cases like Mg may have characteristic features of both limiting cases (Sprunger and Plummer, 1991).

A system where the electronic structure has been studied in some detail is the system H/Pd(111), which we shall discuss below in more detail (Eberhardt et al., 1981; Eberhardt and Plummer, 1983; Shinn, 1986; Shinn and Madey, 1984, 1985).

In Fig. 10.18a electron distribution curves taken in normal emission are shown for several photon energies (Starke et al., 1988; Chubb et al., 1990). The full lines represent the clean surfaces and the broken lines represent the spectra of the surface after saturating the surface with hydrogen at 100 K. The feature at 7.8 eV is easily identified as due to a  $H1s$

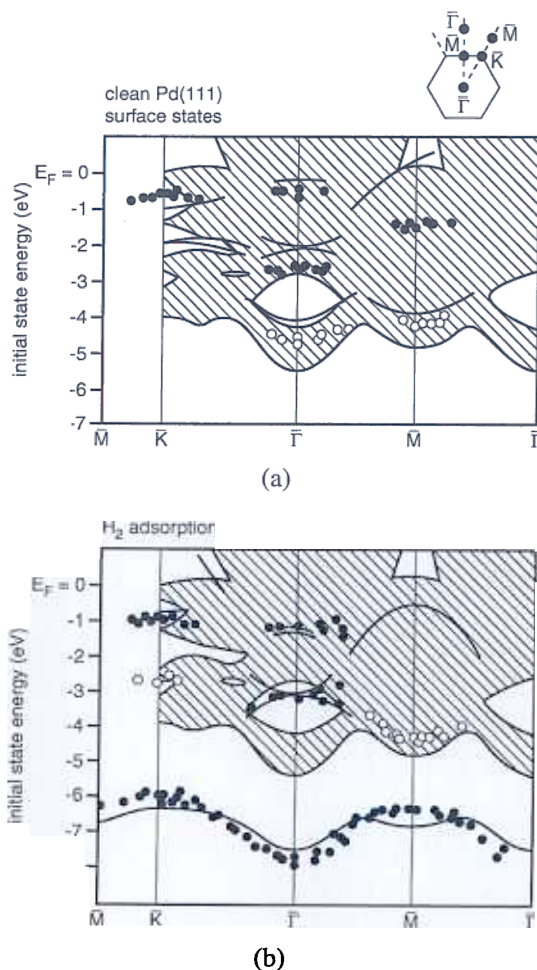


Fig. 10.19. Surface state of clean Pd(111) (a) and one monolayer H on Pd(111) (b). The projected band structure of Pd(111) is indicated by the hatched areas (Eberhardt and Plummer, 1983; Eberhardt et al., 1983).

induced state while the other differences between clean and covered surface are not as easy to assign. In order to get more insight we show in Fig. 10.18b the difference curves. There are systematic changes: While a peak at 1.2 eV appears, the feature at 0.5 eV binding energy is attenuated. In addition there is a decrease at 2.7 eV binding energy and an intensity increase at 3.2 eV. These changes are observed independent of photon energy. Theoretical calculations have been performed and are compared with the experimental observations in Fig. 10.19 (Eberhardt and Plummer, 1983; Eberhardt et al., 1983). The hatched areas indicate the projected bulk band structure. Calculated surface states are shown as fat lines, filled and open circles represent experimental measurements. There is relatively good agreement between experiment and theory. However, a detailed discussion of the bonding characteristics is still rather complicated and we shall not go into the details. This last example

shows that in particular in these systems a discussion of the bonding between adsorbate and substrate is only possible if theoretical calculations are directly available.

### 10.5. Carbon monoxide adsorption

No diatomic adsorbate system has been investigated and analysed in such detail as carbon monoxide adsorbates. This means that much of the fundamental aspects of bonding in molecular chemisorption systems can be demonstrated using experimental results on CO adsorbate systems (Freund and Neumann, 1988). However, certain aspects can be illustrated by including results on other diatomics such as O<sub>2</sub> and N<sub>2</sub>. With the exception of very few examples, e.g., CO on Cr(110) (Shinn, 1986; Shinn and Madey, 1984, 1985), CO on Fe(100) (Saiki et al., 1989) and CO on Mo(100) (Zaera et al., 1985), where the molecule lies flat on the surface, CO is bound vertically towards transition metals if the adsorption energy is characteristic for a chemisorption system (Freund and Neumann, 1988; Plummer and Eberhardt, 1982). Figure 10.20 illustrates on the basis of one electron level diagrams, much in the same spirit as done in Fig. 10.3 for the atomic adsorbate, how the molecule substrate and intermolecular interaction potential determine whether local or global symmetry dominates. Since ARUPS, as will be shown further below, allows us to study symmetry properties of the electronic states of adsorbate systems, it may be possible to disentangle via ARUPS in favourable cases which of these two types of interactions dominates and how they are active in the adsorbate.

We begin the discussion with comments about the molecule substrate interaction. The relevant interactions are described within the "surface molecule" model according to Blyholder. As alluded to above we can look at this process from the view point of the molecule as a  $\sigma$ -donation- $\pi$ -backdonation process. This means that the distribution of electrons among the subsystems, i.e., CO molecule and metal atom, in the metal-CO-cluster is considerably different as compared with the non-interacting subsystems. For example, the electron configuration of the metal atom in the cluster may be different from the isolated metal atom, or the electron distribution within the CO molecule bonded towards the metal atom may look more like the electron distribution of an "excited" CO molecule rather than the ground state CO molecule (Kao and Messmer, 1985). Nevertheless, as a consequence of the relatively weak molecule-substrate interaction only certain electronic levels of the sub-systems are strongly influenced, so that it appears to be justified to classify the electronic levels of the interacting adsorbate system according to the nomenclature used for the isolated subsystems. Naturally, the distortions of the molecular as well as the metal levels are reflected by changes in the ionization energies of those levels, their ionization probabilities, and the line shapes of the ionization bands. Figure 10.21 shows a set of angle resolved, normal emission valence electron spectra of CO adsorbates on different single crystal surfaces (Turner et al., 1970; Eberhardt and Freund, 1983; Schmeisser et al., 1985; Freund et al., 1983; Allyn, 1978; Odörfer, 1987). The binding energy ( $E_B = h\nu - E_{\text{Kin}}$ ) refers to the vacuum level. The region where we expect emission from the three outer valence levels of CO, i.e., the  $5\sigma$ ,  $1\pi$ , and  $4\sigma$  levels (see Fig. 10.20) is shown, and most of the following discussion will concentrate on these levels. From the bottom to the top the heat of adsorption increases from 19 kJ/mol to 142 kJ/mol (Weast, 1973,

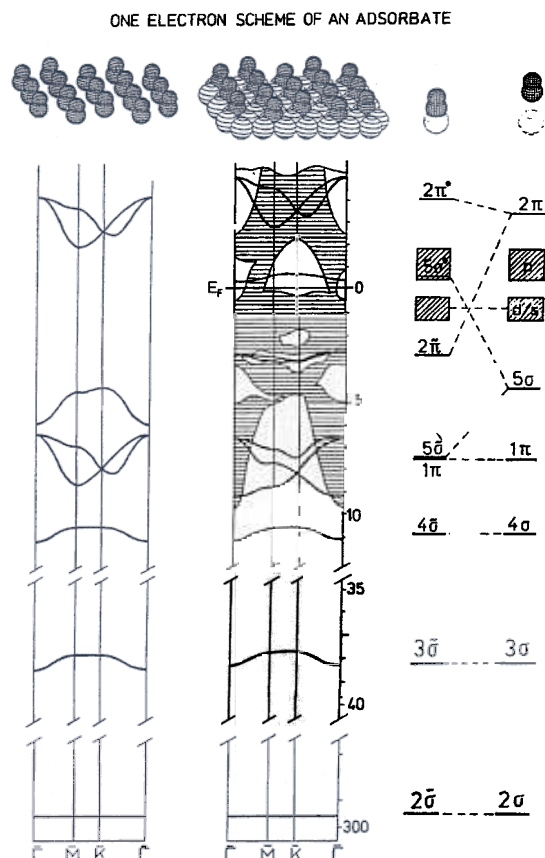


Fig. 10.20. Schematic one-electron level diagrams for diatomic molecules (CO) interacting with a transition metal surface. The level scheme for a molecule-metal cluster (right) is correlated with the band scheme of a free unsupported molecular layer (extreme left) and the band scheme of the quasi-two-dimensional adsorbate (middle). The band structure of the metal projected onto the surface is schematically shown as the hatched area.

1974; Elhiney et al., 1976; Kessler and Thieme, 1977; Christmann et al., 1974; Conrad et al., 1974). This is accompanied by changes in the adsorbate spectra as compared to the gas and solid phase spectra which are shown for comparison. There are several interesting differences in binding energies, line intensities and line shapes between gas, condensed and adsorbate phases, which we shall comment on in the following. In order to do so we have to cover many different aspects such as symmetry considerations, relaxation energies, line widths, shake-up satellites, and so on. We shall use Fig. 10.21 as a guide line to discuss the various aspects as they occur in going from the gas phase via weakly chemisorbed to strongly chemisorbed adsorbates.

In CO/Ag(111) at  $T = 20$  K CO is physisorbed as documented by the small  $E_{ad} = 19$  kJ/mol (Elhiney et al., 1976). This explains why a spectrum similar to condensed CO is observed for this adsorbate. The splittings in the  $4\tilde{\sigma}$  and  $5\tilde{\sigma}$  emissions are connected

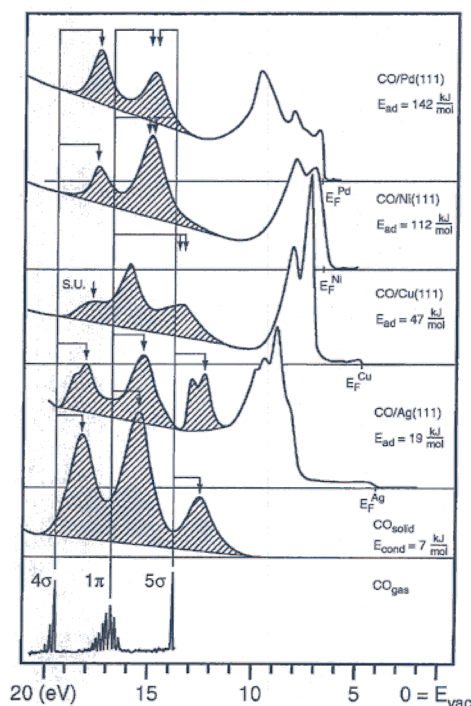


Fig. 10.21. Set of normal emission CO adsorbate spectra (Turner et al., 1970; Eberhardt and Freund, 1983; Schmeisser et al., 1985; Freund et al., 1983; Allyn, 1978; Odörfer, 1987). (S.U. – shake-up satellite.)

with the formation of a two-dimensional overlayer as will be discussed further below. In comparison with the gas phase, however, rather dramatic changes are observed upon condensation and physisorption, namely a shift of about 1 eV towards lower binding energies and a considerable increase in line width which destroys the vibrational structure observed in the gas phase. Very recently new results for weakly adsorbed  $N_2$  layers have been reported and we shall come back to this topic in the section on  $N_2$  adsorption. Chiang et al. (1980) found shifts by comparing the photoelectron spectra of CO, adsorbed on a metal surface (Al(111)), and of CO adsorbed on the same surface precovered with a monolayer of Xe, assisting as a spacer between metal and CO. The bands shift towards higher binding energies, and appear to exhibit smaller line widths when well separated from the surface. Theories have been developed that allow one to understand these observations on the basis of hole hopping and relaxation together with adsorbate–surface vibrations within the condensed quasi-two- or three-dimensional molecular solids (Duke, 1978; Duke et al., 1978; Gadzuk et al., 1982). The shift of the band to lower binding energy is a consequence of the electronic relaxation in the final ion state, which is considerably more pronounced when the molecule is bound to a readily polarizable medium, because metal electrons screen the positive charge introduced by the ionization process more effectively than do the electrons on the isolated molecule. The more pronounced screening stabilizes the final hole



state relative to the initial state, which lowers the binding energy as observed. Measured temperature dependences of line widths in molecular solids and model systems support the developed theoretical ideas (Gadzuk et al., 1982; Salaneck et al., 1980). It is likely that other processes, for example Auger decay or other radiationless decay mechanisms, contribute to these line widths as well (Sandell, 1993; Bjørneholm, 1992).

If the heat of adsorption increases to about 47 kJ/mol (Kessler and Thieme, 1977) (weak chemisorption), like, for example, in the case of a CO adsorbate on a Cu(111) surface, the features in the spectrum shift and the intensities of the lines are altered considerably with respect to the physisorbate. The line widths, on the other hand, are quite comparable in both systems. Three lines are still found, but their assignment is, as we shall see further below, quite different from the one for the condensed molecular solid.

Before we discuss how ARUPS establishes this assignment let us first turn towards the spectra of the strongly chemisorbed adsorbate systems, i.e., CO/Ni(111) and CO/Pd(111), which are only two examples out of a wealth of experimental data (Greuter et al., 1983; Shinn, 1986; Shinn and Madey, 1984, 1985; Saiki et al., 1989; Zaera et al., 1985; Allyn et al., 1977a; Horn et al., 1978a; Kuhlenbeck et al., 1986; Jensen and Rhodin, 1983; Miranda et al., 1984; Horn et al., 1979; Borstel et al., 1980; Hofmann et al., 1982, 1985; Heskett et al., 1985a; Steinkilberg, 1977; Braun et al., 1979; Kuhlenbeck, 1984; Seabury et al., 1980; Rieger et al., 1984; Apai et al., 1976; Smith et al., 1976). In the case of strong chemisorption the spectra show two bands, the binding energies of which are rather independent of the particular system under consideration, but are shifted by more than 2 eV to lower values with respect to the gas phase. ARUPS has been instrumental to show that these two CO induced bands are really caused by three CO ion states, and that the CO molecules are oriented with their axes parallel to the surface normal (Allyn et al., 1977a). Figure 10.22b shows an angular distribution pattern for the  $4\sigma$  ion state intensity of a CO/Pd(111) adsorbate as recorded with an elliptical mirror analyser employing polarized synchrotron light (Miranda et al., 1984). The polarization plane is placed along the  $0^\circ/180^\circ$  azimuth, i.e., the horizontal line in the angular coordinate diagram shown in Fig. 10.22a. With respect to the Pd(111) surface this corresponds to a mirror plane of the system. Figure 10.22c shows a quasi-three-dimensional plot of the emission intensity distribution (shaded areas on the half-sphere) as a function of azimuthal ( $\phi$ ) and polar ( $\theta$ ) angles in direct relation to the geometric structure of the molecular adsorbate (Freund and Neumann, 1988, 1992). The angular distribution pattern clearly shows how the symmetry of the adsorbate wave function with respect to this mirror plane determines the angular distribution of the emitted electron current. If we classify the wave functions of the electron  $\phi_e$  and  $\phi_k$ , (see Eq. (10.2)) as well as the momentum operator  $p$  "even" or "odd" with respect to this mirror plane, we are in the position to differentiate between "even" and "odd" initial states by choosing certain light polarizations and detecting the angular distribution pattern (see above) as long as spin orbit interaction is not important (Borstel et al., 1981). For the above given situation the light polarization direction is within the mirror plane. This corresponds to even symmetry of the momentum operator. Therefore, initial states with even symmetry will emit into the direction of the mirror plane because the final states have to be even in order for the matrix element not to vanish. In principle, one would expect a finite emission probability along the whole mirror plane. In the present case, however, one has to take into account the cylindrical symmetry of a CO molecule, bonded linearly towards the metal surface. Even initial



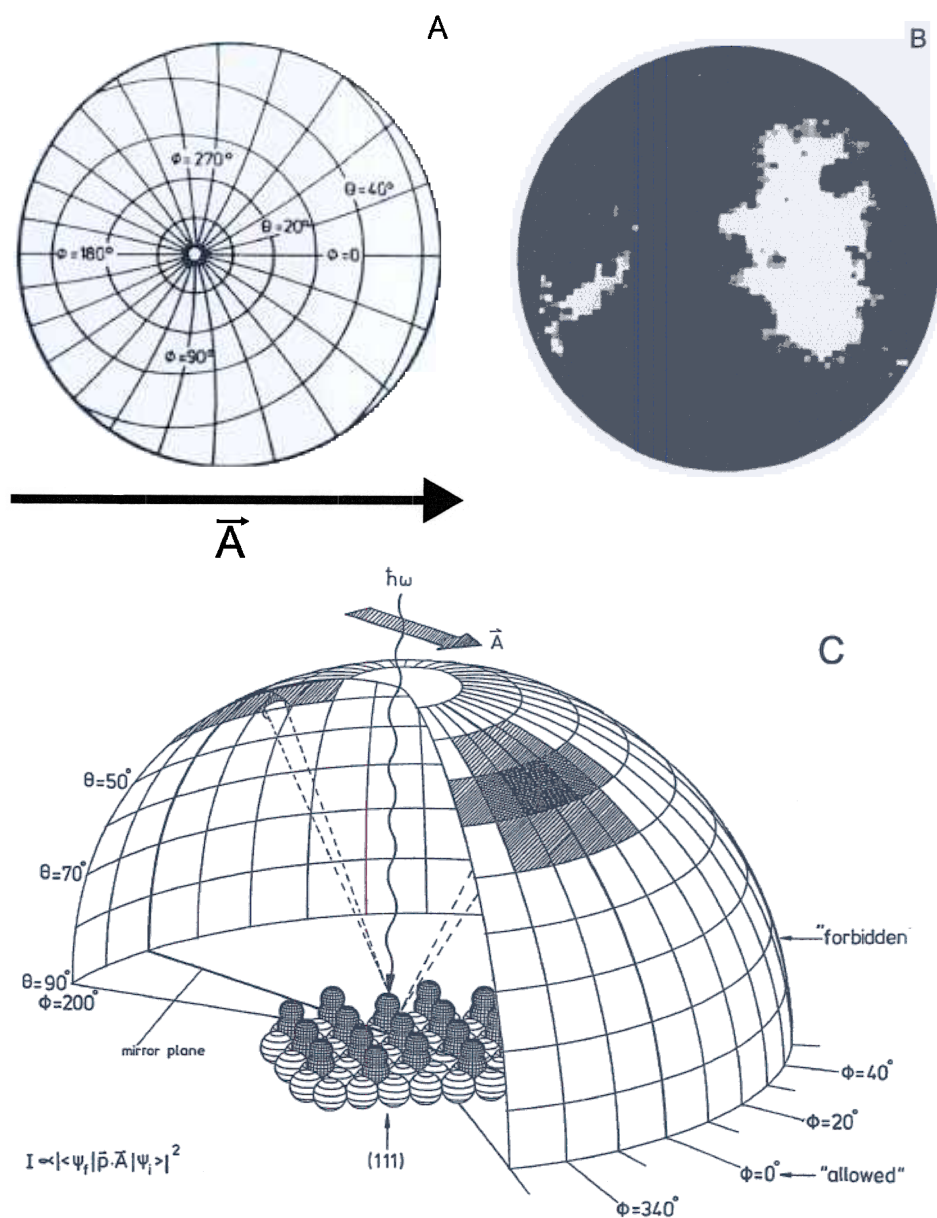


Fig. 10.22. CO  $4\sigma$  emission intensity from CO/Pd(111) as recorded with an elliptical mirror analyser (Miranda et al., 1984). (a) Polar diagram, the direction of the light polarization vector is indicated by an arrow. (b) Intensity distribution pattern. Light regions correspond to high emission current. (c) Quasi three-dimensional representation of the relation between geometric structure of the adsorbate and the measured  $4\sigma$  emission intensity as a function of  $\phi$  and  $\theta$ . The emission intensity is given by the shaded areas.

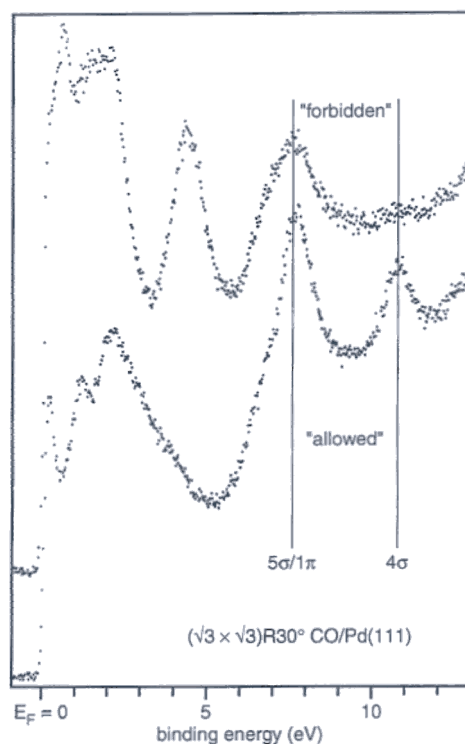


Fig. 10.23. ARUP-spectra of CO/Pd(111) in "forbidden" and "allowed" geometry (see text). The CO induced features are marked. The light polarization was placed along a Pd(210) mirror plane.

states of a cylindrical molecule cannot emit into a direction given by the plane perpendicular to the mirror plane which contains the light polarization vector. This latter property can easily be understood if we remember that any plane in a cylindrical system containing the cylindrical axis is a symmetry plane. Combining this property with the fact that the momentum operator is odd with respect to this second plane means that there cannot be any emission of even states into this direction. Therefore, in order to fulfill both conditions simultaneously, we do not expect an intense CO-4 $\sigma$  emission along the surface normal for light polarized in the surface plane. 4 $\sigma$  emission along the surface normal can only be achieved by using a light polarization perpendicular to the surface plane because in this case the momentum operator is even with respect to any plane perpendicular to the surface plane. If we combine the considerations so far we verify the above angular distribution pattern.

As a consequence of the outlined behaviour of even initial states, we expect a complementary behaviour of odd initial states. This is exactly what is observed experimentally and is shown as a set of electron distribution curves – which is the usual way to look at ARUP-spectra – in Fig. 10.23. In this figure the complementary behaviour of  $\sigma$ - and  $\pi$ -emissions, which was first observed by Lapeyre et al. (Smith et al., 1976) and later by Plummer and coworkers (Allyn et al., 1977a) is obvious: If we record a spectrum perpendicular (so-called "forbidden" geometry) to the incidence plane we do not observe emission in the

region of the  $4\sigma$  level but only in the region of the  $5\sigma/1\pi$  levels. Note, that the  $1\pi$ -ion state of CO has two degenerate components, one of which always transforms according to the even representation. Thus, we expect to see the one odd component of the  $1\pi$ -ion state. A spectrum recorded with the analyser placed within the incidence plane, the so called "allowed" geometry, show all states with even symmetry. From Fig. 10.23 it is clear that the band at 8 eV below the Fermi energy (Fig. 10.21) contains two states, i.e., the  $1\pi$  and the  $5\sigma$  ion states. Their energies are, in contrast to the gas phase, nearly (within a few tenths of an eV) degenerate in the adsorbate. This is a situation, predicted by the simple one-electron level scheme in Fig. 10.20. It is due to the donation of the  $5\sigma$  carbon lone pair into empty metal levels, thus stabilizing the CO  $5\sigma$ -level with respect to the  $1\pi$ -level which is not as intimately involved in the molecule-metal interaction for linear metal-molecule bonding.

The logic so far has been that we have assumed a geometry of the adsorbate site, thus knowing the symmetry of the system, i.e., CO perpendicular to the surface plane, and have verified this via an analysis of the angular photoemission spectra. Usually, the arguments are turned around, namely, the observed angular behaviour is used to deduce an adsorbate site symmetry.

The adsorbate induced features exhibit, in addition to the described angular dependences (Davenport, 1976), characteristic photon energy dependences, which, when recorded in an angle dependent fashion, can be used to get further information about adsorbate site geometry (Allyn et al., 1977a). Figure 10.24 shows a plot of the intensity of the  $4\sigma$  ion state as a function of photon energy. The data have been recorded for the system CO/Co(0001) (Greuter et al., 1983) for three different electron emission angles. The observed resonance feature is caused by the so-called shape resonance, which is well known from CO gas phase studies (Plummer et al., 1977). It can be traced back to a molecular final state of  $\sigma$  symmetry in the ionization continuum, quasi-bound by a centrifugal barrier in the molecular potential. Its symmetry confines the electron emission direction to the molecular axis, and directs the  $4\sigma$  emission out of the oxygen end of the molecule. This means that for the case of a molecule oriented along the surface normal, carbon-end bound to the surface, the resonance should peak along the surface normal.

Experimentally, we find in Fig. 10.24 the expected behaviour, i.e., a pronounced attenuation of the resonance intensity for off normal emission, which corroborates the assumed adsorbate orientation. Another interesting property of this resonance is its coherent-forward-emission character (Gustafsson, 1980). Coherent-forward-emission leads to an oscillatory behaviour of the photoionization cross-section. The periodicity is determined by the distance of the interfering sources, which are in the present case the carbon and oxygen atoms participating in the ion state wave function under consideration ( $4\sigma$ ). Examples are shown in Fig. 10.25 for the system CO/Pd(111) (Geisler et al., 1996). At a photon energy of 35 eV the resonance corresponding to the one shown in Fig. 10.24 is found. As predicted by theoretical calculations (Gustafsson, 1980), at about 95 eV and 220 eV a second and a third feature with larger widths and smaller amplitudes are observed. Potentially, the energy separation can be used to estimate the CO bond length in adsorbates as proposed by Gustafsson (1980). For the  $5\sigma$  emission the second and third features are missing due to back scattering.

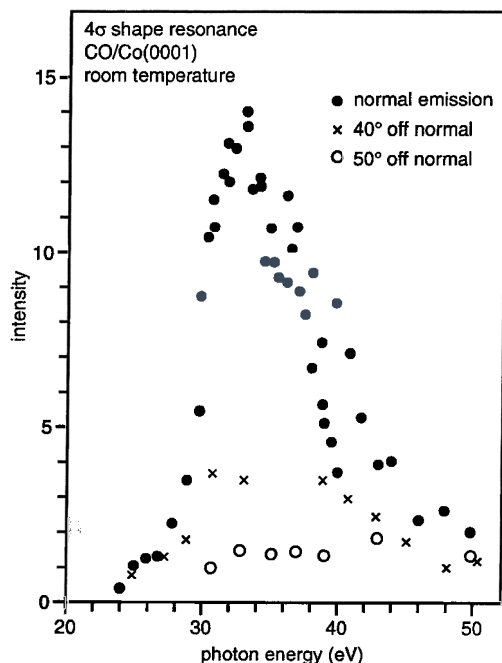


Fig. 10.24. Intensity variations of the  $4\sigma$  intensity in CO/Co(0001) as a function of photon energy. Filled circles refer to normal emission, open circles and crosses to off-normal emission as indicated (Greuter et al., 1983).

If we apply the geometry sensitive experiments, just presented, to investigate the geometric structure of physisorbed molecules, for example CO/Ag(111) (Schmeisser et al., 1985), Fig. 10.21, or CO/Al(111) (Chiang et al., 1980), we find that the orientation of the molecular axis is not, like in the chemisorbates perpendicular, but rather parallel to the surface. The reason is that due to the electronic structure of the substrate, not enough energy can be gained via the above mentioned  $\sigma$ -donor- $\pi$ -acceptor interaction, for which a vertical orientation is a necessary prerequisite. As we shall see further below, intermolecular interactions are rather important to understand the electronic structure of physisorbates.

At this point we can return to the assignment and analysis of the spectra of the weakly chemisorbed system. The assignment of the spectrum of the CO/Cu(111) system, given in Fig. 10.21 indicates that the considerations presented so far are not complete and sufficient to explain all experimental findings. It has been shown theoretically that for weakly chemisorbed systems so called shake up excitations accompanying the "normal" electron emission have to be considered (Hermann et al., 1981; Messmer and Lamson, 1979; Freund and Plummer, 1981; Saddeh et al., 1980; Schönhammer and Gunnarsson, 1978; Mariani et al., 1982; Wendin, 1981; Umbach, 1982; Martensson and Nilsson, 1990; Sandell, 1993; Bjørneholm, 1992). These shake-up excitations are manifestations of the fact that the ionization process is a rather complicated many-electron process (Cederbaum and Domcke, 1977; Wendin, 1981). They can be assigned to electron excitations in addition to electron emission. Their intensity is determined by the second matrix element in Eq. (10.2) whose

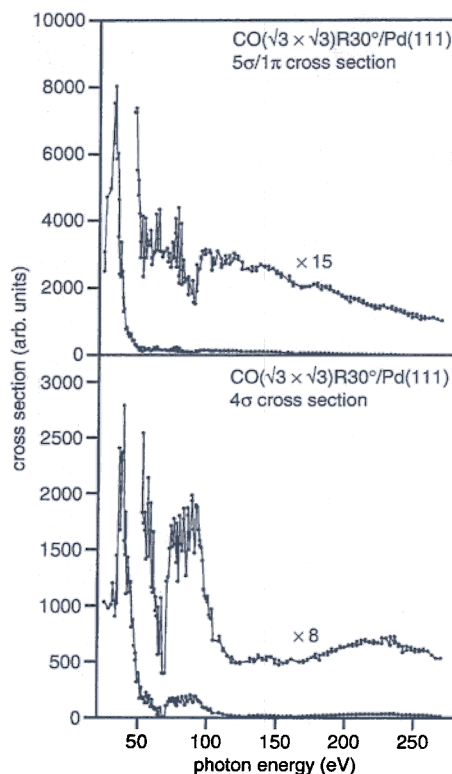


Fig. 10.25. Cross sections of the CO valence orbitals of  $(\sqrt{3} \times \sqrt{3})R30^\circ$  CO/Pd(111) as a function of the photon energy (Odörfer, 1987).

magnitude is governed by the projection of the wave function of the shake-up state  $N-1\psi_{e,E}$  onto the “frozen” ion state  $a_{\mathbf{k}}\varphi_i$ . Shake-up intensities are rather low for chemisorbed and for physisorbed systems but reach the maximum for intermediate metal–molecule coupling, i.e., weak chemisorption (Messmer and Lamson, 1979; Freund and Plummer, 1981; Saddei et al., 1980; Schönhammer and Gunnarsson, 1978; Mariani et al., 1982; Umbach, 1982; Martensson and Nilsson, 1990). Again, ARUPS can be employed to support the assignment as given in Fig. 10.21 for the CO/Cu(111) system. If the most intense CO features were due to  $1\pi$  emission, as might be suspected by comparing the spectra of the CO/Cu(111) system with CO/Ag(111), a resonance behaviour for this particular peak would not be allowed. Horn et al. (Mariani et al., 1982) showed that both bands at higher binding energy are due to states of  $\sigma$  symmetry by investigating the shape resonance discussed above. The  $4\sigma$  ion state as well as the accompanying shake-up transition exhibited parallel resonance behaviour as expected according to the assignment in Fig. 10.21. A spectrum rather similar to the one of the CO/Cu system, but with even slightly more intense satellite structure, has been found for the system CO/Au (Sandell, 1993; Bonzel, private communication). In the latter system the adsorption energy is between the one for CO/Ag

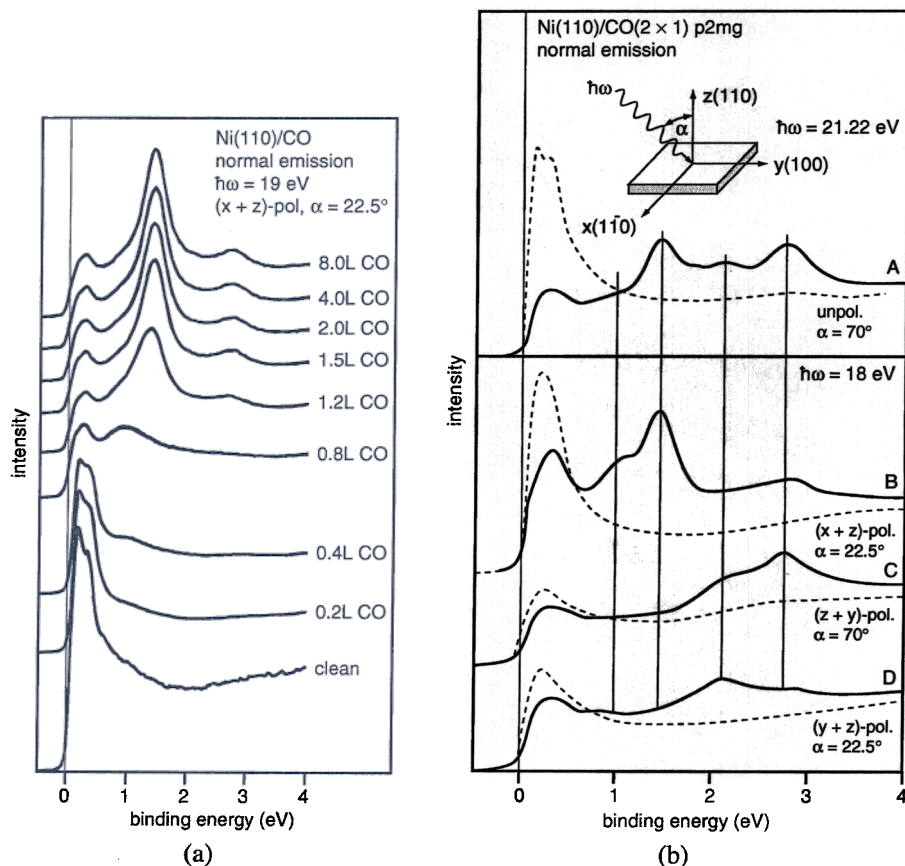


Fig. 10.26. (a) Normal emission ARUPS spectra of CO on Ni(110) as a function of coverage. (b) ARUP-spectra in normal emission for different light polarization directions of CO(2 x 1)p2mg/Ni(110) (full lines) in comparison with the clean Ni(110) surface (broken lines) in the region of the metal emissions (Kuhlenbeck et al., 1989).

and CO/Cu which leads us to expect more intense satellites, and corroborates the ideas presented.

In our discussion so far we have only considered the molecule induced peaks at binding energies higher than the metal states, i.e., those states that correspond to "molecular" ion states. However, as is obvious from Fig. 10.20 there are levels of the adsorbate system within the region of the metal projected density of states, due to the coupling of unoccupied molecular states to occupied metal states. There have been several attempts to identify these states (Smith et al., 1980; Boszo et al., 1983; Kuhlenbeck et al., 1987). The most recent one was done on the system CO(2 x 1)p2mg/Ni(110), whose structure will be discussed in detail in connection with intermolecular interactions (Kuhlenbeck et al., 1986). Figure 10.26a shows how these states develop as a function of coverage. The symmetry and high CO density of the system with highest coverage allows to measure the adsorbate induced peaks in the d-band region of the Ni substrate (Kuhlenbeck et al., 1987). Figure 10.26b shows a

selected set of spectra that demonstrate the intensity, symmetry and energy position of the CO induced, d-like states for this system. The spectra of the clean surface are given as dashed curves for comparison. The usually dominant CO molecular ionizations (Kuhlenbeck et al., 1986) are not shown in this figure. The various peak intensities are strongly polarization dependent, and, together with the measured dispersion, discussed in the section intermolecular interactions, support an assignment of these features to CO-2 $\pi$ -Ni-3d states. We shall come back to these states further down.

To complete the picture of the electronic structure we consider as the next step intermolecular interactions. As an introduction to the quasi two-dimensional band structure of molecular overlayers we discuss the band dispersions and the symmetry properties of a hexagonal overlayer (Greuter et al., 1983) of CO molecules on a fcc(111) surface as shown in Fig. 10.20.

We can illustrate the qualitative features of the dispersion by plotting schematically the real parts of a tight-binding wave function in real space for values of  $k$  corresponding to high symmetry points in reciprocal space. Figure 10.27a shows the real- and reciprocal-space unit cells for the hexagonal structure. The real and reciprocal lattices have two mirror planes: one along the  $\Gamma$ -M- $\Gamma$  line (in reciprocal space) and the other one along the line  $\Gamma$ -K-M-K. The wave functions along these lines will be even (a') or odd (a''). Figure 10.27b illustrates the phases of a  $\sigma$  and the two  $\pi$  states at  $\Gamma$  and M. The discussion of band dispersions is analogous to the one discussed for sulphur on Ni(100) in Fig. 10.8 and we refer to literature for details. The dispersions connected with the wave functions are the ones shown in Fig. 10.20 on the left hand side.

Such dispersions can be determined via ARUPS. Figure 10.27c shows a comparison of calculated dispersions for the 4 $\sigma$ -derived band with measured 4 $\sigma$  dispersions of CO/Co(0001) adsorbates in  $\Gamma$ -M direction in two hexagonal ( $\sqrt{3} \times \sqrt{3}$ )R30° and ( $2\sqrt{3} \times 2\sqrt{3}$ )R30° layers (Freund and Neumann, 1992). We have artificially set the lengths of the two Brillouin zones equal for a more convenient comparison. Due to the smaller CO-CO distance in the ( $2\sqrt{3} \times 2\sqrt{3}$ )R30° layer, the overlap of the 4 $\sigma$ -CO wave functions increases, and concomitantly, the band width increases. Figure 10.27c illustrates that the increase in band width can be quantitatively reproduced by simple tight binding calculations in the case of 4 $\sigma$  derived bands. In the present case the comparison can be made directly because the number of nearest neighbours is the same in both systems. If, on the other hand, we want to compare dispersions in hexagonal and quadratic systems, the observed band widths have to be corrected for the different number of nearest neighbours. Such a correction is straightforward on the basis of simple tight binding considerations. The result of such a comparison for several different adsorbate systems is shown in Fig. 10.28 (Freund et al., 1983; Allyn et al., 1977a; Horn et al., 1978a, b, 1979; Kuhlenbeck et al., 1986; Jensen and Rhodin, 1983; Greuter et al., 1983; Miranda et al., 1984; Hofmann et al., 1982, 1985; Heskett et al., 1985a; Rieger et al., 1984; Odörfer et al., 1988; Batra et al., 1979; Seaburg et al., 1981; Heskett, private communication; Schneider et al., 1988). The data points follow an exponential dependence on the nearest neighbour distance with a decay length on 1.25 Å if we disregard the CO-K co-adsorbate for the moment. This strongly supports the conclusion that the 4 $\sigma$  dispersion is caused by direct CO-CO overlap. Intuitively, this is reasonable, because the 4 $\sigma$ -CO level is not strongly involved in the metal substrate bonding. At the same time we expect a completely different behaviour for the

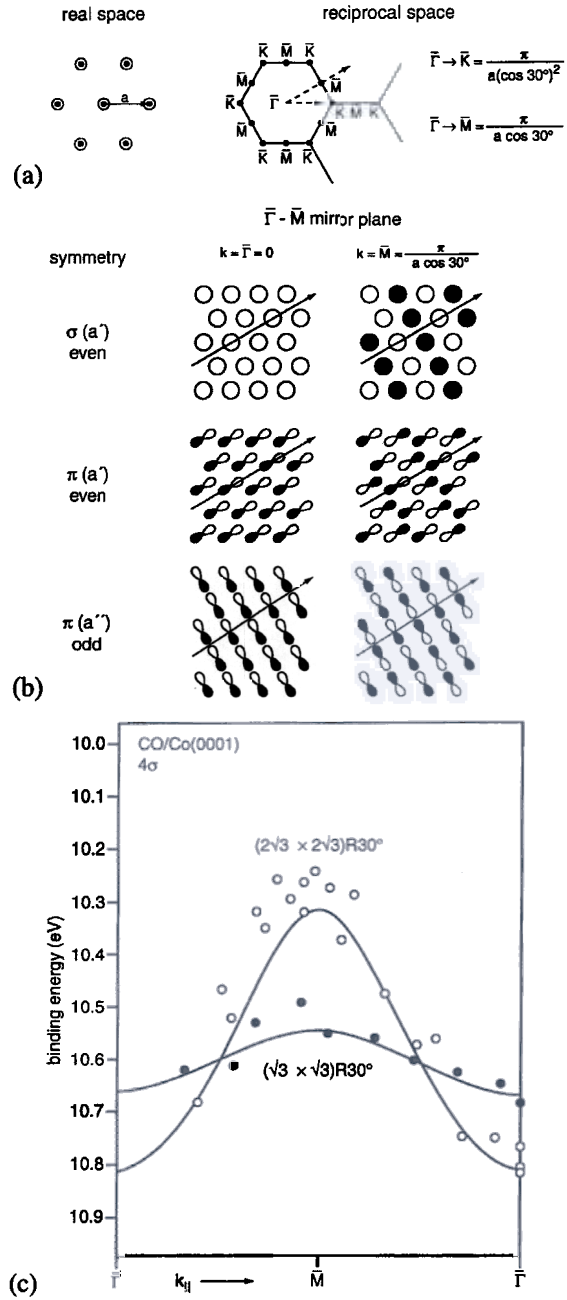


Fig. 10.27. Schematic two-dimensional wave functions of a hexagonal CO layer along the  $\bar{\Gamma}$ - $\bar{M}$  direction. (a) Real and reciprocal space representation of the hexagonal layer, (b) wave functions, (c) comparison of experimental and theoretical dispersions for two CO overlayers on Co(0001) of varying CO density (Freund and Neumann, 1992).



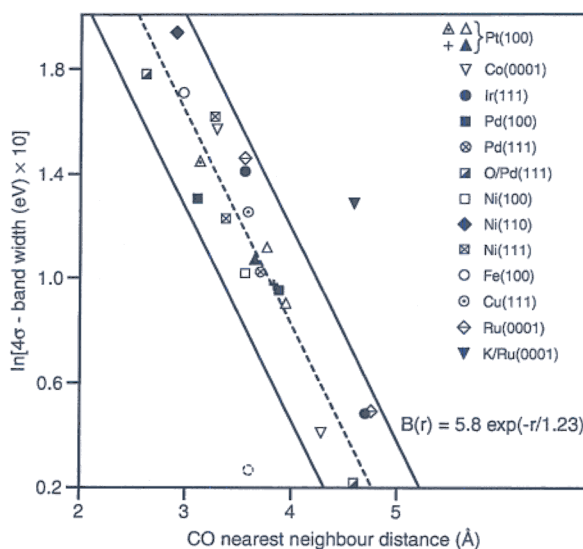


Fig. 10.28. Observed  $4\sigma$  bandwidths as a function of intermolecular separation. Six nearest neighbours are used as reference (Greuter et al., 1983; Freund et al., 1983; Allyn et al., 1977a; Horn et al., 1978a, b, 1979; Kühlenbeck et al., 1986; Jensen and Rhodin, 1983; Miranda et al., 1984; Hofmann et al., 1982, 1985; Heskett et al., 1985a; Rieger et al., 1984; Odörfer et al., 1988; Batra et al., 1979; Seaburg et al., 1981; Heskett, private communication; Schneider et al., 1988).

$5\sigma$  level, because in this case the interaction with the substrate as indicated in the middle of Fig. 10.20 should have a marked influence on measured dispersion. There is no such linear dependence of the observed band width as a function of CO–CO distances as for the  $4\sigma$  level (Heskett et al., 1985a). A similar plot as for the  $4\sigma$  level exhibits no particular functional dependence, which may be an expression of the participation of indirect through substrate interactions in intermolecular interaction. Care has to be exercised not to jump to this conclusion prematurely, because, due to the stabilization of the  $5\sigma$  level into the region of the  $1\pi$  level (see Fig. 10.20) we expect strong  $5\sigma/1\pi$  hybridization effects which have to be taken into account in the prediction of band dispersions (Greuter et al., 1983).

There are only very few cases, where the complete band structure in the  $5\sigma/1\pi$  region has been determined. One such example, which shall be considered in the following, is the system CO( $2 \times 1$ )p2mg/Ni(110) (Kühlenbeck et al., 1986). In this system the coverage is  $\Theta = 1$ , and the lateral stress is particularly demanding. Figure 10.29 shows a model of this structure. The interesting structural feature is the glide plane along the densely packed rows ( $1\bar{1}0$  azimuth) of the Ni(110) surface. The unit cell of this overlayer contains two CO molecules, which leads to peculiar consequences for the ARUP-spectra. Figure 10.30 shows the full band structure of the system including the unoccupied part. The occupied part was determined by measuring the binding energies of the CO induced features as a function of the electron emission angle along two azimuths with respect to the Ni(110) substrate, i.e., the  $[1\bar{1}0]$  and the  $[001]$  directions. Together with the experimental data (Kühlenbeck et al., 1986, 1989; Schneider et al., 1990; Memmel et al., 1989; Rangelov

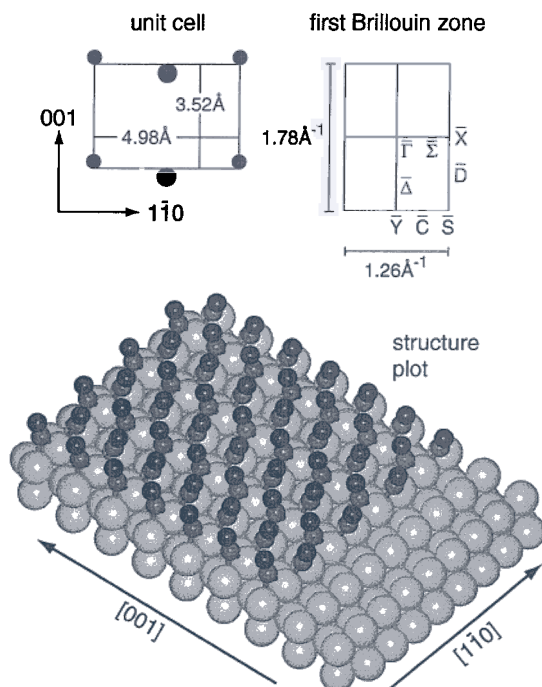


Fig. 10.29. Schematic representation of the CO(2 × 1)p2mg/Ni(110) structure, the unit cell and the surface Brillouin zone (Kuhlenbeck et al., 1986).

et al., 1991) we have plotted the result of a band structure calculation where the position of the lowest occupied  $4\sigma^+$ -valence orbital (see below) has been shifted to agree with experiments and the tilt angle has been used as a parameter. The best fit resulted for a tilt angle of  $17^\circ$  with respect to the surface normal. On the right hand side of the collected dispersion data we show a set of photoelectron spectra at the  $\Gamma$  point (normal emission). Clearly, the number of outer valence features which are bound at binding energies above 6 eV is larger than four, which would be the maximum number of features for a single molecule within the unit cell ( $5\sigma$ ,  $4\sigma$  and two  $1\pi$  components). This indicates that the unit cell contains more than one molecule (Kuhlenbeck et al., 1986). The region of the energetically well separated  $4\sigma$ -emissions shows a splitting into two features consistent with two molecules in the unit cell.

For a description of the band structure the wave functions of a single molecule are therefore not appropriate. However, linear combinations

$$\begin{aligned}\chi_1 &= c_1|\text{CO}^1\rangle + c_2|\text{CO}^2\rangle \quad (\text{symmetric}), \\ \chi_2 &= c_1|\text{CO}^1\rangle - c_2|\text{CO}^2\rangle \quad (\text{antisymmetric})\end{aligned}\tag{10.4}$$

of molecular CO wave functions located at the positions of the two molecules within the unit cell allow one to construct two-dimensional adlayer wave functions that transform

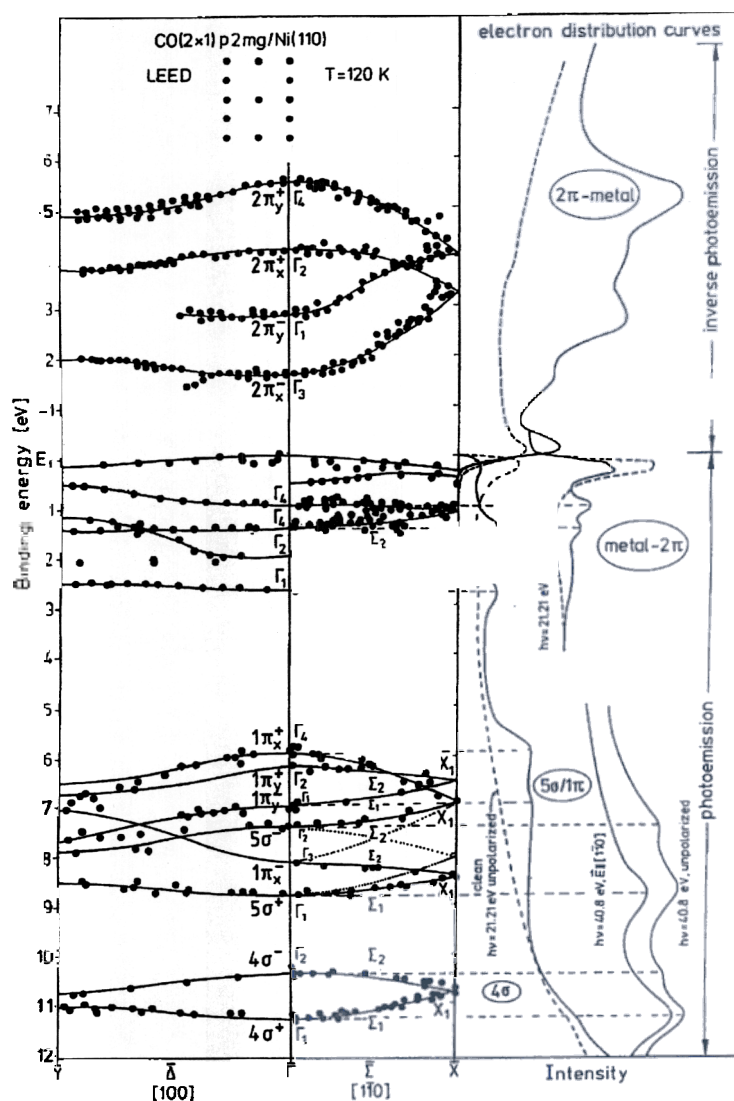


Fig. 10.30. Occupied and unoccupied band structure for CO(2 × 1)p2mg/Ni(110). In the right panel some typical electron distribution curves are shown (Kuhlenbeck et al., 1986; Memmel et al., 1989; Rangelov et al., 1991).

according to p2mg symmetry and which give rise to bands (E vs.  $k_{\parallel}$ ) easy to label by their irreducible representations at the points of high symmetry. Figure 10.31 schematically shows two-dimensional adlayer wave functions at  $\Gamma$ , X, and Y based on  $\sigma$  molecular wave functions. The unit cell is indicated,  $\chi_1$  and  $\chi_2$  are plotted. Consider Fig. 10.31a to represent the  $4\sigma$ -orbitals of CO. Unlike the case of one molecule per unit cell leading to a single band per non-degenerate molecular orbital (MO) in the Brillouin zone, we have two

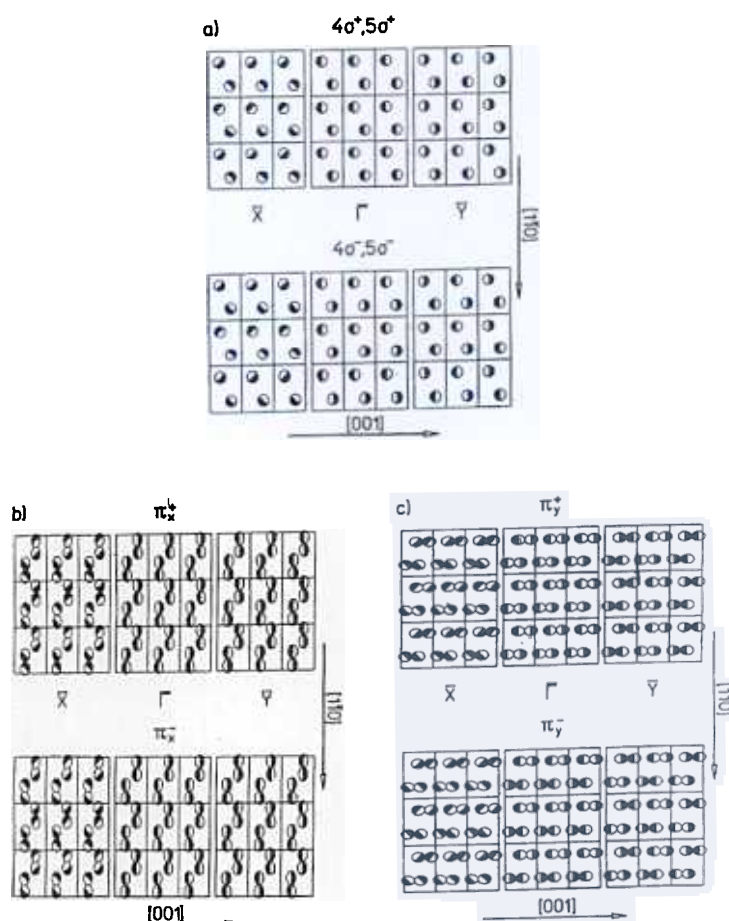


Fig. 10.31. Schematic representation of the  $\sigma$  (a) and  $\pi$  (b, c) derived wave functions of the CO overlayer for different  $\mathbf{k}$ -points. Each orbital lobe is half hatched. The direction of the line separating open and hatched part of the lobe marks the phase of the respective molecular wave function. In the zero phase situation the direction of the separating line points along the  $[1\bar{1}0]$  direction and the left part of the lobe is hatched.

bands in the present case, namely, one associated with the symmetric, the other one with the antisymmetric combination of molecular orbitals. In the band structure the bands are labelled '+' and '-', respectively. At  $\Gamma$  the splitting of the two  $4\sigma$  derived bands is about 0.85 eV, caused by the strong lateral interaction. In the symmetric combination all MOs have the same phase, i.e., the two-dimensional wave function is strongly bonding which leads to a stabilization on a binding energy scale compared to a laterally non-interacting adsorbate. The antisymmetric combination at  $\Gamma$  is antibonding with respect to the direction of the glide plane  $[1\bar{1}0]$ , but bonding with respect to the  $[001]$  direction. The interaction is stronger along the close packed  $[1\bar{1}0]$  direction leading to a net destabilization on a binding energy scale. If we follow the bands in  $\mathbf{k}_{\parallel}$ -space along  $\Gamma$ -X (the  $\Sigma$  direction),

the '+' band increases, while the '-' band decreases in energy until they are degenerate at X. Figure 10.31a allows us to visualize the situation: at X the phase between adjacent unit cells changes by  $180^\circ$  along  $[1\bar{1}0]$ . Consequently, for the symmetric combination this yields a two-dimensional wave function with phase changes only between rows in  $[001]$  direction. For the antisymmetric combination a similar wave function results is evident from Fig. 10.31a. In fact, these wave functions are degenerate. As was shown by Hund (1936) the bands have to be degenerate on the entire line X-S, which is perpendicular the glide plane (see Fig. 10.29), i.e., the line perpendicular to the glide plane. Clearly, the wave function plots indicate that the energy position of the bands at X has to be intermediate between the energies at  $\Gamma$  since there is increasing antibonding character for the symmetric combination while there is loss of antibonding character for the asymmetric combination. At Y the wave functions and thus the bands are non-degenerate energetically, since the spacial separation between sites of equal phase is larger for the '-' than for the '+' band. The splitting at Y is 0.3 eV, which should be compared with 0.85 eV at  $\Gamma$ . In order to specify the character of the wave functions within the band structure plot the irreducible representations of the wave functions are indicated.

Next we consider the region of the band structure of occupied levels at lower binding energies, namely, the region of the  $5\sigma$  and  $1\pi$  molecular orbitals. Due to the low symmetry of the overlayer  $5\sigma$  and  $1\pi$  derived adlayer bands are allowed to hybridize. The solid lines in this region (Fig. 10.30) refer to the bands after hybridization has been taken into account, while the dotted lines refer to the non-hybridized bands. We start the discussion by first considering the band dispersion neglecting hybridization. Clearly the dispersion of the nonhybridized  $5\sigma$ -bands should be similar to the  $4\sigma$ -dispersion. In fact, this is our result. The splittings calculated for various symmetry points, however, differ considerably. This is expected since the spatial extent of the  $5\sigma$  molecular orbitals is different from the  $4\sigma$  molecular orbitals. This aspect has been discussed in detail by Greuter et al. (Freund and Neumann, 1988). Compared with the  $4\sigma$ -bands the  $5\sigma$ -bands show a splitting of 1.35 eV at  $\Gamma$  and 0.63 eV at Y since the  $5\sigma$  molecular orbitals are more diffuse than the  $4\sigma$  molecular orbitals.

The dispersion associated with the nonhybridized  $1\pi$  molecular orbitals is, due to their twofold degeneracy on the molecular level, slightly more complicated than the  $\sigma$  band dispersions. Since the global symmetry of the adlayer is only twofold, the two  $1\pi$ -components cannot be degenerate and, due to the formation of symmetric and asymmetric combinations, give rise to four bands at  $\Gamma$ . In order to label the bands, we have chosen  $x$  to denote the component in  $[1\bar{1}0]$ ,  $y$  to denote the component in  $[001]$  direction. The wave functions belonging to the  $x$  components are shown in Fig. 10.31b. Again, symmetric and antisymmetric phase relations are identical to those for the  $\sigma$ -bands shown in Fig. 10.31a. Unlike the  $\sigma$ -bands, however, the antibonding combination is symmetric (+) and the bonding combination is antisymmetric (-) in the  $1\pi$ -case. As outlined above, the + or - signs refer to phase factors within the unit cell, while bonding and antibonding refer to the interaction of the wave functions within the unit cell: an in-phase combination of two  $\pi$  functions is antibonding and thus energetically destabilized, the out-of-phase combination of two  $\pi$  functions is bonding and thus energetically stabilized. In other words,  $\pi$  bands associated with phase factors + and - are energetically reversed with respect to the  $\sigma$ -bands. The splitting between + and - bands differs for the  $x$  and  $y$  components, in agreement with

Table 10.1  
Dipole selection rules for CO(2 × 1)p2mg

Electric field vector E orientation	Initial state bands		
	Symmetry	Molecular assignment	Symmetry
$E_{\parallel}[110]$ : z-polarization	$\Gamma_1$	$4\sigma^+, 5\sigma^+, 1\pi_y^-$	$\Gamma_1$
$E_{\parallel}[001]$ : y-polarization	$\Gamma_2$	$4\sigma^-, 5\sigma^-, 1\pi_y^+$	$\Gamma_2$
—	$\Gamma_3$	$1\pi_x^-$	$\Gamma_3$
$E_{\parallel}[1\bar{1}0]$ : x-polarization	$\Gamma_4$	$1\pi_x^+$	$\Gamma_4$

expectations since the lateral interactions along  $[1\bar{1}0]$  are much stronger than along  $[001]$ . The magnitudes of the splitting are 2.1 eV and 0.78 eV at  $\Gamma$ , respectively. At  $\Gamma$ ,  $1\pi_x^+$ ,  $1\pi_x^-$ ,  $1\pi_y^+$  and  $1\pi_y^-$  all belong to different irreducible representations. At X the bands degenerate pairwise for the same reason as the  $\sigma$ -bands. The bonding character of the wave functions at X is clearly higher for the x-component than for the y-component as is evident from Fig. 10.31b and Fig. 10.31c. Along the  $\Sigma$  line there are only two irreducible representations. The bands are labelled according to Litvin's compatibility relations (Litvin, 1983, 1984). The  $1\pi_y^-$  band has the same symmetry as the  $1\pi_x^+$  band along  $\Sigma$ , leading to a very small gap around the crossing point. The gap is very small since the interaction is "weak" for topological reasons. Perpendicular to the  $\Sigma$  direction, namely in the  $\Delta$  direction, the  $\pi$ -bands, like the  $\sigma$ -bands, are not degenerate at the zone boundary. Figure 10.31c shows on the right hand side that the  $1\pi_y^-$  band is, in addition to its bonding character in  $[001]$ , antibonding along  $[1\bar{1}0]$ . The  $1\pi_y^+$ -band is bonding in both directions.

$\sigma/\pi$ -hybridization can only occur if the bands of  $\sigma$  and  $\pi$  parentage transform according to the same irreducible representations. Along  $\Gamma$ -X, i.e., in the  $\Sigma$ -direction, the  $1\pi_x^-$ -band hybridizes with the  $5\sigma^-$ -band, shifting the energetic position of the point of degeneracy. Note that the degeneracy at X is not lifted by  $\sigma/\pi$ -hybridization. However, it is evident that the hybridized band structure is considerably different from the nonhybridized one. At  $\Gamma$ , for instance, the  $\sigma/\pi$ -hybridization leads to reversal of the  $1\pi_x^-$  and  $5\sigma^-$  binding energies.

So far we have discussed the development of the band structure without explicit reference to the experimental observations. The basis for an experimental analysis is Table 10.1 where the dipole selection rules for the p2mg system at  $\Gamma$  are summarized. At  $\Gamma$  the symmetry is  $C_{2v}$  and the symmetry selection rules shown in Table 10.1 may be applied. Because the final state of the electron must be totally symmetric ( $\Gamma_1$ ) there is evidence for a  $\Gamma_2$ - and a  $\Gamma_1$ -state in the range of the  $4\sigma$ -ionization if we compare the spectra recorded with polarized (electric field vector  $E$  parallel to the  $[1\bar{1}0]$  direction) and unpolarized light in Fig. 10.30. The symmetry restrictions for the  $4\sigma^-$ - and  $4\sigma^+$ -bands hold in the same way for the  $5\sigma^-$ - and  $5\sigma^+$ -band. The comparison of the same two spectra supports this conclusion. If the photon energy is smaller, i.e., around 20 eV the cross section of the  $\pi$  derived components becomes more prominent. The  $\pi$  derived  $\Gamma_4$ -band at lowest binding energy can be well used to demonstrate that the symmetry of the ordered overlayer is p2mg and not p1g1.

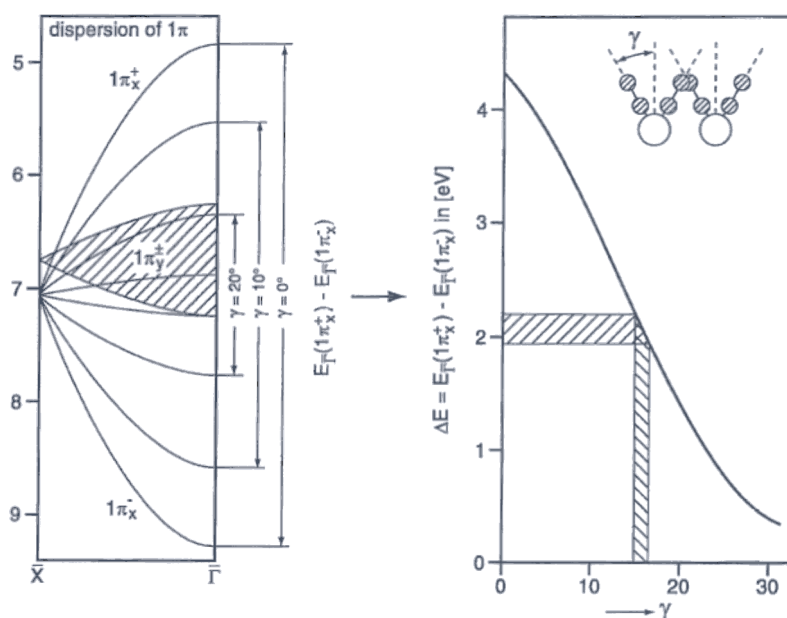


Fig. 10.32. Calculated  $1\pi$ -bandwidths as a function of the tilt angle of the molecular axis ( $\gamma$ ) with respect to the surface normal. In the right hand panel the observed splitting is used to deduce a tilt angle (Kuhlenbeck et al., 1986).

The splitting of the  $1\pi$ -levels has been discussed above and the experimental data basically corroborate the conclusions as is evident from Fig. 10.30. The strong splitting of the  $1\pi_x$  components can be used – and has been used – to estimate the CO tilt angle of the CO molecules. The procedure can be visualized with the help of Fig. 10.32. In the left panel we show the dispersion of the  $1\pi_y$ - and the  $1\pi_x$ -bands as a function of the tilt angle  $\gamma$ . The  $1\pi_y$ -bands disperse within the hatched area for the considered angular variations. We use the  $1\pi_x$ -bands as an example because for these bands the angular variations are largest and the fitting procedure is rather precise. For  $\gamma = 0^\circ$  the splitting is calculated to be  $\approx 4$  eV between the bands belonging to the bonding and the antibonding combination. Note that for  $\gamma = 0^\circ$  the glide plane disappears and we reach a  $p(1 \times 1)$  structure. In this case the unit cell contains only one molecule, and therefore, instead of having a splitting at  $\Gamma$  into two bands, the size of the Brillouin zone doubles. However, for comparison we have folded back the bands into a reduced zone, identical to the one of the  $p2mg$  structure. Clearly, as soon as we allow the CO molecules to avoid each other by tilting the splitting decreases dramatically, until we reach agreement with the experimentally observed splitting of 2.2 eV at  $\gamma = (17 \pm 2)^\circ$ . This is graphically shown in the panel on the right-hand side of Fig. 10.32. This strong variation of the  $1\pi_x$ -splitting is a consequence of the strong variation of intermolecular overlap as a function of  $\gamma$ . The splitting of the  $1\pi$ -levels in the range of occupied orbitals should be compared with the corresponding splitting of the  $2\pi$ -orbitals in the unoccupied range shown in Fig. 10.30. The experimental results have been taken from



inverse photoemission studies by (Mommel et al., 1989; Rangelov et al., 1991). The observed splitting for both the  $2\pi_x$  (3.8 eV) and the  $2\pi_y$  (1.2 eV) components is considerably larger than observed for the  $1\pi$ -levels. This may be caused again by substrate mediated interaction due to  $2\pi$ -backdonation but an additional role may be played by the  $2\pi$ -wave functions themselves which are expected to be considerably more diffuse as compared with the  $1\pi$ -levels. This point can be supported through a very nice series of experiments performed by Bertel and coworkers (Rangelov et al., 1991) on three isomorphic structures, i.e.,  $\text{CO}(2 \times 1)\text{p2mg/Ni}(110)$ ,  $\text{CO}(2 \times 1)\text{p2mg/Pd}(110)$ , and  $\text{CO}(2 \times 1)\text{p2mg/Pt}(110)$  where the intermolecular CO spacing varies and also the substrate mediated interaction changes. The comparison between the Ni and the Pd systems reveal that the splitting in the  $2\pi$  manifold is slightly smaller for Pd due to the increase in CO–CO separation. For Pt the situation is more complicated. Here it has been shown that the metal molecule interaction has a stronger  $5\sigma$  donation component than for Pd and Ni (Tüshaus et al., 1987). This in turn would lead to the shift of the  $5\sigma$ -metal antibonding component in the unoccupied region while for Ni and Pd both the bonding and antibonding combinations are occupied.

A direct observation of the substrate mediated interaction is possible for the system CO p2mg on Ni(110) by following the CO induced features in the region of the metal band structure, i.e., between the Fermi energy and a binding energy of 3 eV (Kuhlenbeck et al., 1989). In this energy range Fig. 10.30 shows bands which exhibit dispersions of up to 0.5–1.0 eV indicating a substantial contribution via this type of interaction. A way to investigate the substrate mediated intermolecular interactions may be the analysis of the dispersion of the above mentioned molecule induced changes in the region of the metal-substrate ionizations (see solid lines in the region of the projected band structure in Fig. 10.20). Such an analysis has been carried out for the  $\text{CO}(2 \times 1)\text{p2mg/Ni}(110)$  system [110]. Before the dispersions are analysed we have to ensure that the bands are really localized at the surface of the solid, i.e., the  $\text{CO}2\pi$ –Ni3d features should not exhibit a dispersion as a function of photon energy in normal emission, which is the usually applied criterion for a surface state. Once this has been done, we can determine the dispersion via off normal emission and vary the photon energy such that we choose an appropriate cross section of the feature under consideration. The result of such a very tedious analysis has been carried out by Kuhlenbeck et al. (1987, 1989) and is shown in Fig. 10.33 for two directions of the surface Brillouin zone. There are two important qualitative features of the dispersion curves. First, there are no band gaps at the zone boundary X, which – as Hund pointed out in 1936 (Hund, 1936) – is a consequence of the glide plane in the  $\Sigma$  direction. Secondly, the lower well resolved band can be fitted closely with a tight binding type curve (full lines). A detailed discussion, for which we refer to the original literature (Kuhlenbeck et al., 1987), reveals a rather clear picture of the nature of the  $\text{CO}2\pi$ –Ni3d interaction. For the case Ni(110) this interaction creates new surface resonances positioned from 1 to 2.7 eV below the Fermi energy with the appropriate symmetry and intensity. We have not found direct indications of the  $5\sigma$ -metal antibonding combination, although we also cannot exclude its existence in this energy range. This picture seems to be quite incompatible with a model where the  $\text{CO}2\pi$  orbital close to the Fermi level is resonantly broadened by interaction with the metal. The tails of this broadened band would extend below the Fermi energy and therefore create a degree of  $2\pi$  occupancy. In the “surface molecule” model, on the other hand we have a  $2\pi$  level, the width of which is not very important, far above the Fermi energy as



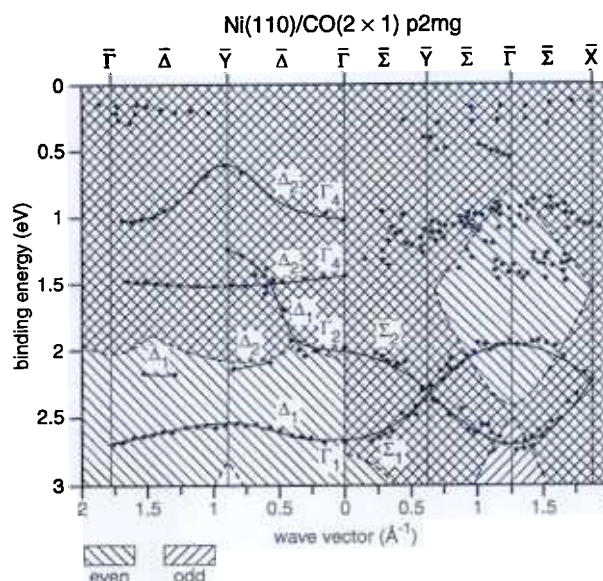


Fig. 10.33. Measured dispersions of the  $2\pi$ -d wave functions plotted on top of the calculated bulk band structure projected onto the [110] surface. The projection has been done separately for even and odd bands (Kuhlenbeck et al., 1989).

the molecule approaches the surface. This level (or the symmetry adapted combination of levels) mixes into the metal levels because there is a finite overlap between them. Since the overlap is a matter of symmetry it determines which of the metal bands will couple with the  $\text{CO}2\pi$ . The question which of the  $2\pi$ -induced bands are actually observed is then determined by the strength of the  $\text{CO}2\pi$ -metal coupling, and will depend upon the nature of the metal, the crystal face, and the structure of the CO layer.

The examples for dispersions in quasi two-dimensional systems were chosen so far from the many examples of strongly chemisorbed systems. One question is what happens to the dispersions when weakly chemisorbed or physisorbed systems are considered. The latter case is easy: Fig. 10.34 shows the dispersions measured via ARUPS for the system  $\text{CO}/\text{Ag}(111)$  (Schmeisser et al., 1985). We know from the previous section that in this system the CO molecules are oriented with their axis parallel to the surface. It is known from LEED studies that CO molecules physisorbed on graphite form herring-bone structures (Diehl and Fain, 1983) as shown in the inset in Fig. 10.34. Such structures again belong to nonsymmorphic space groups with two molecules in the unit cell. This is the reason why the molecular ionization bands appear as split in two components, i.e., a bonding and an antibonding combination at  $\Gamma$ . From symmetry considerations it is clear that these two bands are degenerate at the zone boundary. The splitting is larger for the  $\sigma$  levels than for the  $\pi$  level, which is not unreasonable on the basis of intermolecular overlap considerations. A particularly interesting observation has been made for this system if the temperature is increased. These physisorbed overlayers are known to undergo order-disorder transitions (Diehl and Fain, 1983). The CO molecules are then no longer locked into a herring-bone structure but rotate freely on their site. This destroys the nonsymmorphic

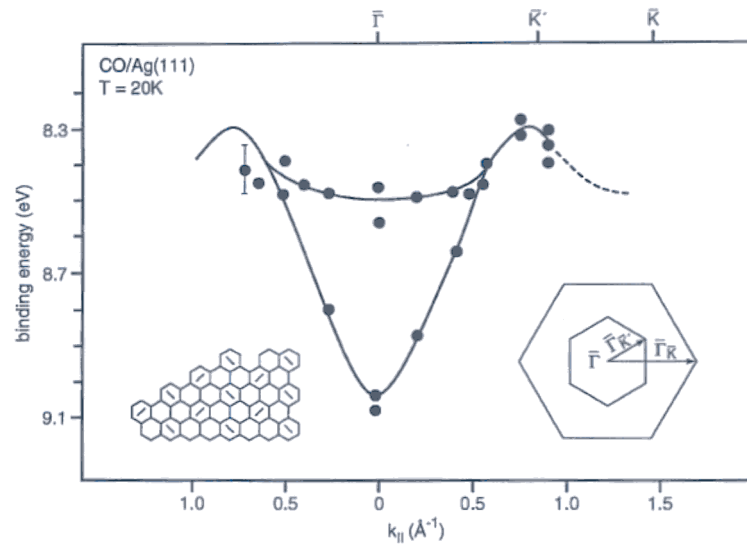


Fig. 10.34. Measured dispersion the  $5\sigma$  CO levels of CO/Ag(111) (Schmeisser et al., 1985).

phic structure and, concomitantly, the splitting of the  $\sigma$  levels disappears. CO/Ag(111) is a system where ARUPS can be used to study phase transitions in quasi-two-dimensional systems (Schmeisser et al., 1985).

In the case of weakly chemisorbed systems the situation is slightly more complicated. The reason for this complication is the shake-up structure identified in the previous section (Freund et al., 1983). Figure 10.35 shows the dispersions for the system  $(\sqrt{7} \times \sqrt{7})\text{CO}/\text{Cu}(111)$ , for which Fig. 10.2 showed an electron distribution curve (Freund et al., 1983). In this case the CO molecules are oriented perpendicular to the surface as in the case of the strongly chemisorbed systems. While the integrated  $5\sigma/1\pi$  dispersion is compatible with other CO overlayer systems, the  $4\sigma$  dispersion is considerably smaller than expected for the given intermolecular separation. The observed value is represented in Fig. 10.28 by the dashed circle. The shake-up which is – as noted above – associated with the  $4\sigma$  ionization shows almost no dispersion, but a slight variation in relative intensity with respect to the  $4\sigma$  ionization. There are sum rules (Hedin, 1979; Lundquist, 1967, 1968, 1969) relating intensity and ionization energy of the peaks in the observed spectral function with the quasi-particle energy. These sum rules are of the type

$$\varepsilon_k^{\text{HF}} = \int_{-\infty}^{\infty} \omega A(\omega, k) d\omega. \quad (10.5)$$

We can apply this sum rule to the observed data and regain a dispersion shown as the open circles in Fig. 10.35. This renormalized  $4\sigma$  band widths can now be favourably compared with the values measured for the strongly chemisorbed systems. This shows that it is the ionization process that introduces the deviations in the observed band widths and not a different intermolecular interaction potential in this case.

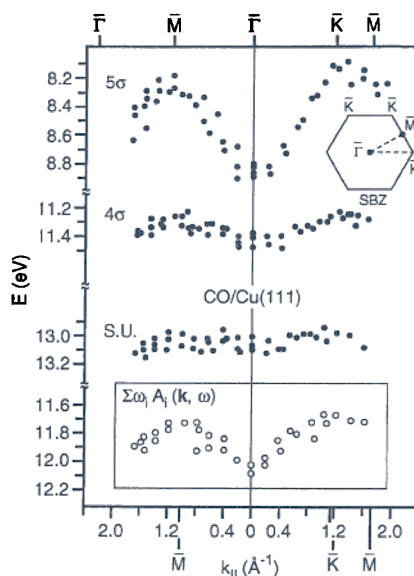


Fig. 10.35. Measured dispersion of the CO induced levels of the system CO/Cu(111). The renormalized dispersion of the 4 $\sigma$ -levels is plotted as open circles (Freund et al., 1983).

### 10.6. Nitrogen adsorption

N<sub>2</sub> on Fe(111) has been the model system to investigate the mechanism of ammonia synthesis (Ertl, 1983). It is known that N<sub>2</sub> dissociation is the rate limiting step, and that there exist molecular precursor states for dissociation where N<sub>2</sub> has been presumed to be side-on bonded to the iron surface (Grunze et al., 1984). Via ARUPS a strongly inclined N<sub>2</sub> species was identified (Freund et al., 1987) in addition to a vertically bound N<sub>2</sub> species which only exists at lower temperature. Figure 10.10 shows a set of angle resolved spectra at low temperature (vertically bound N<sub>2</sub>) and higher ( $T = 110$  K) temperature (N<sub>2</sub> bond inclined). Figure 10.36 reveals the  $\sigma$ -shape resonance in normal emission for  $z$ -polarized light at  $T < 77$  K. Figure 10.36 shows a  $\sigma$  resonance, but only in off-normal emission for  $s$ -polarized light (compare left and right part of this figure) at  $T = 110$  K, supporting the proposed inclined geometry in the second case.

Very similar observations have been made in a very detailed study by Shinn (1990) on N<sub>2</sub> bonding on Cr(110). Figure 10.37 shows a correlation of the outer valence ionizations of N<sub>2</sub> adsorbates including those where the N<sub>2</sub> molecule is bound "end-on" to the metal (b) and two where the molecule is  $\pi$ -bonded "side-on" to the metal surface. There are only slight differences between the two groups as compared with the gas phase and physisorbates (a). The reason for this similarity is still not quite clear. One might expect some major differences, in particular the  $1\pi_u$  level should be split. However, there is no convincing experimental evidence for this. One reason may be that the mixing of the levels, especially in the highly asymmetric bonding sites on the Fe(111) surface, is so strong that a definitive differentiation between the two  $\sigma$  levels and the  $1\pi_u$  component with  $\sigma$

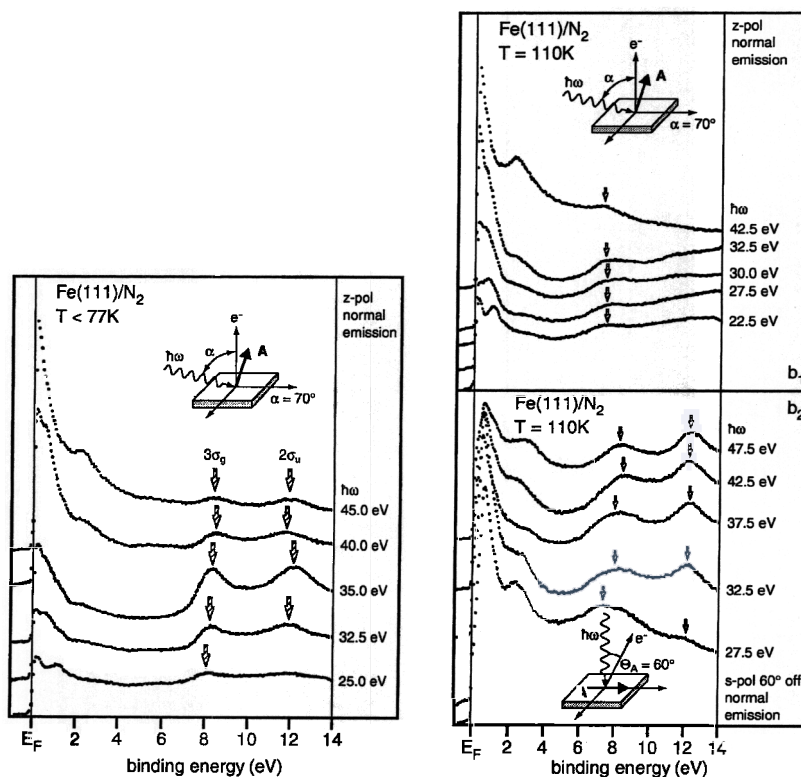


Fig. 10.36. ARUPS-spectra of  $\text{N}_2/\text{Fe}(111)$  for grazing light incidence and normal emission (left panel), and s-polarization (near normal incidence, right panel) and two electron emission angles: ( $b_1$ ) normal emission; ( $b_2$ ) off-normal ( $60^\circ$ ) emission. For each measurement geometry typical spectra at different photon energies are plotted (Freund et al., 1987).

symmetry is not possible. Another interesting feature can be demonstrated on the basis of the present results. Both, the  $3\sigma_g$  as well as the  $2\sigma_u$  state exhibit the shape resonance behaviour, while in the gas phase the  $\sigma_g$  resonance is symmetry forbidden. The reason is very simple: the inversion symmetry of the homonuclear  $\text{N}_2$  molecule is broken upon adsorption which makes the final resonance state accessible to both  $\sigma$  states. This was demonstrated earlier by Horn et al. (1982) for the system  $\text{N}_2/\text{Ni}(110)$ . In contrast to the case  $\text{N}_2/\text{Fe}(111)$  where  $\text{N}_2$  dissociates at low temperature ( $T > 140$  K),  $\text{N}_2$ -metal coupling is usually rather weak (Heskett et al., 1985a; Horn et al., 1982; Umbach et al., 1980; Dowben et al., 1984; Breitschäfer et al., 1986). This leads to the existence of rather intense shake-up structure as noted for several  $\text{N}_2$ -transition metal systems (Heskett et al., 1985a; Horn et al., 1982; Umbach et al., 1980; Dowben et al., 1984; Breitschäfer et al., 1986; Schichl et al., 1984; Messmer, 1984; Freund et al., 1985). The experimental findings are corroborated by several theoretical calculations (Heskett et al., 1985a; Horn et al., 1982; Umbach et al., 1980; Dowben et al., 1984; Breitschäfer et al., 1986; Schichl et al., 1984; Messmer, 1984; Freund et al., 1985).

Binding energies of molecular nitrogen valence orbitals (UPS data)

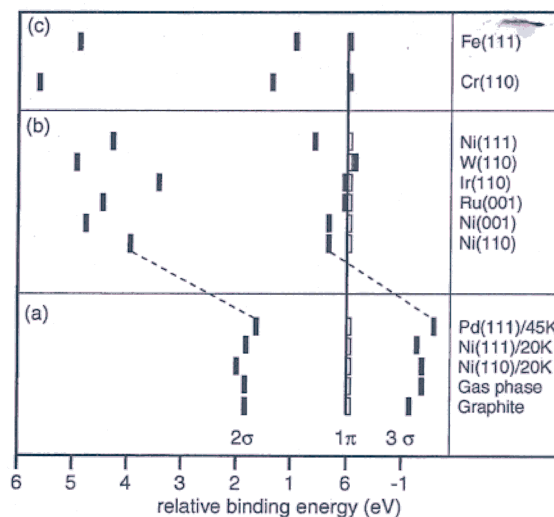


Fig. 10.37. Relative UPS molecular binding energies plotted with respect to the  $N_2(1\pi_u)$  peak: (a) physisorption systems and gas phase, (b) weak chemisorption systems, and (c) strong chemisorption systems (Freund et al., 1987).

In the introduction we alluded to the question of line widths in weakly bound molecules. We shall deepen this aspect slightly at this point because Umbach and his group (Höfer et al., 1990), as well as Jacobi and coworkers (Bertolo et al., 1991) have recently presented interesting data for  $N_2$  molecules adsorbed on a monoatomic Xe spacer layer on a metal surface. Figure 10.38 shows the region of the  $N_2$  ionizations and indicates the pronounced vibrational structure in the  $1\pi_u$  derived band. We note in passing that the splitting of the  $3\sigma_g$  band in the present system is similar to observations in  $N_2$  layers on graphite and CO layers on Ag, discussed above. The observed vibrational line shape of the  $1\pi_u$  ionization cannot be reproduced by just convoluting the gas-phase data with the appropriate broadening function. Instead, both the vibrational progression of  $N_2^+$  as well as of neutral  $N_2$  had to be included, indicating that the hole life time is finite and the hole hops to another molecule in the physisorbed layer. From the fits a life time may be estimated to  $(2-3) \times 10^{-15}$  s. The hopping of the hole is most effective for those levels between which the overlap is largest. This can be experimentally shown by taking the spectra as a function of incidence angle.  $N_2$  is oriented with its axis parallel to the surface plane and thus the  $1\pi_u$  splits into components parallel and perpendicular to the surface. At normal light incidence the  $1\pi_u$  component parallel to the surface may lead to normally emitted electrons. At growing light incidence angle the perpendicular component leads to normal emission. Due to the larger overlap of the  $1\pi_u$  component parallel to the surface the hopping is more effective for those levels. Therefore at near normal incidence the neutral contribution to the spectrum increases considerably. This is demonstrated by Fig. 10.38.

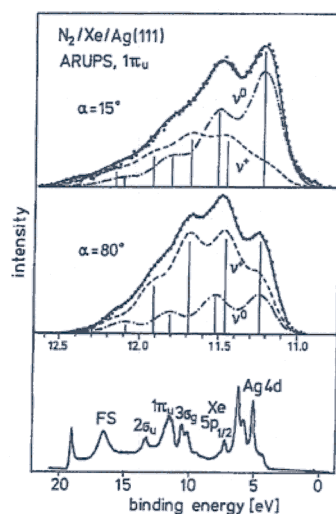


Fig. 10.38. Photoelectron spectra of  $\text{N}_2/\text{Xe}/\text{Ag}(111)$ . At the bottom the full spectrum taken with a photon energy of 23 eV is shown. FS denotes a final state peak which appears at a fixed kinetic energy irrespective of the photon energy. It is due to the unoccupied  $1\pi_g$  level. The other panels show spectra of the  $1\pi_u$  state recorded in normal emission. For the spectrum at the top the light incidence angle was  $\alpha = 15^\circ$  and for the spectrum in the center it was  $\alpha = 80^\circ$  (Bertolo et al., 1991).

### 10.7. Carbondioxide adsorption

$\text{CO}_2$  has been the subject of many surface science studies (Bartos et al., 1987a, b; Freund et al., 1987; Peled and Asscher, 1987; Asscher et al., 1988; Brosseau et al., 1991; D'Evelyn et al., 1986; Walsh, 1913; Freund and Messmer, 1986; Wambach et al., 1991). Besides simple molecular physisorption also under certain circumstances transformation into a bent anionic species has been observed (Bartos et al., 1987a, b; Freund et al., 1987; Peled and Asscher, 1987; Asscher et al., 1988; Brosseau et al., 1991; D'Evelyn et al., 1986; Walsh, 1913; Freund and Messmer, 1986; Wambach et al., 1991). The latter cases are  $\text{CO}_2/\text{Ni}(110)$  (Bartos et al., 1987a, b),  $\text{CO}_2/\text{Fe}(111)$  (Freund et al., 1987),  $\text{CO}_2/\text{Re}(0001)$  (Peled and Asscher, 1987; Asscher et al., 1988), and  $\text{CO}_2/\text{Pd}(110)$  (Brosseau et al., 1991). Since the results are rather similar we will concentrate in the following on one of these systems, i.e.,  $\text{CO}_2/\text{Ni}(110)$ . A series of ARUPS spectra as a function of temperature is shown in Fig. 10.39. By comparison with the gas-phase spectrum (Turner et al., 1970) one finds that at  $T = 80$  K  $\text{CO}_2$  is molecularly adsorbed with out significant changes of the electronic structure. Angular-dependent measurements have shown that  $\text{CO}_2$  adsorbs in a lying down geometry at this temperature (Bartos et al., 1987a, b). Upon heating the intense features in the photoelectron spectrum gradually fade away until at  $T = 200$  K a spectrum (e) is observed that could neither be assigned to  $\text{CO}_2$  nor to CO or O (confer Fig. 10.39). Further heating leads to a dissociation of this species into  $\text{CO} + \text{O}$  as indicated by spectrum (f) so that the species leading to spectrum (e) may be viewed as a precursor for  $\text{CO}_2$  dissociation. On the basis of *ab initio* calculations this species has been assigned to bent anionic  $\text{CO}_2^-$ .



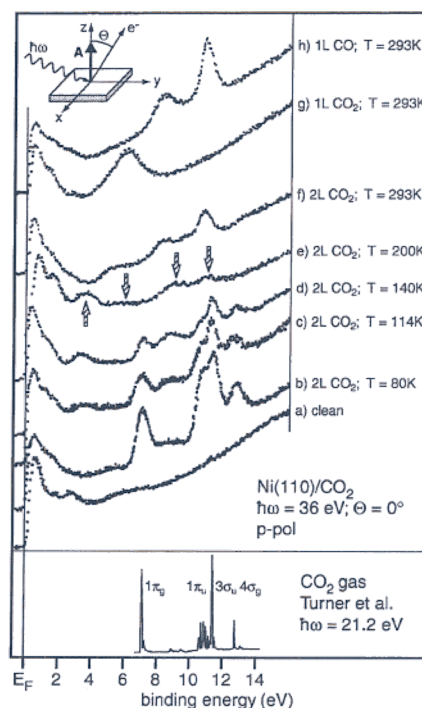


Fig. 10.39. Photoelectron spectra of a CO<sub>2</sub>/Ni(110) adsorbate at various temperatures in comparison with the clean surface (a), an oxygen covered surface (g), and a CO covered surface (h). At the bottom a spectrum of CO<sub>2</sub> in the gas phase is shown (Turner et al., 1970).

which has also previously been proposed from the results of molecular-beam experiments on different metal surfaces (D'Evelyn et al., 1986). It is formed by an electron transfer from the substrate to the CO<sub>2</sub> molecule. According to the Walsh rules (Walsh, 1913) the molecular axis is no longer linear but bent, as is also the case for NO<sub>2</sub> which is isoelectronic to CO<sub>2</sub><sup>-</sup>. The assignment of the CO<sub>2</sub><sup>-</sup> valence band features on the basis of *ab initio* calculations is shown in Fig. 10.40. Generally, all CO<sub>2</sub> levels shift to lower binding energy. The feature at about 3.5 eV (6a<sub>1</sub>), which is not observed in the spectrum of linear CO<sub>2</sub>, is due to the extra electron which is located at the carbon atom of the CO<sub>2</sub><sup>-</sup> anion. The respective level is unoccupied in linear CO<sub>2</sub>. Angular dependent measurements indicate that the symmetry of the CO<sub>2</sub><sup>-</sup> anion is most likely C<sub>2v</sub>. In this context the CO<sub>2</sub><sup>-</sup> molecules may bond to the substrate via the carbon atom (carbon end-down) or the oxygen atoms (carbon end-up). Due to the unpaired electron at the carbon end this species is rather reactive. Using HREELS it could be shown that the CO<sub>2</sub><sup>-</sup> anions readily react to form formate upon hydrogen exposure (Wambach et al., 1991). Formate differs from CO<sub>2</sub><sup>-</sup> only by a hydrogen atom which is bonded to the carbon atom. For steric reason it is therefore rather likely that CO<sub>2</sub><sup>-</sup> bonds to the substrate via the oxygen atoms since otherwise the molecule would have to turn around to form formate. This result is consistent with the behaviour of the work function which increases upon CO<sub>2</sub><sup>-</sup> formation.

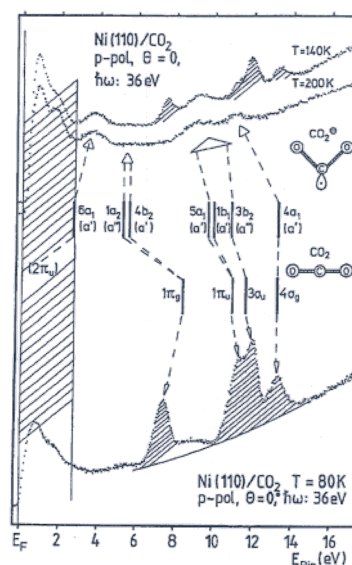


Fig. 10.40. Assignment of the photoelectron spectra of  $\text{CO}_2$  at 80 K, 140 K, and 200 K and adsorbed  $\text{CO}_2^-$  on the basis of *ab initio* calculations (Freund and Messmer, 1986).

The bonding of formate to Ni(110) and Cu(110) has recently been studied by several groups (Lindner et al., 1987; Hofmann and Menzel, 1987; Peyerimhoff, 1967; Woodruff et al., 1988; Puschmann et al., 1985; Madix et al., 1983; Jones et al., 1988; Jones and Richardson, 1989). Surface formate may be formed by adsorption of formic acid with subsequent annealing at temperatures above  $T = 270$  K. Photoelectron spectroscopy (ARUPS) has been employed to deduce the orientation of the surface formate species. In Fig. 10.41 a set of ARUPS spectra taken from Hofmann and Menzel (1987) is shown. The spectra have been taken for different light incidence angles and polarizations, but always detecting the electrons along the surface normal. The assignment of the spectral features within the coordinate system of an isolated adsorbate molecule is indicated in the figure. Assuming a  $\text{C}_{2v}$  geometry of the adsorbate complex the dipole operator transforms according to the irreducible representations  $b_1$ ,  $b_2$  and  $a_1$  of the adsorbate/substrate complex for  $x$ ,  $y$  and  $z$  polarized light, respectively. For a light incidence angle of  $65^\circ$  with respect to the surface normal the  $z$ -component of the light is stronger than for  $20^\circ$ . Therefore orbitals with  $a_1$  symmetry are expected to emit stronger in spectra (c) and (d) than in spectra (a) and (b). By changing the azimuth of the A-vector of the light from  $[1\bar{1}0]$  to  $[001]$  it is possible to differentiate between  $b_1$  and  $b_2$  orbitals. Orbitals with  $b_2$  symmetry should emit when the light contains a component polarized along  $[001]$  ( $y$ ) whereas orbitals with  $b_1$  symmetry may be ionized by light polarized along  $[1\bar{1}0]$  ( $x$ ). The observed intensity variations observed in Fig. 10.41 are compatible with formate ions that are standing upright on the surface with the molecular plane oriented along the  $[1\bar{1}0]$  azimuth. The same geometry has been deduced by Bradshaw and co-workers from their data (Lindner et al., 1987). This is also in agreement with the results of an X-ray absorption study by Puschmann et al.



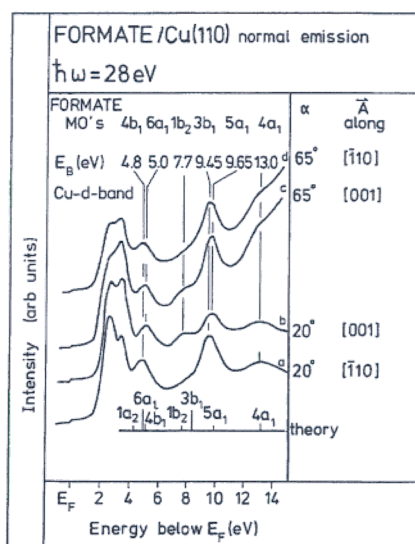


Fig. 10.41. Normal emission spectra of formate on Cu(110) taken for different polarizations of the incident light in normal emission (Hofmann and Menzel, 1987). At the bottom the assignment of the photoelectron peaks as derived from theoretical work (Peyerimhoff, 1967) is indicated.

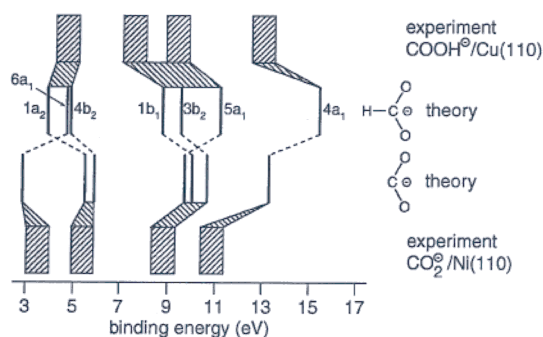


Fig. 10.42. Energy level diagram showing the correlation between the energy levels of  $\text{COOH}^-$  and  $\text{CO}_2^-$ . The theoretical and experimental data have been taken from D'Evelyn et al. (1986); Hofmann and Menzel (1987) and Bartos et al. (1987a, b); Hofmann and Menzel (1987), respectively.

(Kimura et al., 1981) and a photoelectron diffraction study by Woodruff et al. (Woodruff et al., 1988; Puschmann et al., 1985). The influence of the adsorbate/substrate interaction on the binding energies of the valence levels indicates that for formate on Cu(110) the bonding to the substrate occurs via oxygen coordination. This is compatible with the proposed geometry of the  $\text{CO}_2^-$  anion on Ni(110).

We see in Fig. 10.42 the direct comparison between the  $\text{CO}_2^-$  and  $\text{CHO}_2^-$  orbital energies (Bartos et al., 1987a, b; Freund et al., 1987; Peled and Asscher, 1987; Asscher et al., 1988; Brosseau et al., 1991; D'Evelyn et al., 1986; Walsh, 1913; Freund and Mess-

mer, 1986; Wambach et al., 1991; Hofmann and Menzel, 1987) and we may undertake a direct correlation of the observed ion states on the basis of the available molecular orbital calculations. The hydrogen-carbon bond formation leads to a stabilization of the totally symmetric orbitals with respect to all other orbitals. The effect is most pronounced for the low energy  $4a_1$  orbital. In this case the stabilization effect may clearly be deduced from the experimental data.

### 10.8. Ethylene adsorbates (Sheppard, 1988)

Rather complete studies of the electronic structure of more complex adsorbate systems, such as chemisorbed hydrocarbons are relatively rare. Very recently, Steinrück and co-workers (Weinelt et al., 1992a, b) published an interesting study of ethylene adsorption on Ni(110) where the aspect of local and global symmetry has been discussed. We want to summarize their results in the following.

Saturation coverage of Ni(110) by  $C_2H_4$  at  $T = 120$  K results in a  $c(2 \times 4)$  LEED pattern. This pattern represents a very dense layer containing two molecules per unit cell (i.e.,  $\Theta = 0.5$ ) as revealed through coverage determination with temperature programmed desorption (TPD) (Weinelt et al., 1992a).

The primary task, though, as in the case of the CO adsorbates, is the determination of the local symmetry of the molecule at the surface. This is done for a dilute ethylene layer ( $\Theta \sim \Theta_{\text{sat}}/2$ ) where lateral interactions are not important. We shall see that the local geometry prevails in the dense layer. There are indications from high resolution electron energy loss spectroscopy (HREELS) that the ethylene species is di- $\sigma$ -bonded as opposed to  $\pi$ -bonded with the C-C-axis parallel to the surface and that the site symmetry is actually lower than  $C_{2v}$  (Stroscio et al., 1984). Theoretical results, however, indicate that the adsorbate bonding is quite similar in both the di- $\sigma$ -bonded and the  $\pi$ -bonded cases, i.e.,  $\pi$ -donation from  $C_2H_4$  to the substrate is stronger as compared to  $\pi^*$ -backdonation (Hofmann et al., 1985) from the substrate towards the  $C_2H_4$  molecule.

#### 10.8.1. Symmetry considerations and ethylene-substrate interaction

Angle resolved photoemission spectra of the dilute layer are shown in Fig. 10.43 (Weinelt et al., 1992a). The photon energy of 30 eV was chosen to optimize the intensity of the adsorbate induced features. For comparison the angle integrated photoelectron spectrum of gas phase ethylene (Kimura et al., 1981) including assignment is plotted. The spectra have been aligned at the  $3a_g$  and  $1b_{3u}$  levels (gas phase nomenclature) as is frequently done in the literature (Weinelt et al., 1992a). The comparison reveals that the adsorbate spectrum is characteristic of a molecularly adsorbed species. It also shows that the  $1b_{2u}$  ion-state is shifted by 1.1 eV to higher binding energies. This is by far the largest differential shift observed in this system. The shape of the ethylene orbitals in the gas phase is plotted in Fig. 10.44 (Jorgensen and Salem, 1974). It shows that the  $1b_{2u}$  orbital is characteristic for a  $\pi$ -bond. The large shift indicates that the main interaction of the molecule with the surface takes place through this orbital.

The site symmetry and the orientation of the adsorbed ethylene molecules in the dilute layer can be derived from the polarization, polar angle and azimuthal dependences

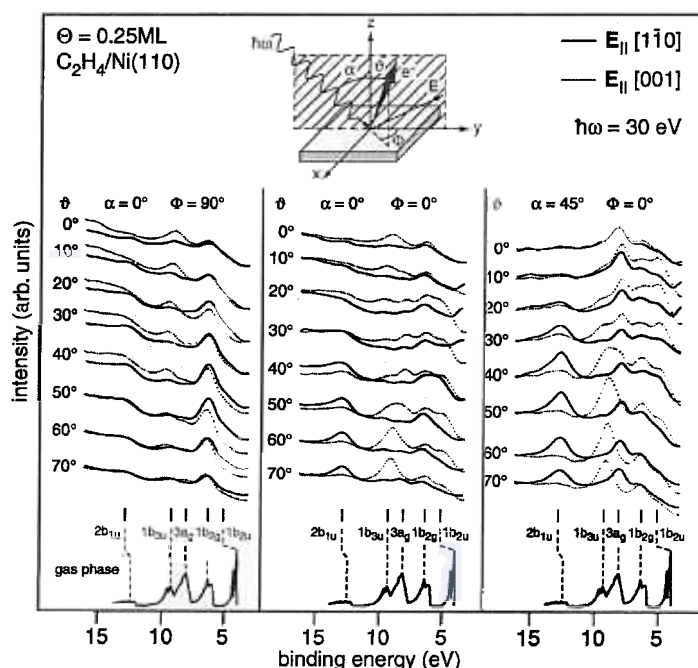


Fig. 10.43. Angle resolved electron distribution curves for a dilute  $C_2H_4$  layer on Ni(110) in comparison to the gas phase (Weinelt et al., 1992a).

of the observed ionization bands, which are shown in Fig. 10.43 and are discussed below. Figure 10.44 shows how the irreducible representations of the molecular orbitals in the isolated molecule correlate with the corresponding irreducible representations when ethylene is bound to the surface in four different point group symmetries of the hypothetical sites. The real-space geometries corresponding to the site symmetries are shown in Fig. 10.44. Due to the twofold symmetry of the Ni(110) surface there are two possibilities for a  $C_s$  site as indicated.

There is an important experimental detail in the experiments by Steinrück et al. (Weinelt et al., 1992a, b) that must be mentioned at this point. The electron analyzer allows to measure angular distributions of electrons by means of multichannel detection techniques including normal emission also at light incidence normal to the surface (Engelhardt et al., 1981a, b). At these particular experimental conditions two bands ( $3a_g$  at 8.0 eV and  $1b_{2u}$  at 5.0 eV) show no normal emission intensity for normal incidence, but rather strong normal emission for incidence at  $45^\circ$ , with detection in the plane of incidence. It is clear from Fig. 10.44 that this experimental observation is strong evidence for a basically flat lying geometry. Both orbitals  $3a_g$  and  $1b_{2u}$  belong to the totally symmetric representation in any considered point group and are only allowed in normal emission for a nonvanishing  $z$ -component of the electric field vector. Note that both orbitals show rather weak emission for normal incidence if the electrons are detected in a plane perpendicular to the incidence plane. This detection geometry is called “forbidden” geometry for diatomic adsorbates as











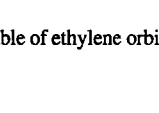
<div style="display: inline-block; transform: rotate(-45deg); transform-origin: center;">           symmetry orbitals         </div>	<div style="display: flex; justify-content: space-around; align-items: center;">      </div>				
	D <sub>2h</sub>	C <sub>2v</sub>	C <sub>2</sub>	C <sub>s</sub> (xz)	C <sub>s</sub> (yz)
	1b <sub>2u</sub>	a <sub>1</sub>	a	a'	a'
	1b <sub>2g</sub>	a <sub>2</sub>	a	a''	a''
	3a <sub>g</sub>	a <sub>1</sub>	a	a'	a'
	1b <sub>3u</sub>	b <sub>2</sub>	b	a''	a'
	2b <sub>1u</sub>	b <sub>1</sub>	b	a'	a''
	2a <sub>g</sub>	a <sub>1</sub>	a	a'	a'

Fig. 10.44. Correlation table of ethylene orbital symmetries in the gas phase with those in varying adsorbed phases on Ni(110).

discussed above. The azimuthal orientation can be extracted from the intensity variations in the 2b<sub>1u</sub> (12.7 eV) and 1b<sub>3u</sub> (9.2 eV) emission (see Fig. 10.43). These states transform according to the b<sub>1</sub> and b<sub>2</sub> representations if C<sub>2v</sub> point group symmetry is assumed. They exhibit opposite intensity variations if the plane of light incidence is changed from [001] to [1 $\bar{1}$ 0]. The b<sub>1</sub> state shows strong emission in the [001] plane and weak emission in the [1 $\bar{1}$ 0] plane, while the b<sub>2</sub> is weak along [001] and strong along [1 $\bar{1}$ 0], respectively. Figure 10.44 shows that the b<sub>2</sub> orbital has a node along the C–C axis, while the b<sub>1</sub> orbital has a node perpendicular to the C–C axis. Consequently, if the electric field vector points along the C–C axis the orbital with the node perpendicular to the C–C axis (b<sub>1</sub>) should lead to normal emission intensity, and if the electric field vector is oriented perpendicular to the C–C axis the b<sub>2</sub> orbital should yield electron ejection in normal direction from Fig. 10.43 it is therefore quite obvious that the C–C axis of the C<sub>2</sub>H<sub>4</sub> molecule is to a first approximation oriented along the [1 $\bar{1}$ 0] azimuth. However, the intensities do not completely go to zero in the appropriate directions indicating that the alignment is not perfect. In other words, the symmetry of the adsorption complex is lower than C<sub>2v</sub>. This is also in line with intensity

variations observed for the  $1b_{2g}$  (6.2 eV) ion state which belongs to the  $a_2$  representation in point group  $C_{2v}$ . In fact, a detailed analysis shows that the observed intensity of the  $a_2$  ion state in normal emission can only be explained by either a slight tilting of the C–C axis, a lower symmetry adsorption site or a twisting of the molecule. Steinrück et al. (Weinelt et al., 1992a, b) exclude the former due to the vanishing normal emission intensity of the  $3a_g(a_1)$  ion state and therefore favour a lower adsorption site, i.e., slightly displaced from a high symmetry adsorption site or twisting of the molecule as shown in Fig. 10.44.

Rösch and co-workers have analyzed the bonding via cluster calculations (Weinelt et al., 1992a, b) on the basis of the local-density functional approach. Their analysis shows that the molecule substrate interaction follows the standard description of olefin bonding towards transition metal atoms:  $\pi$ -donation to the metal and backdonation from the metal into the  $\pi^*$ -orbital of  $C_2H_4$ . However, the calculations do not allow discrimination between the two main adsorption modes,  $\pi$  or di- $\sigma$ .

#### 10.8.2. Ordered ethylene overlayers

After having discussed the local site geometry as determined via ARUPS on a dilute  $C_2H_4$  layer we come back to the study of the layer at saturation coverage. Steinrück et al. (Weinelt et al., 1992a, b) showed that for the strongly laterally interacting  $C_2H_4$  layer the local site is similar to the dilute layer so that we do not have to discuss the spectra in detail in this case.

From the variation of the binding energy with the emission angle, the two-dimensional band structure of the saturated ethylene layer can be evaluated. The two-dimensional band structure has been determined along the two high-symmetry directions of the substrate, i.e.,  $[1\bar{1}0]$  and  $[001]$ . Note that these directions are not necessarily mirror planes of the adsorbate Brillouin zone. The LEED Brillouin zone is shown in Fig. 10.45. The structure of the layer derived from this pattern is shown in the same figure. The molecules are put in the proposed asymmetric adsorption sites and are aligned along the  $[1\bar{1}0]$  direction with 5 Å separation. Molecules in neighbouring rows are shifted with respect to each other by 1.25 Å. This results in translational equivalence at every fourth row, i.e., a  $c(2 \times 4)$  structure. The ARUPS measurements combined with molecular dynamics simulations reveal that the active intermolecular  $C_2H_4$  potentials lead to a band structure which is not directly compatible with the Brillouin zone derived from the LEED pattern (Weinelt et al., 1992a, b). The plot of the data  $E_B$  vs.  $k_{||}$  is shown in Fig. 10.46. Some high symmetry points in the extended Brillouin zone scheme deduced from the LEED pattern are indicated at the top of Fig. 10.46, and it is quite obvious that the observed band dispersions do not follow the true Brillouin zone symmetry. The observed band structure may be explained if the interaction of the molecule with the substrate is neglected for all but the  $\pi$  ( $1b_{2u}$ ) ion state and the molecules are displaced with respect to each other in neighbouring rows as indicated in the middle panel of Fig. 10.47. In other words the periodic potential leading to the fourfold repeat unit is not important. The molecular dynamics simulations energetically favour this interpretation. It is known from other hydrocarbons that the intermolecular interaction is dominated by the repulsive hydrogen–hydrogen interactions which are minimized in the geometry shown in the middle panel of Fig. 10.47 with respect to the other two limiting cases (left and right panels in Fig. 10.47). Without consideration of the substrate

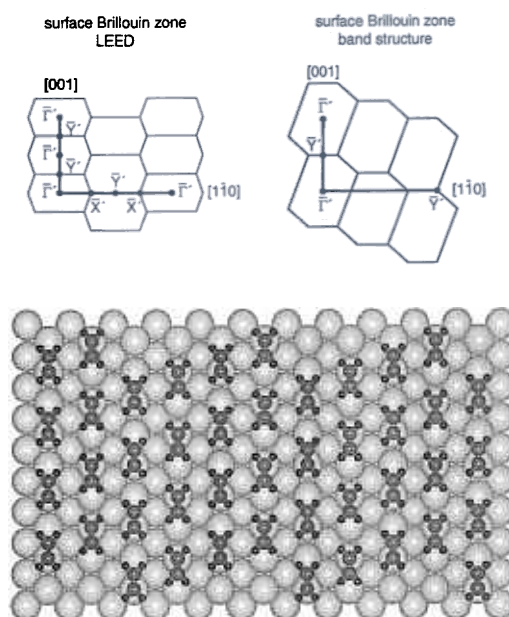


Fig. 10.45. Brillouin zones of the  $c(4 \times 2)\text{C}_2\text{H}_4/\text{Ni}(111)$  system as observed with LEED (on the left) and as determined via band structure measurements (on the right). A real space model is included (Weinelt et al., 1992a, b).

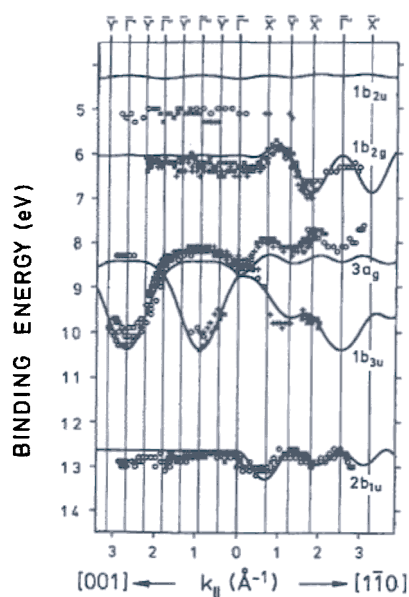


Fig. 10.46. Measured band structure for the system  $c(4 \times 2)\text{C}_2\text{H}_4/\text{Ni}(111)$ . Points of high symmetry according to the LEED Brillouin zone (top) and the band structure Brillouin zone (bottom) are indicated (Weinelt et al., 1992a, b).

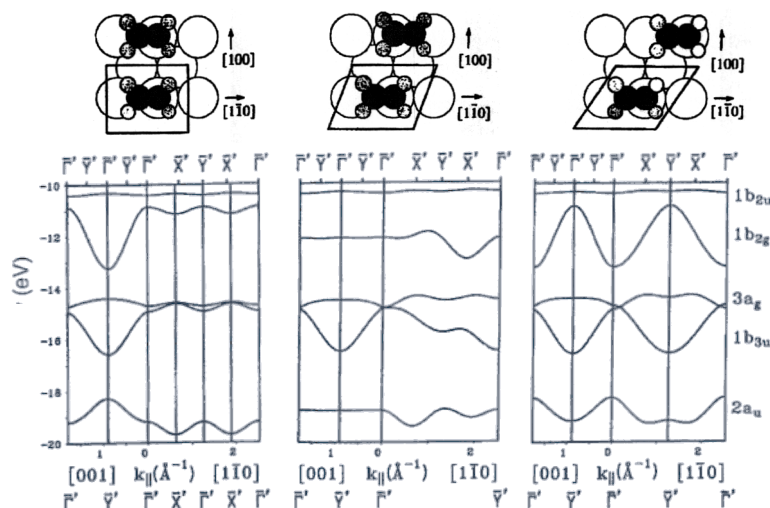


Fig. 10.47. Calculated band structures for three different lateral arrangements of  $C_2H_4$  molecules (Weinelt et al., 1992a, b).

the adsorbate unit cell only contains a single molecule. The unit cell in reciprocal space is shown in Fig. 10.45. The experimentally chosen  $[001]$  and  $[1\bar{1}0]$  directions of the substrate are included in the figure. They do not represent high symmetry directions in the adsorbate mesh, but rather the paths from  $\Gamma$  to  $Y$  along  $[1\bar{1}0]$ . The calculated band structure along these paths for the energetically favoured arrangement is depicted in Fig. 10.47 middle panel and may be directly compared with the calculated band structures for other geometries. If we now compare the calculated band structure with the measured data, as done in Fig. 10.46, we find very good agreement for four out of five ion states. The only noticeable exception is the  $b_{2u}$  ion state which couples the ethylene molecule to the substrate. It is obvious that none of the other considered geometries (left and right panels) would yield a band structure that agrees with experiment anywhere near to this one. The dispersions observed can be explained on the basis of nearest neighbour interactions. Let us consider for simplicity the  $[001]$  direction. The highest binding energy ion state has  $b_{1u}$  symmetry. The molecular wave function can be taken from Fig. 10.44. For a two-dimensional array of molecules (Fig. 10.48a) the relative phases lead to a mainly nonbonding wave function at  $\Gamma$ . If the relative phases of the molecule rows change at  $Y$ , the nonbonding character is not changed. Consequently, there is no dispersion of this orbital along the  $[001]$  direction. The two-dimensional wave function derived from the  $1b_{3u}$  orbital as shown in Fig. 10.48b is strongly antibonding at  $\Gamma$ . Upon going to the zone boundary along  $[001]$  the wave function becomes strongly bonding, therefore leading to strong downward dispersions. In the case of the  $3a_g$  derived wave function (see Fig. 10.48c), it is essentially nonbonding or weakly bonding at  $\Gamma$ . At  $Y$  it remains basically nonbonding or weakly antibonding. The  $1b_{2g}$  orbital leads to a two-dimensional wave function as depicted in Fig. 10.48d. The overall character is nonbonding at  $\Gamma$  and it remains nonbonding at  $Y$ . We do not expect any strong dispersion for this orbital. The  $b_{2u}$  orbital couples to the substrate and thus we

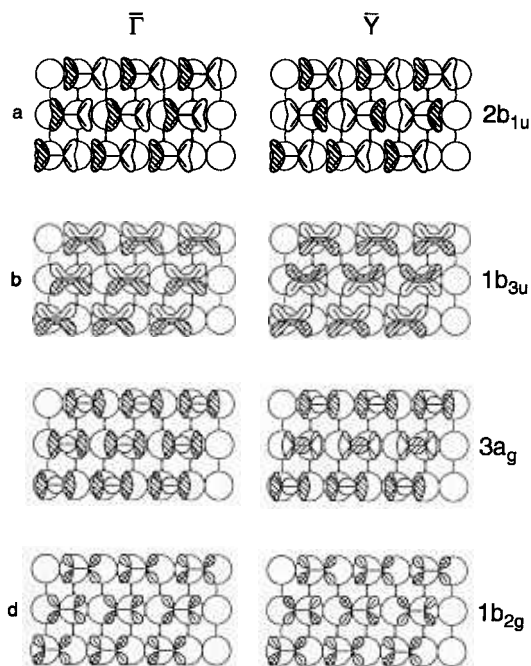


Fig. 10.48. Schematic two-dimensional wave functions for the ethylene overlayer for the center (left) and the border (right) of the Brillouin zone: (a)  $2b_{1u}$ , (b)  $1b_{3u}$ , (c)  $3a_g$ , (d)  $1b_{2g}$ .

cannot expect correspondence to the simple band structure calculation on an unsupported layer. Similar arguments hold for the other directions but they are slightly more involved because the  $[1\bar{1}0]$  direction is not a high symmetry direction within the adsorbate structure.

Summarizing this section it has been demonstrated that a close packed ethylene overlayer exhibits a pronounced band structure which is completely determined by nearest neighbour interactions. The overall structure documented in the band structure is determined via ARUPS. Calculations on a free unsupported ethylene layer completely account for the observations. It should be noted that independent of the packing of the molecules,  $C_2H_4$  occupies almost certainly a nonsymmetric surface site and interacts with the surface through its  $\pi$ -electrons. The band derived from the  $\pi$ -electron level does not follow the calculated band structure. It behaves like a localized state created via interaction with the substrate. The interaction with the substrate is documented predominantly in a more pronounced differential binding energy shift of this ion state.

### 10.9. Benzene adsorbates

Even more complex systems which nevertheless have been extensively studied during recent years are the various benzene adsorbates. Out of the many investigations performed so far (see, e.g., Table 10.2, Steinrück et al., 1989; Bertolini et al., 1977; Huber et al., 1991a, b; Ramsey et al., 1991; Jakob and Menzel, 1988; Bertel et al., 1986; Chiang et al., 1988;



Table 10.2  
Ordered benzene overlayers on metal substrates

Substrate	Structure	$\Theta$ (ML)	References
Ni(111)	$(\sqrt{7} \times \sqrt{7})R19.1^\circ$	0.143	Steinrück et al. (1989) Huber et al. (1991b)
Ni(100)	$c(4 \times 4)$	0.125	Bertolini et al. (1977)
Ni(110)	$c(4 \times 2)$	0.250	Huber et al. (1991a) Ramsey et al. (1991)
Ru(0001)	$(\sqrt{7} \times \sqrt{7})R19.1^\circ$	0.143	Jakob and Menzel (1988)
	$(2\sqrt{3} \times 2\sqrt{3})R30^\circ$	0.083	Jakob and Menzel (1988)
Rh(111)	$(2\sqrt{3} \times \sqrt{3})_{\text{rect}}$	0.166	Bertel et al. (1986) Chiang et al. (1988) Markert and Wandelt (1985) Mate et al. (1986, 1988)
	$(\sqrt{19} \times \sqrt{19})23.4^\circ$	0.159	Neuber et al. (1991) Neuber (1992)
	$(\sqrt{7} \times \sqrt{7})R19.1^\circ$	0.143	Koel et al. (1984)
	$(2\sqrt{3} \times 2\sqrt{3})R30^\circ$	0.083	Uhlenbrock (private communication)
Pd(110)	$c(4 \times 2)$	0.250	Netzer (1990)
Pd(100)	$c(4 \times 4)$	0.125	Hofmann et al. (1981)
Ag(111)	$(3 \times 3)$	0.111	Dudde et al. (1990)
Os(0001)	$(\sqrt{7} \times \sqrt{7})R19.1^\circ$	0.143	Graen et al. (1990)
	$(\sqrt{21} \times \sqrt{21})R10.9^\circ$	0.19	Neuber (private communication)
Ir(111)	$(3 \times 3)$	0.111	Mack et al. (1985) Nieuwenhuys et al. (1976)
Pt(100)	$c(4 \times 4)$	0.125	Richardson and Palmer (1982)

Markert and Wandelt, 1985; Mate et al., 1986, 1988; Neuber et al., 1991; Neuber, 1992, private communication; Koel et al., 1984; Uhlenbrock, private communication; Netzer, 1990; Hofmann et al., 1981; Dudde et al., 1990; Graen et al., 1990; Mack et al., 1985; Nieuwenhuys et al., 1976; Richardson and Palmer, 1982; Huber et al., 1991b, for a selection of structures) only rather few contain detailed band structure studies.

We shall review in the following data gained on adsorbates on (111) faces and choose as an example the Ni(111) (Steinrück et al., 1989; Huber et al., 1991a) and Os(0001) (Graen et al., 1990) surfaces. To further discuss the determination of further azimuthal ordering we turn then to the analysis on a surface with twofold symmetry, i.e., Ni(110) (Huber et al., 1991a).

#### 10.9.1. Symmetry considerations on the molecule–substrate interaction in a dilute disordered layer of $C_6H_6/Ni(111)$ (Huber et al., 1991b)

For Ni(111) Huber et al. (1991b) have determined the structure for dilute layers of  $C_6H_6$  from angle resolved photoemission. Figure 10.49 shows the comparison of the angle integrated spectrum for a disordered  $C_6H_6$  layer at  $\Theta = 0.1$  ML ( $\Theta_{\text{sat}} = 0.143$  ML) with the gas phase spectrum (Turner et al., 1970). The assignment of the observed spectral features

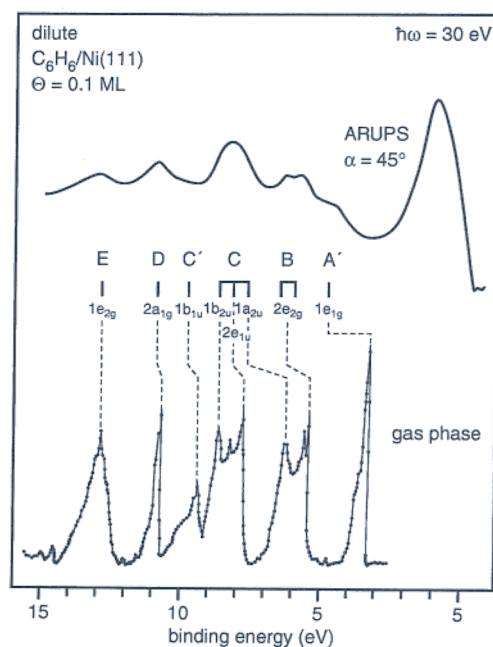


Fig. 10.49. Angle integrated photoelectron spectrum for a dilute  $C_6H_6/Ni(111)$  system (Huber et al., 1991b) in comparison with the gas phase (Turner et al., 1970).

in the adsorbate to the bands of the gas phase photoelectron spectrum has been discussed in detail by many authors (Steinrück et al., 1989; Bertolini et al., 1977; Huber et al., 1991a, b; Ramsey et al., 1991; Jakob and Menzel, 1988; Bertel et al., 1986; Chiang et al., 1988; Markert and Wandelt, 1985; Mate et al., 1986, 1988; Neuber et al., 1991; Neuber, 1992, private communication; Koel et al., 1984; Uhlenbrock, private communication, Netzer, 1990; Hofmann et al., 1981; Dudde et al., 1990; Graen et al., 1990; Mack et al., 1985; Nieuwenhuys et al., 1976; Richardson and Palmer, 1982). The shifts observed between gas and adsorbate phase strongly suggest that the interaction between molecule and substrate basically involves the  $\pi$  electrons of benzene as is well known from transition metal benzene complexes, i.e.,  $(C_6H_6)Cr$  (Cotton and Wilkinson, 1980). Of course, the symmetry of the molecule, which is  $D_{6h}$  in the gas phase is reduced upon interaction with the substrate at least to  $C_{6v}$ . If there is moderate interaction between molecule and substrate the threefold symmetry of the substrate is likely to reduce the sixfold molecular symmetry to a threefold  $C_{3v}$  symmetry. The three symmetry planes may either correspond to the  $\sigma_v$  or the  $\sigma_d$  symmetry planes of the sixfold symmetry. On a surface with twofold symmetry the point group could be further reduced to  $C_{2v}$ . Figure 10.50 contains a correlation table for the molecular orbitals symmetries of  $C_6H_6$  according to the various point groups. The + and - signs correspond to allowed and forbidden normal emission of the electrons for the two limiting light polarization directions, i.e., in the ring plane ( $x, y$ ) and perpendicular to the ring plane ( $z$ ). Due to the broad peaks in the adsorbate spectrum some ion states are su-

orbitals	$D_{6h}$	symmetry					
		$C_{6v}$	$C_{3v, \sigma v}$	$C_{3v, \sigma v}$	$C_{2v}$		
		xy z	xy z	xy z	xy z	xy	z
	$1e_{1g}(\pi)$	$e_1 + -$	$e + -$	$e + -$	$b_1 + b_2$	+	-
	$2e_{2g}(\sigma)$	$e_2 - -$	$e + -$	$e + -$	$a_1 + a_2$	-	+
	$1a_{2u}(\pi)$	$a_1 - +$	$a_1 - +$	$a_1 - +$	$a_1$	-	+
	$2e_{1u}(\sigma)$	$e_1 + -$	$e + -$	$e + -$	$b_1 + b_2$	+	-
	$1b_{2u}(\sigma)$	$b_2 - -$	$a_1 - -$	$a_1 - +$	$b_2$	+	-
	$1b_{1u}(\sigma)$	$b_1 - -$	$a_1 - +$	$a_2 - -$	$b_1$	+	-
	$2a_{1g}(\sigma)$	$a_1 - +$	$a_1 - +$	$a_1 - +$	$a_1$	-	+
	$1e_{2g}(\sigma)$	$e_2 - -$	$e + -$	$e + -$	$a_1 + a_2$	-	+

Fig. 10.50. Correlation table of the orbital symmetries of  $C_6H_6$  in the gas phase ( $D_{6h}$ ) with those in different adsorbed phases on Ni(111). The + and - signs denote whether the orbitals can be excited with light polarized along the xy or the z directions.

perimposed. The bands in the experimental spectrum are therefore labelled in alphabetical order. Figure 10.50 can be used to establish the symmetry of the adsorption site by evaluating the experimental data shown in Fig. 10.51. The spectra show negligible emission from the  $2a_{1g}$  orbital for  $\alpha = 0$ , i.e., normal incidence and normal emission, but strong emission for  $\alpha = 45^\circ$ , i.e., a non vanishing z-component of the light. Together with the fact that the  $b_{1u}$  state shows no normal emission for both light incidence angles this proves that the ring plane is oriented parallel to the surface. From the observation that the  $1b_{1u}$  state shows negligible emission at all angles whereas the  $1b_{2u}$  orbital is rather intense we conclude that the detector is placed in the  $\sigma_d$  mirror plane of the molecule, indicating that this plane acts as a mirror plane for the molecular symmetry. This is then compatible with a  $C_{3v}(\sigma_d)$  symmetry of the adsorbate complex. Since the spectra have been collected along the  $[1\bar{1}0]$  direction of the substrate, Steinrück et al. (Huber et al., 1991b) concluded that the benzene molecules are azimuthally oriented with the carbon-hydrogen bonds pointing along the  $[2\bar{1}1]$  directions of the substrate as shown in Fig. 10.52a. The alternative local structure with  $C_{3v}(\sigma_v)$  symmetry favoured by a recent cluster calculation, shown also in Fig. 10.51a is less likely but cannot completely be ruled out because measurements were only performed in one azimuth. Thus the structure marked  $C_{3v}(\sigma_d)$  depicted in Fig. 10.52a is assumed to represent the interaction of an isolated benzene molecule with a Ni(111) surface.

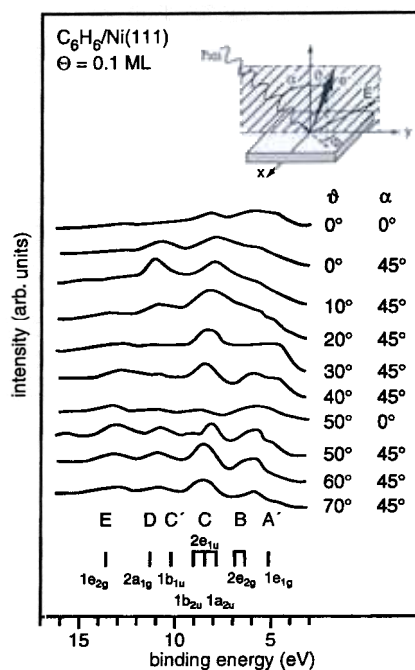


Fig. 10.51. Angle resolved electron distributions curves for a dilute  $C_6H_6$  layer on Ni(111) (Huber et al., 1991b).

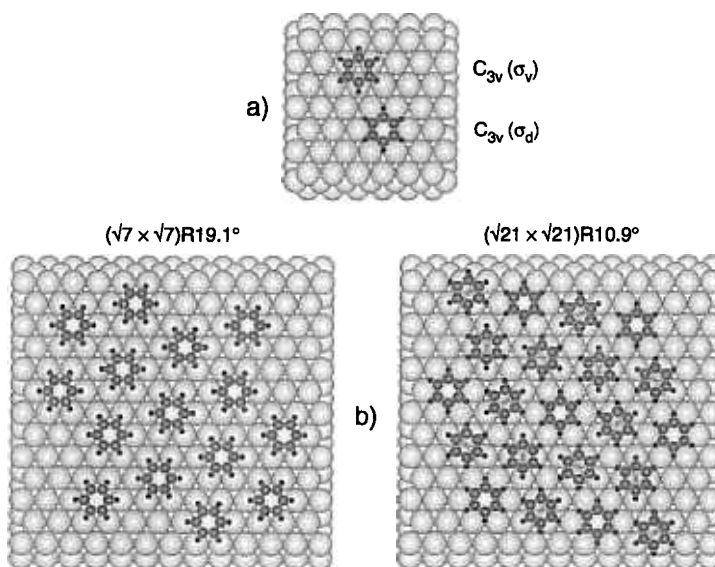


Fig. 10.52. Schematic representation of some  $C_6H_6$  structures on (111) surfaces: (a) two possible adsorption sites of isolated  $C_6H_6$  molecules; (b) left panel:  $(\sqrt{7} \times \sqrt{7})R19.1^\circ$  structure model, right panel:  $(\sqrt{21} \times \sqrt{21})R10.9^\circ$  structure model.

10.9.2. Ordered layers:  $C_6H_6/Ni(111)$  (Huber et al., 1991b) and  $C_6H_6/Os(0001)$  (Graen et al., 1990)

$C_6H_6$  on  $Ni(111)$  as well as on  $Os(0001)$  which are examples of close packed surfaces of a fcc and a hcp metal, form ordered overlayers of the type  $(\sqrt{7} \times \sqrt{7})R19.1^\circ$  and sometimes, i.e., on  $Os(0001)$ , even more close packed layers of  $(\sqrt{21} \times \sqrt{21})R10.9^\circ$  structure. Models of these structures are shown in Fig. 10.52b. The angle resolved spectra of a saturated  $(\sqrt{7} \times \sqrt{7})R19.1^\circ$   $C_6H_6$  on  $Ni(111)$  exhibit characteristic differences if compared with those of the dilute layer (Huber et al., 1991b). The spectra (not shown) indicate strong emission from the  $1b_{2u}$  ion state except at particular angles. Huber et al. (1991b) take this as indications that the detection plane is no longer the  $\sigma_d$  mirror plane of adsorbed  $C_6H_6$ . An explanation would be an azimuthal rotation of the molecule due to strong lateral interactions. Figure 10.52b shows an anticipated model of the benzene layer keeping the adsorption site determined for the dilute layer, but allowing for a rotation by  $30^\circ$ .

Experimental evidence for strong lateral interaction is gained from the observation of dispersion of some of the ion states. Intermolecular interaction between planar hydrocarbon is mainly mediated through the hydrogen–hydrogen interaction. Therefore one expects those ion states to show the strongest effect that have considerable wave function coefficients at the hydrogen positions. Figure 10.50 shows that there are several candidates. However, for a clear experimental identification of the dispersion an energetically isolated level should be used in order to avoid problems with overlapping levels. We consider the system  $(\sqrt{7} \times \sqrt{7})R19.1^\circ$   $C_6H_6$  on  $Os(0001)$  (Graen et al., 1990). In Fig. 10.53 the dispersions of the  $2a_{1g}$  level are plotted for two photon energies along the direction indicated in the inset. The two possible domains of the overlayer are indicated. There exists a common direction  $\Gamma \rightarrow A$  in both domains along which the experiments have been performed. Tight-binding calculations on an unsupported benzene layer have been performed in which the relative arrangement of the molecules within the layer has been varied in order to simulate the probable structures shown in Fig. 10.54a. Two extreme cases have been chosen, i.e., a parallel arrangement (Fig. 10.54b<sub>1</sub>), and an “interlocked” arrangement (Fig. 10.54b<sub>2</sub>).

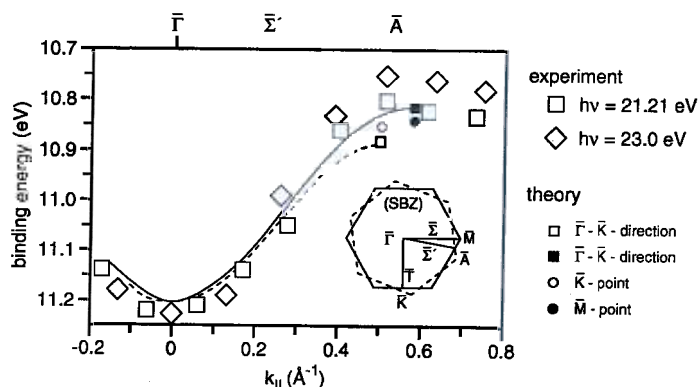


Fig. 10.53. Dispersion relation for the  $2a_{1g}$  ion state of the system  $C_6H_6(\sqrt{7} \times \sqrt{7})R19.1^\circ/Os(0001)$  (Graen et al., 1990).

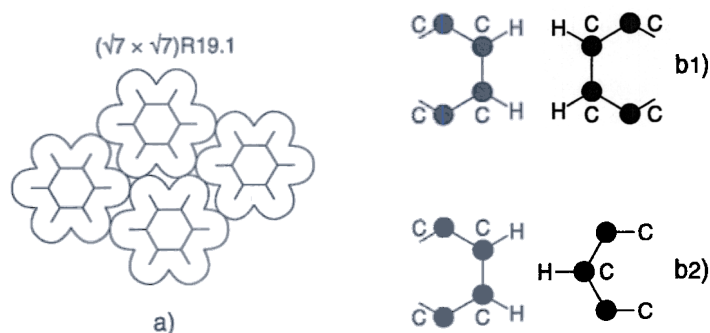


Fig. 10.54. Arrangement of the  $C_6H_6$  molecules in the  $(\sqrt{7} \times \sqrt{7})R19.1^\circ$  structure (a) schematic representation of molecules in van der Waals contact, (b<sub>1</sub>) eclipsed arrangement of two  $C_6H_6$  molecules, (b<sub>2</sub>) staggered arrangement of two  $C_6H_6$  molecules.

Figure 10.54a obviously represents an intermediate case where the repulsion between interacting molecules is minimized. The calculated dispersion curves (Graen et al., 1990) are included in Fig. 10.53. They correspond to the two azimuthal directions, i.e.,  $\Gamma \rightarrow K$  and  $\Gamma \rightarrow M$  applying intermolecular interaction parameters derived from the geometries shown in Fig. 10.54b<sub>1</sub> and Fig. 10.54b<sub>2</sub>. The energy position of the band at the M point is always higher than at the K point, independent of the absolute value of the interaction parameter. The former value can be estimated almost quantitatively via a simple procedure: we consider a parallel arrangement of  $C_6H_6$  moieties (Fig. 10.54b<sub>1</sub>). On both molecules an  $2a_1$ -orbital is placed. The overlap between the two molecules will be dominated by the overlap of the adjacent hydrogen atomic orbitals. The reason is that the overlap depends exponentially on the distance. A calculation of the interaction parameter  $\beta$  yields 0.045 eV. Since the band constructed from the  $2a_{1g}$ -levels is of  $\sigma$ -type, we expect a band dispersion from high binding energy at  $\Gamma$  to lower binding energy at the zone boundary. In the simplest version of the tight-binding theory the band dispersion of a  $\sigma$ -type band in  $\Gamma-M$  and  $\Gamma-K$  direction are given by  $9\beta$  and  $8\beta$ , respectively. This yields 0.4 eV and 0.36 eV if we use the above mentioned  $\beta$  value. Those values are very close to the dispersion plotted in Fig. 10.53 as a result of the full calculation. A similar estimate can be made for the other geometry in Fig. 10.54b<sub>2</sub>. This yields 0.36 eV and 0.32 eV, respectively. In conclusion we realize that the observed dispersion can be explained on the basis of simple considerations. Very similar results have been gained for the system  $(\sqrt{7} \times \sqrt{7})R19.1^\circ C_6H_6/Ni(111)$  and  $(\sqrt{19} \times \sqrt{19})R23.4^\circ C_6H_6/Rh(111)$ . The observed dispersions are basically the same as for the Os(0001) surface layer and have been interpreted in a similar way by Huber et al. (1991b) and Neuber (1992).

Graen and Neumann (Graen, 1991; Graen and Neumann, private commun.) have also determined the dispersion for a more densely packed layer with a  $(\sqrt{21} \times \sqrt{21})R10.9^\circ$  structure (Fig. 10.52b). Here the bandwidth increases due to the shorter nearest neighbour distance. With such data one may now establish a bandwidth vs. distance plot quite similar to the one presented for CO adsorbates (Neuber, 1992; Graen, 1991; Graen and Neumann, private communication).

A different situation is found for the adsorption of  $C_6H_6$  on Ni(110). An ordered approximate  $c(4 \times 2)$  structure forms for saturation coverage which shows pronounced intermolecular interactions. Before we discuss the band structure, the interaction of a  $C_6H_6$  molecule with the surface of twofold symmetry has to be discussed. A priori, one might expect that the molecules are no longer adsorbed in a flat geometry due to the troughs of the surface, different from other close packed surfaces. In fact, such a tilt has been proposed for  $C_6H_6$  on Pd(110) (Netzer et al., 1988) while on other surfaces such as Pt(110) ( $1 \times 2$ ) (Surman et al., 1987), Cu(110) (Bader et al., 1986) and Ag(110) (Kelemen and Fischer, 1981; Liu et al., 1990) flat lying geometries have been suggested. Huber et al. (1991a) have recently presented a very detailed study on the adsorption geometry of  $C_6H_6$  on Ni(110). The dilute layer corresponds to a coverage of  $\sim 0.1$  monolayer which is half of the saturation coverage. The layer is disordered. A series of angle resolved spectra is shown in Fig. 10.55. A parallel orientation of the molecule is concluded from the fact that the  $2a_{1g}$  state is only observed for  $\alpha = 45^\circ$  and normal emission but at no emission angle in a plane perpendicular to the plane of light incidence. This means that the mirror planes of the benzene molecule must coincide with the  $[001]$  and  $[1\bar{1}0]$  directions of the substrate which is a strong indication of an azimuthally oriented benzene molecule. The  $1a_{2u}$  ion state behaves similarly and corroborates the above conclusion. Obviously, the adsorbate complex seems to exhibit  $C_{2v}$  symmetry. Consequently, the doubly degenerate e-levels should split. By comparing the normal emission spectra for normal incidences obtained at the two different

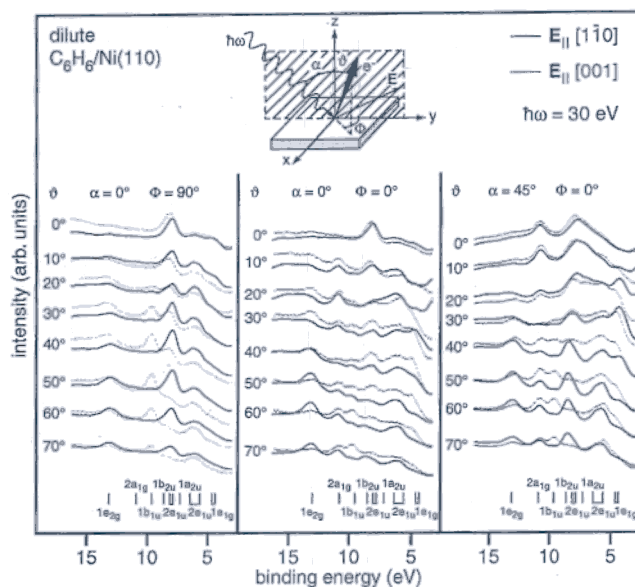


Fig. 10.55. Angle resolved electron distribution curves for a dilute  $C_6H_6/Ni(110)$  system (Huber et al., 1991a).



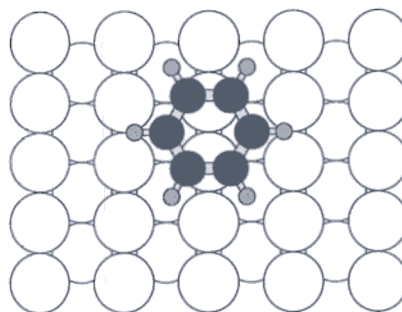


Fig. 10.56. Schematic representation of a single  $C_6H_6$  molecule interacting with a Ni(110) surface.

azimuths there are indications (e.g., at 7.8 eV and 8.1 eV) for a split  $2e_{1u}$  level. A characteristic angular intensity is exhibited by the  $1b_{1u}$  ion state. Its intensity is very weak for the polarization of the light along the  $[1\bar{1}0]$  azimuth but very strong for the light polarization parallel to  $[001]$ . Taking into account that for  $\alpha = 45^\circ$  the emission of the  $1b_{1u}$  ion state is large along  $[001]$  and strongly attenuated along  $[1\bar{1}0]$  corroborates the orientation of the molecule with its corners along the  $[001]$  direction. The behaviour of the  $1b_{2u}$  ion state is in full agreement with this conclusion. It is therefore very likely that the symmetry of the adsorbate site is  $C_{2v}$ . We should note at this point that not all levels can be simply analyzed according to the above rules. For example the  $2e_{2g}$  level shows a splitting which is due to a Jahn-Teller effect (Herzberg, 1966; Köppel et al., 1988; Eiding et al., 1991; Neumann et al., 1985), also known from the free molecule. Summarizing so far we realize that the plane of the molecule is parallel to the surface and the corners are oriented along the  $[001]$  direction. The mirror planes of the molecule coincide with the  $[1\bar{1}0]$  and  $[001]$  directions of the substrate and thus the symmetry of the adsorption complex is  $C_{2v}$ . This is depicted in Fig. 10.56.

#### 10.9.4. Ordered overlayer: $C_6H_6/Ni(110)$ (Huber et al., 1991a)

The saturated layer exhibits a coverage of  $\Theta \sim 0.25$  ML and a  $c(4 \times 2)$  LEED pattern. A detailed analysis of the spectra (Huber et al., 1991a) finally leads to the conclusion that the symmetry of the adsorption complex is  $C_1$ , and that this symmetry is achieved by a molecule oriented parallel to the surface, azimuthally rotated with respect to the  $[1\bar{1}0]$  direction and an adsorption site slightly asymmetric. As mentioned above, the  $2a_{1g}$  ion state exhibits significant dispersions. The band structure has been determined along the two high symmetry directions of the substrate Brillouin zone and is plotted in Fig. 10.57. Data have been obtained using various photon energies. The fact that these data coincide shows that the dispersion is caused by an electronic state with periodicity in two dimensions. The magnitude of the dispersion is 0.8 eV and thus considerably larger as compared with, e.g., the  $(\sqrt{7} \times \sqrt{7})R19.1^\circ$  structure on the close packed surfaces. We shall come back to this point later. Real space models for the approximate  $c(4 \times 2)$  layer are shown in Fig. 10.58. Figure 10.58a shows the situation if the molecules were not rotated with respect to the geometry in the dilute layer. Obviously, the van der Waals areas overlap strongly indica-



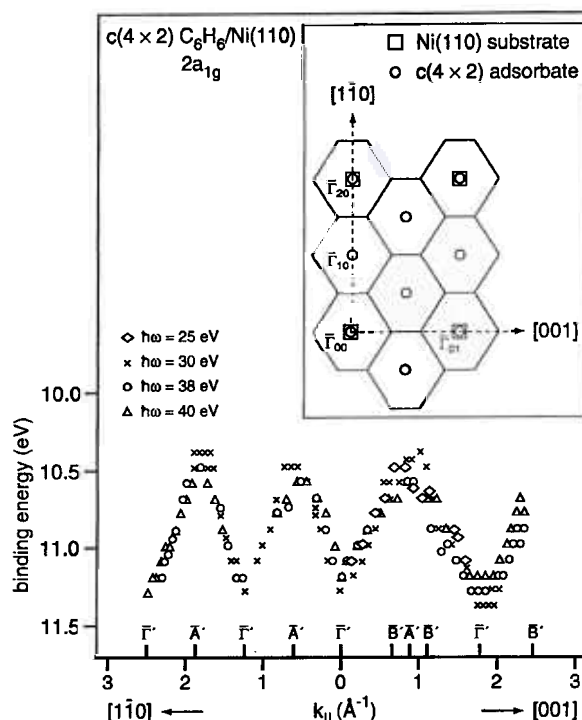


Fig. 10.57. Measured dispersion for a  $c(4 \times 2)$   $\text{C}_6\text{H}_6/\text{Ni}(110)$  system along two directions in  $k$ -space as indicated in the inset (Huber et al., 1991a).

tive of strong steric repulsion. While the geometry in Fig. 10.58b is sterically favourable, the molecule wants to assume the local geometry as in Fig. 10.58a. The arrangement in Fig. 10.58c is therefore a compromise with reduced steric repulsion and a geometry reasonably close to the local geometry. Such an arrangement has also been favored via a force field calculation by Fox and Rösch (1991).

As mentioned above, the dispersion in the present system is by a factor of two larger as compared to  $\text{C}_6\text{H}_6$  on  $\text{Ni}(111)$  (Richardson and Palmer, 1982) and  $\text{Os}(0001)$  (Graen et al., 1990). This must result from the significantly closer packing of the molecules. For  $\text{C}_6\text{H}_6$  on  $\text{Ni}(110)$  the coverage of  $\Theta = 0.25$  ML corresponds to a unit cell area of  $35.2 \text{ \AA}^2$  with a nearest neighbour distance of  $6.11 \text{ \AA}$ . This should be compared with a unit cell area of  $37.6 \text{ \AA}^2$  for the  $(\sqrt{7} \times \sqrt{7})\text{R}19.1^\circ$  structure and a coverage of  $\Theta = 0.143$  ML for  $\text{Ni}(111)$ . The 6–7% denser packing in the layer obviously has a strong nonlinear response. This is due to the fact that the intermolecular overlaps scale exponentially with distance and in addition the local arrangement is such that the repulsive interaction between the hydrogen atoms is rather large. This effect has been discussed above for the  $(\sqrt{7} \times \sqrt{7})\text{R}19.1^\circ$  structure. Clearly, the interaction energy of a single  $\text{C}_6\text{H}_6$  molecule with the metal surface must be rather strong to tolerate the considerable intermolecular repulsions in the layer which in turn leads to the pronounced band structure effects in this system.

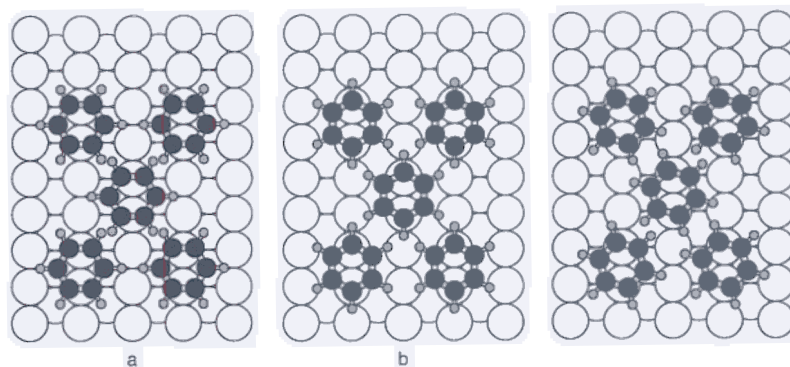


Fig. 10.58. Schematic representations of the relative arrangements in a  $c(4 \times 2)$   $C_6H_6/Ni(110)$  layer: (a) assuming the same site as in the dilute layer, (b) rotation by  $30^\circ$  with respect to the orientation in the dilute layer, (c) arrangement intermediate between (a) and (b).

### 10.10. Co-adsorbates

The adsorption of atomic hydrogen induces marked changes in the electronic structure of co-adsorbed CO on Ni(100), as was recently shown with ARUPS by Bradshaw and his group (Klauser et al., 1987; Hayden et al., 1987; Kulkarni et al., 1991). This is shown in Fig. 10.59 where spectra of a pure CO (a), a H+CO co-adsorbate, with both gases exposed to saturation coverage (b), and a H+CO co-adsorbate, the so-called  $\Sigma$ -state (c), where the hydrogen coverage is lower than in case (b) are presented. The spectra are taken with polarized synchrotron radiation at non-normal emission and a light incidence angle of  $45^\circ$  with respect to the surface normal. In spectra (a) and (b) we find the normal behaviour documented in Fig. 10.21. This is typical for strongly chemisorbed CO molecules oriented perpendicular to the surface plane. In spectrum (c), however, there are indications of weak satellite structure on the high binding energy side of the  $4\sigma$  ionization. This is in line with the finding that the adsorption energy (Goodman et al., 1980) of the  $\Sigma$ -state of CO+H/Ni(100) is considerably weaker as compared to CO/Ni(100), and is similar to CO/Cu(100) (Allyn et al., 1977a), where we expect intense satellite structure similar to CO/Cu(111) (Fig. 10.21) (Freund et al., 1983) discussed above. The orientation of the CO axis in the  $\Sigma$ -state has been shown to be perpendicular to the surface plane.

CO-alkali-co-adsorbates (Bonzel, 1988) are the most frequently tackled co-adsorbate systems with ARUPS. Several different metal surfaces have been studied (Bonzel, 1988). The most complete sets of ARUP-spectra exist for Ru(001) and Cu(100) surfaces (Eberhardt et al., 1985; Heskett and Plummer, 1986; Heskett et al., 1985a, 1986; Weimer and Umbach, 1984; Weimer et al., 1985; Wurth et al., 1986). Some important conclusions have been drawn from these studies which were partially in contrast to existing models of CO-alkali interaction at the time (Goodman et al., 1980). As monitored by the angular distribution pattern and the peaking of the shape-resonance the CO orientation with respect to the surface normal does not change upon alkali co-adsorption independent of alkali-coverage, except for a thick alkali film (Eberhardt et al., 1985; Heskett and Plummer, 1986; Heskett et al., 1985a, 1986; Weimer and Umbach, 1984; Weimer et al., 1985; Wurth et al., 1986).

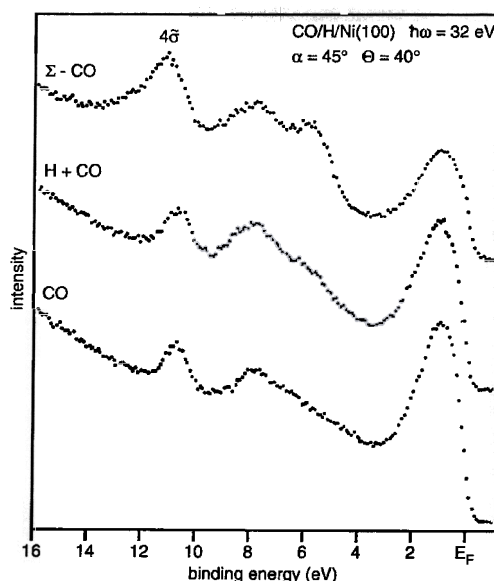


Fig. 10.59. Typical photoemission spectra for the CO/H/Ni(100) system at high emission angle showing the increase in intensity in the satellite region of the  $4\sigma$  feature (Klauser et al., 1987; Hayden et al., 1987; Kulkarni et al., 1991).

In the case of the alkali-CO-co-adsorbates on Cu surfaces (Heskett and Plummer, 1986), interesting variations in the shake up structure have been observed by Heskett and Plummer (1986) as shown in Fig. 10.60, where both the pure CO and the co-adsorbate spectra are presented for comparison. As outlined above, the decrease of the satellite intensity can be a sign of stronger or weaker metal-CO coupling. Since, however, there are still only two CO bands we must conclude that the metal-CO-bond strength actually increases. In addition to this variation of the CO-metal bond strength direct CO-alkali short range interactions involving the alkali-s- and the CO- $1\pi$ -orbitals have been postulated (Fox and Rösch, 1991). Figure 10.61 shows two sets of spectra, one for the pure CO adsorbate, equivalent to Fig. 10.21, and another one for the alkali-co-adsorbate. The spectra in the so-called "allowed" geometry are fairly similar, but in the "forbidden" geometry they are substantially different. The  $1\pi$  peaks in spectra (b) and (c) are located at different energies and the  $4\sigma$  peak for CO/K has more residual intensity than expected for an unperturbed, perpendicularly adsorbed CO molecule. The shift of the  $1\pi$  level in the CO/K-system to lower binding energy is similar to that observed on Pt(111) (Kiskinova et al., 1983) or on Fe(110) (Brodén et al., 1979). The fact that  $\sigma$  states are visible in the "forbidden" geometry may be caused by a slight tilting of the CO molecule or be due to the immediate vicinity of the K species, such that the symmetry of the coadsorbed CO molecule is broken. The spectra of the K/CO system are interestingly similar to those of systems like CO/Fe(111) (Freund et al., 1987). This may mean that in the latter case similar interactions, i.e., between the CO  $1\pi$  and the metal surface are active. Very often alkali co-adsorption leads to stronger molecule-surface interactions (Bonzel, 1988), but there are cases where the

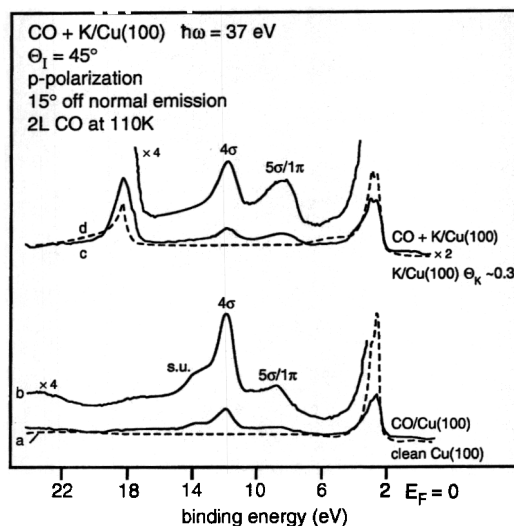


Fig. 10.60. Photoelectron spectra for CO/Cu(100) ( $\Theta_{CO} = 0.5$ ) and CO+K/Cu(100) ( $\Theta_K = 0.3$ ,  $\Theta_{CO} = 0.3$ ) in comparison. The spectra of the CO free system are shown as broken lines (Heskett and Plummer, 1986).

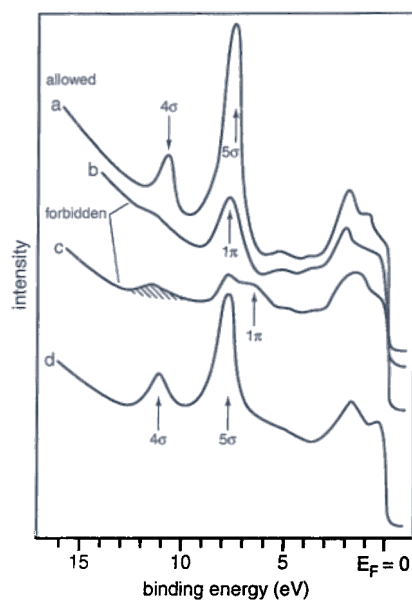


Fig. 10.61. Photoelectron spectra in "allowed" and "forbidden" geometry for CO/Ru(001) (c and d) and CO+K/Ru(001) ( $\Theta_K = 0.33$ ) (a and b) (Eberhardt et al., 1985).

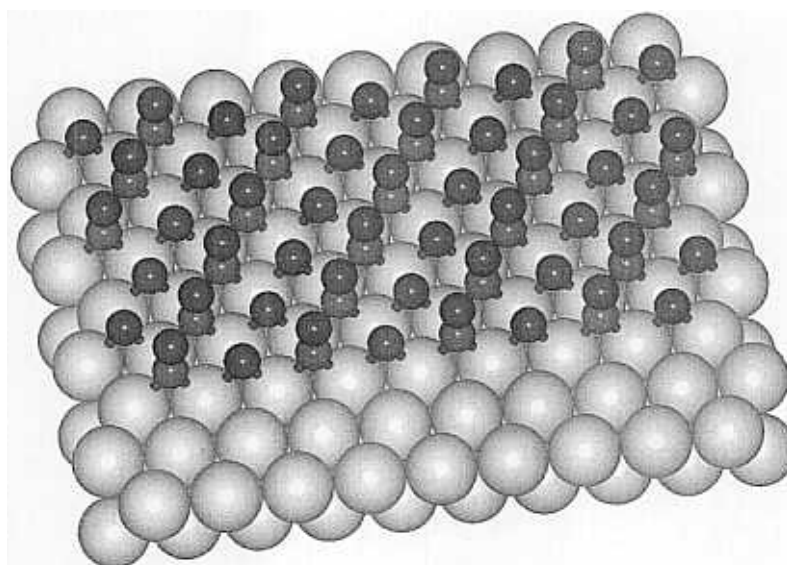


Fig. 10.62. Schematic representation of the structure of the  $(2 \times 1)\text{CO}+\text{O}/\text{Pd}(111)$  coadsorption system.

opposite effect is observed. For example, small amounts of alkali precoverages lead to a very strong repulsive interactions with  $\text{N}_2$  and attenuates  $\text{N}_2$  adsorption by a factor of 4 while the electronic structure of the adsorbed  $\text{N}_2$  appears to be the same as without alkali precoverage (Kiskinova et al., 1983). ARUPS was used to prove this (DePaola et al., 1987), and it has been interpreted as an indication for long range alkali- $\text{N}_2$  repulsion. Tentatively, a lack of d- $\pi$ -backdonation in the case of  $\text{N}_2$ -transition metal bonding has been argued to be the reason for this behaviour (DePaola et al., 1987).

Many other alkali co-adsorbates have been studied using photoelectron spectroscopy (Bonzel, 1988). A use of angular resolution, on the other hand, has only been reported in a few cases. An ordered CO/O co-adsorbate on Pd(111) has been studied using ARUPS (Odörfer et al., 1988). Figure 10.62 shows a schematic picture of the structure proposed to explain the observed  $(2 \times 1)$  LEED pattern. Early angle integrated photoemission results (Conrad et al., 1978) were basically reproduced. The co-adsorption of oxygen shifts the positions of the  $4\sigma$  and  $5\sigma/1\pi$  bands to higher binding energies. This has been taken as evidence for a strong oxygen CO interaction. The  $4\sigma$  dispersion is, however, basically caused by the strong lateral interaction along the CO rows. The ARUPS study shows that the  $4\sigma$  dispersion, as presented in Fig. 10.28 is in line with those of pure CO adsorbates. Therefore, if there is any distortion of the wave function then it is smaller than in the case of K/CO adsorbates. Further comparison with other pure CO adsorbates on Pd(111) revealed that the observed chemical shift of the CO peaks can be explained exclusively via CO-CO interaction. Therefore, the reason for the high tendency of the CO+O/Pd(111) system to form  $\text{CO}_2$  well below room temperature (Conrad et al., 1978) must be due to CO-CO and O-O repulsive interactions rather than strong attractive CO-O interactions within the adsorbate.

### Acknowledgements

We thank the Deutsche Forschungsgemeinschaft, the Bundesministerium für Forschung und Technologie, the Ministerium für Wissenschaften und Forschung des Landes Nordrhein-Westfalen and the Fonds der chemischen Industrie for support. Many coworkers have contributed over the years. Their names are mentioned in the references. We would like to thank Heiko Hamann for a critical reading of the manuscript.

### References

- Allyn, C.L., 1978, Thesis, University of Pennsylvania.
- Allyn, C.L., T. Gustafsson and E.W. Plummer, 1977a, *Chem. Phys. Lett.* **47**, 127.
- Allyn, C.L., T. Gustafsson and E.W. Plummer, 1977b, *Solid State Commun.* **24**, 531.
- Anderson, R.W., 1961, *Phys. Rev.* **124**, 41.
- Apai, G., R.S. Wehner, R.W. Williams, J. Stöhr and D.A. Shirley, 1976, *Phys. Rev. Lett.* **37**, 1497.
- Asscher, M., C.T. Kao and G. Somorjai, 1988, *J. Phys. Chem.* **92**, 2711.
- Bader, M., J. Haase, K.-H. Frank, C. Ocal and A. Puschmann, 1986, *J. Phys. (Paris) Coll.* **C8**, 491.
- Bader, M., J. Haase, A. Puschmann and C. Ocal, 1987, *Phys. Rev. Lett.* **59**, 2435.
- Bagus, P.S., K. Hermann and C.W. Bauschlieher, Jr., 1984, *J. Chem. Phys.* **80**, 4378; 1984, *J. Chem. Phys.* **81**, 1966.
- Bartos, B., H.-J. Freund, H. Kuhlenbeck and M. Neumann, 1987a, *Kinetics of Interface Reactions*, eds. M. Grunze and H.-J. Kreuzer, Springer Series in Surface Science, Vol. 8. Springer-Verlag, Berlin, p. 164.
- Bartos, B., H.-J. Freund, H. Kuhlenbeck, M. Neumann, H. Lindner and K. Müller, 1987b, *Surf. Sci.* **179**, 59.
- Batra, I.P., K. Hermann, A.M. Bradshaw and K. Horn, 1979, *Phys. Rev. B* **20**, 801.
- Bertel, E., G. Rosina and F.P. Netzer, 1986, *Surf. Sci.* **172**, L515.
- Bertolini, J.C., G. Dalmei-Imelik and J. Rousseau, 1977, *Surf. Sci.* **67**, 478.
- Bertolo, M., W. Hansen and K. Jacobi, 1991, *Phys. Rev. Lett.* **67**, 1898.
- Björneholm, O., 1992, Ph.D. Thesis, Uppsala University.
- Blyholder, G., 1964, *J. Phys. Chem.* **68**, 2792;
- Blyholder, G., 1974, *J. Vac. Sci. Technol.* **11**, 865.
- Bonzel, H.P., private communication.
- Bonzel, H.P., 1988, *Surf. Sci. Rep.* **8**, 43.
- Bonzel, H.P., A.M. Bradshaw and G. Ertl (eds.), 1989, *Physics and Chemistry of Alkali Metal Adsorption*. Elsevier, Amsterdam.
- Borstel, G., M. Neumann, G. Seitz and W. Braun, 1980, in: *Proc. 4th Intern. Conf. Solid Surf.*, Vol. 1, p. 357.
- Borstel, G., M. Neumann and M. Wöhlecke, 1981, *Phys. Rev. B* **23**, 3121.
- Boszo, T., I. Arias, T.E. Yates, R.M. Martin and H. Metiu, 1983, *Chem. Phys. Lett.* **94**, 243.
- Braun, W., G. Meyer-Ehmsen, M. Neumann and E. Schwarz, 1979, *Surf. Sci.* **89**, 354.
- Breitschaffer, M.J., E. Umbach and D. Menzel, 1986, *Surf. Sci.* **178**, 725.
- Brodén, G., G. Gaffner and H.P. Bonzel, 1979, *Surf. Sci.* **84**, 295.
- Brosseau, R., T.H. Ellis and H. Wang, 1991, *Chem. Phys. Lett.* **177**, 118.
- Brundle, C.R. and J.Ch. Broughton, 1990, in: *The Chemical Physics of Solid Surfaces and Heterogeneous Catalysis*, Vol. 3, eds. D.A. King and D.P. Woodruff. Elsevier, Amsterdam, p. 131.
- Burchhardt, J., M.M. Nielsen, D.L. Adams, E. Lundgren, J.N. Andersen, C. Stampfl, M. Scheffler, A. Schmalz, S. Aminpirooz and J. Haase, 1995, *Phys. Rev. Lett.* **74**, 1617.
- Cederbaum, L.S. and W. Domcke, 1977, *Adv. Chem. Phys.* **36**, 205.
- Chatt, J. and C.A. Duncauson, 1953, *J. Chem. Soc.* **3**, 2939.
- Chiang, S., R.J. Wilson, C.M. Mate and H. Ohtani, 1988, *J. Microsc.* **152**, 567.
- Chiang, T.C., G. Kaindl and D.E. Eastman, 1980, *Solid State Commun.* **36**, 25.
- Christmann, K., 1988, *Surf. Sci. Rep.* **9**, 1.
- Christmann, K., O. Schober and G. Ertl, 1974, *J. Chem. Phys.* **60**, 4719.

- Chubb, S.R., P.M. Marcus, K. Heinz and K. Müller, 1990, *Phys. Rev. B* **41**, 5417.
- Conrad, H., G. Ertl, J. Koch and E.E. Latta, 1974, *Surf. Sci.* **43**, 462.
- Conrad, H., G. Ertl and J. Küppers, 1978, *Surf. Sci.* **76**, 323.
- Cotton, F.A. and G. Wilkinson, 1980, *Advanced Inorganic Chemistry*, 4th edn. Wiley, New York.
- Coulman, D.J., J. Winterlin, G. Ertl and R.J. Behm, 1990, *Phys. Rev. Lett.* **64**, 1761.
- Courths, R., private communication.
- Courths, R., B. Cord, H. Wern and H. Saalfeld, 1986, *BESSY Annual Report*, p. 203.
- Courths, R., B. Cord, H. Wern, H. Saalfeld and S. Hüfner, 1987, *Solid State Commun.* **63**, 619.
- Davenport, J.W., 1976, Thesis, University of Pennsylvania; Davenport, J.W., 1976, *Phys. Rev. Lett.* **36**, 945.
- Demuth, I.E., D.W. Jepsen and P.M. Marcus, 1973, *Phys. Rev. Lett.* **31**, 540.
- DePaola, R.A., F.M. Hoffmann, D. Heskett and E.W. Plummer, 1987, *Phys. Rev. B* **35**, 4236.
- D'Evelyn, M.P., A.V. Hamza, G.E. Gidowski and R.J. Madix, 1986, *Surf. Sci.* **167**, 451.
- Dewar, M.J.S., 1951, *Bull. Soc. Chem. Fr.* **18**, C71.
- Didio, R.A., D.M. Zehner and E.W. Plummer, 1984, *J. Vac. Sci. Technol. A* **2**, 852.
- Diehl, R.D. and S.C. Fain, 1983, *Surf. Sci.* **125**, 116.
- Dowben, P.A., Y. Sakisaka and T.N. Rhodin, 1984, *Surf. Sci.* **147**, 89.
- Dudde, R., K.H. Frank and E.E. Koch, 1990, *Surf. Sci.* **225**, 267.
- Duke, C.B., 1978, *Surf. Sci.* **70**, 674.
- Duke, C.B., W.R. Salaneck, F.-J. Fabisch, J.J. Ritsko, H.R. Thomas and A. Paton, 1978, *Phys. Rev. B* **18**, 5717.
- Eberhardt, W. and H.-J. Freund, 1983, *J. Chem. Phys.* **78**, 700.
- Eberhardt, W., F. Greuter and E.W. Plummer, 1981, *Phys. Rev. Lett.* **46**, 1085.
- Eberhardt, W., F.M. Hoffmann, R. DePaola, D. Heskett, I. Strathy, E.W. Plummer and H.R. Moser, 1985, *Phys. Rev. Lett.* **54**, 1856.
- Eberhardt, W., S.G. Lonie and E.W. Plummer, 1983, *Phys. Rev. B* **28**, 465.
- Eberhardt, W. and E.W. Plummer, 1983, *Phys. Rev. B* **28**, 3605.
- Eiding, J., W. Domcke, W. Huber and H.-P. Steinrück, 1991, *Chem. Phys. Lett.* **180**, 133.
- Einstein, T.L. and J.R. Schrieffer, 1973, *Phys. Rev. B* **7**, 3629.
- Engelhardt, H.A., W. Bäck, D. Menzel and H. Liebl, 1981a, *Rev. Sci. Instr.* **52**, 835.
- Engelhardt, H.A., A. Zartner and D. Menzel, 1981b, *Rev. Sci. Instr.* **52**, 1161.
- Ertl, G., 1982, *Ber. Bunsenges. Phys. Chem.* **86**, 425.
- Ertl, G., 1983, *J. Vac. Sci. Technol. A* **1**, 1247.
- Ertl, G. and J. Küppers, 1985, *Low Energy Electrons and Surface Chemistry*. Verlag Chemie, Weinheim.
- Fink, J., 1992, *Transmission Electron Energy Loss Spectroscopy*, in: *Unoccupied Electronic States*, Vol. 69, Topics in Applied Physics, eds. J.C. Fuggle and J.E. Inglesfield. Springer-Verlag, Berlin, p. 203 and references therein.
- Fox, T. and N. Rösch, 1991, *Surf. Sci.* **256**, 159.
- Freund, H.-J., B. Bartos, R.P. Messmer, M. Grunze, H. Kühlenbeck and M. Neumann, 1987, *Surf. Sci.* **185**, 187.
- Freund, H.-J., H. Behner, B. Bartos, G. Wedler, H. Kühlenbeck and M. Neumann, 1987, *Surf. Sci.* **180**, 550.
- Freund, H.-J., W. Eberhardt, D. Heskett and E.W. Plummer, 1983, *Phys. Rev. Lett.* **50**, 768.
- Freund, H.-J. and R.P. Messmer, 1986, *Surf. Sci.* **172**, 1.
- Freund, H.-J., R.P. Messmer, C.M. Kao and E.W. Plummer, 1985, *Phys. Rev. B* **31**, 4848.
- Freund, H.-J. and M. Neumann, 1988, *Appl. Phys. A* **47**, 3.
- Freund, H.-J. and M. Neumann, 1992, in: *Angle Resolved Photoemission*, ed. S.D. Kevan, *Studies in Surface Science and Catalysis*, Vol. 74. Elsevier, p. 319.
- Freund, H.-J. and E.W. Plummer, 1981, *Phys. Rev. B* **23**, 4859.
- Gadzuk, J.W., S. Holloway, K. Horn and C. Mariani, 1982, *Phys. Rev. Lett.* **48**, 1288.
- Geisler, H., J. Wambach, H. Kühlenbeck, H.-J. Freund, M. Neuber and M. Neumann, 1996, *J. Electron Spectrosc. Relat. Phenom.* **77**, 33.
- Goldmann, A., 1992, in: *Angle Resolved Photoemission*, ed. S.D. Kevan, *Studies in Surface Science and Catalysis*, Vol. 74. Elsevier, p. 291.
- Goodman, D.W., J.T. Yates and T.E. Madey, 1980, *Surf. Sci.* **93**, L135.
- Graen, H.H., 1991, Thesis, Universität Osnabrück.
- Graen, H.H., M. Neuber, M. Neumann, G. Odörfer and H.-J. Freund, 1990, *Europhys. Lett.* **12**, 173.



- Graen, H.H. and M. Neumann, private communication.
- Greuter, F., D. Heskett, E.W. Plummer and H.-J. Freund, 1983, *Phys. Rev. B* **27**, 7117.
- Grimley, T.B., 1960, *Adv. Catal.* **12**, 1.
- Grimley, T.B., 1967, *Proc. Phys. Soc.* **90**, 751; **92**, 776.
- Grimley, T.B., 1971, *Ber. Bunsenges. Phys. Chem.* **75**, 1003.
- Grunze, M., M. Golze, W. Hirschwald, H.-J. Freund, H. Pulm, U. Seip, N.C. Tsai, G. Ertl and F. Küppers, 1984, *Phys. Rev. Lett.* **53**, 850.
- Guerney, R.W., 1935, *Phys. Rev.* **47**, 479.
- Gumhalter, B., K. Wandelt and Ph. Avouris, 1988, *Phys. Rev. B* **37**, 8048.
- Gustafsson, T., 1980, *Surf. Sci.* **94**, 593.
- Höfer, U., M.J. Breitschäfer and E. Umbach, 1990, *Phys. Rev. Lett.* **64**, 3050.
- Hayden, B.E., R. Klauser and A.M. Bradshaw, 1987, *Surf. Sci.* **183**, L279.
- Harris, J. and S. Andersson, 1985, *Phys. Rev. Lett.* **55**, 1383.
- Hedin, L., 1979, *Phys. Sci.* **21**, 477.
- Henzler, M. and W. Göpel, 1991, *Oberflächenphysik des Festkörpers* Teubner Studienbücher, Stuttgart.
- Hermann, K., P.S. Bagus, C.R. Brundle and D. Menzel, 1981, *Phys. Rev. B* **24**, 7025.
- Hermanson, J., 1977, *Solid State Commun.* **22**, 9.
- Herzberg, G., 1966, *Molecular Spectra and Molecular Structure*, Vol. 3, *Electronic Spectra and Electronic Structure of Polyatomic Molecules*. Van Nostrand-Reinhold, New York.
- Heskett, D., private communication.
- Heskett, D. and E.W. Plummer, 1986, *Phys. Rev. B* **33**, 2322.
- Heskett, D., E.W. Plummer, R.A. DePaola and W. Eberhardt, 1986, *Phys. Rev. B* **33**, 5171.
- Heskett, D., E.W. Plummer, R.A. DePaola, W. Eberhardt and F.M. Hoffmann, 1985a, *Surf. Sci.* **164**, 490.
- Heskett, D., I. Strathy, E.W. Plummer and R.A. DePaola, 1985b, *Phys. Rev. B* **32**, 6222.
- Hjelmberg, H., 1979, *Surf. Sci.* **81**, 539.
- Hofmann, P., S.R. Bare and D.A. King, 1982, *Surf. Sci.* **117**, 245.
- Hofmann, P., J. Gossler, A. Zartner, M. Glanz and D. Menzel, 1985, *Surf. Sci.* **161**, 303.
- Hofmann, P., K. Horn and A.M. Bradshaw, 1981, *Surf. Sci.* **105**, L260.
- Hofmann, P. and D. Menzel, 1987, *Surf. Sci.* **191**, 353.
- Horn, K., A.M. Bradshaw, K. Hermann and I.P. Batra, 1979, *Solid State Commun.* **31**, 257.
- Horn, K., A.M. Bradshaw and K. Jacobi, 1978a, *Surf. Sci.* **72**, 719.
- Horn, K., J.N. Di Nardo, W. Eberhardt, H.-J. Freund and E.W. Plummer, 1982, *Surf. Sci.* **118**, 465.
- Horn, K., A. Hohlfeld, J. Somers, Th. Lindner, P. Holling and A.M. Bradshaw, 1988, *Phys. Rev. Lett.* **61**, 2488.
- Horn, K., M. Scheffler and A.M. Bradshaw, 1978b, *Phys. Rev. Lett.* **41**, 822.
- Huber, W., M. Weinelt, P. Zebisch and H.-P. Steinrück, 1991a, *Surf. Sci.* **253**, 72.
- Huber, W., P. Zebisch, T. Bornemann and H.-P. Steinrück, 1991b, *Surf. Sci.* **258**, 16.
- Hund, F., 1936, *Z. Phys.* **99**, 119.
- Ishida, H., 1988, *Phys. Rev. B* **38**, 8006.
- Ishida, H., 1990, *Phys. Rev. B* **42**, 10899.
- Jacob, W., V. Dose and A. Goldmann, 1986, *Appl. Phys. A* **41**, 145.
- Jakob, P. and D. Menzel, 1988, *Surf. Sci.* **201**, 503.
- Jensen, E.S. and T.N. Rhodin, 1983, *Phys. Rev. B* **27**, 3338.
- Jones, H., 1975, *The Theory of Brillouin Zones and Electronic States in Crystals*. North-Holland, Amsterdam.
- Jones, T.S. and N.V. Richardson, 1989, *Surf. Sci.* **211/212**, 377.
- Jones, T.S., N.V. Richardson and A.W. Joshi, 1988, *Surf. Sci.* **207**, 2948.
- Jorgensen, W.L. and L. Salem, 1974, *Orbitale Organischer Moleküle*. Verlag Chemie, Weinheim.
- Kao, C.M. and R.P. Messmer, 1985, *Phys. Rev. B* **31**, 4835.
- Kelemen, S.R. and T.E. Fischer, 1981, *Surf. Sci.* **102**, 45.
- Kessler, J. and F. Thieme, 1977, *Surf. Sci.* **67**, 405.
- Kevan, S.D. (ed.), 1992, *Angle Resolved Photoemission: Theory and Current Applications*, Vol. 74, *Studies in Surface Science and Catalysis*. Elsevier, Amsterdam (and references therein).
- Kimura, K., S. Katsumata, Y. Achiba, T. Yamakaki and S. Iwata, 1981, *Handbook of HeI Photoelectron Spectra of Fundamental Organic Molecules*. Halsted, New York.



- Kingdom, K.H., 1923, *I. Langmuir*, *Phys. Rev.* **21**, 380.
- Kiskinova, M., G. Pirug and H.P. Bonzel, 1983, *Surf. Sci.* **133**, 321.
- Klauser, R., M. Surman, Th. Lindner and A.M. Bradshaw, 1987, *Surf. Sci.* **183**, L279.
- Kleyn, A.W., A.C. Luutz and D.J. Auerbach, 1982, *Surf. Sci.* **117**, 33.
- Koel, B.E., J.E. Crowell, C.M. Mate and G.A. Somorjai, 1984, *J. Phys. Chem.* **88**, 1988.
- Köppel, H., L.S. Cederbaum and W. Domcke, 1988, *J. Chem. Phys.* **89**, 2023.
- Koutecky, J., 1958, *Trans. Faraday Soc.* **54**, 1038.
- Kuhlenbeck, H., 1984, *Diplomarbeit*, Universität Osnabrück.
- Kuhlenbeck, H., M. Neumann and H.-J. Freund, 1986, *Surf. Sci.* **173**, 194.
- Kuhlenbeck, H., H.B. Saalfeld, U. Buskotte, M. Neumann, H.-J. Freund and E.W. Plummer, 1989, *Phys. Rev. B* **39**, 3475.
- Kuhlenbeck, H., H.B. Saalfeld, M. Neumann, H.-J. Freund and E.W. Plummer, 1987, *Appl. Phys. A* **44**, 83.
- Kulkarni, S.K., J. Somos, A.W. Robinson, D. Ricken, Th. Lindner, P. Hollins, G.J. Lapeyre and A.M. Bradshaw, 1991, *Surf. Sci.* **259**, 70.
- Lapeyre, G.J., J. Anderson and R.J. Smith, 1979, *Surf. Sci.* **89**, 304.
- Lang, N.D., 1971, *Solid State Commun.* **9**, 1015.
- Langmuir, I., 1918, *J. Am. Chem. Soc.* **40**, 1361.
- Lennard-Jones, J.E., 1932, *Trans. Farad. Soc.* **28**, 333.
- Lindner, Th., J. Somers, A.M. Bradshaw and G.P. Williams, 1987, *Surf. Sci.* **185**, 75.
- Litvin, D.B., 1983, *Thin Solid Films* **106**, 203.
- Litvin, D.B., 1984, *J. Phys. C* **17**, L37.
- Liu, A.C., J. Stöhr, C.M. Friend and R.J. Madix, 1990, *Surf. Sci.* **235**, 107.
- Lundquist, B.I., 1967, *Phys. Cond. Mater.* **6**, 193, 203.
- Lundquist, B.I., 1968, *Phys. Cond. Mater.* **7**, 117.
- Lundquist, B.I., 1969, *Phys. Cond. Mater.* **9**, 2236.
- Lundquist, B.I., O. Gunnarsson, H. Hjeernberg and J.K. Nyrkov, 1979, *Surf. Sci.* **89**, 196.
- Mack, J.U., E. Bertel and F.P. Netzer, 1985, *Surf. Sci.* **159**, 265.
- Madix, R.J., J.L. Gland, G.E. Mitchell and B.A. Sexton, 1983, *Surf. Sci.* **125**, 481.
- Mariani, C., H.-U. Middelmann, M. Iwan and K. Horn, 1982, *Chem. Phys. Lett.* **93**, 308.
- Markert, K. and K. Wandelt, 1985, *Surf. Sci.* **159**, 24.
- Martensson, N. and A. Nilsson, 1990, *J. Electron Spectrosc. Relat. Phenom.* **52**, 1.
- Mate, C.M., B.E. Bent and G.A. Somorjai, 1986, *J. Electron Spectrosc. Relat. Phenom.* **39**, 205.
- Mate, C.M., C.-T. Kao and G.A. Somorjai, 1988, *Surf. Sci.* **206**, 145.
- McElhiney, G., H. Papp and J. Pritchard, 1976, *Surf. Sci.* **54**, 617.
- Mammel, N., G. Rangelov, E. Bertel, V. Dose, K. Kometer and N. Rösch, 1989, *Phys. Rev. Lett.* **63**, 1884.
- Messmer, R.P. and S.H. Lamson, 1979, *Chem. Phys. Lett.* **65**, 465.
- Messmer, R.P., 1984, *J. Vac. Sci. Technol. A* **2**, 899.
- Nielsen, M.M., J. Burchhardt, D.L. Adams, E. Lungren and J.N. Andersen, 1994, *Phys. Rev. Lett.* **72**, 3370.
- Miranda, R., K. Wandelt, D. Rieger and R.D. Schnell, 1984, *Surf. Sci.* **139**, 430.
- Muscat, J.P. and D.M. News, 1978, *Surf. Sci.* **74**, 355.
- Netzer, F.P., 1990, *Vacuum* **41**, 49.
- Netzer, F.P., G. Rangelov, G. Rosina, H.B. Saalfeld, M. Neumann and D.R. Lloyd, 1988, *Phys. Rev. B* **37**, 10399.
- Neuber, M., private communication.
- Neuber, M., 1992, *Thesis*, Universität Osnabrück.
- Neuber, M., S. Witzel, C. Zubrägel, H.H. Graen and M. Neumann, 1991, *Surf. Sci.* **251/252**, 911.
- Neumann, M., J.U. Mack, E. Bertel and F.P. Netzer, 1985, *Surf. Sci.* **155**, 629.
- News, D.M., 1969, *Phys. Rev.* **178**, 1123.
- Nieuwenhuys, B.E., D.I. Hagen, G. Rovida and G.A. Somorjai, 1976, *Surf. Sci.* **59**, 155.
- Odörfer, G., 1987, *Diplomarbeit*, Universität Erlangen-Nürnberg.
- Odörfer, G., E.W. Plummer, H.-J. Freund, H. Kuhlenbeck and M. Neumann, 1988, *Surf. Sci.* **198**, 331.
- Peyerimhoff, S.D., 1967, *J. Chem. Phys.* **47**, 349.
- Peled, H. and M. Asscher, 1987, *Surf. Sci.* **183**, 201.
- Plummer, E.W. and W. Eberhardt, 1982, *Adv. Chem. Phys.* **49**, 533.

- Plummer, E.W., T. Gustafsson, W. Gudat and D.E. Eastman, 1977, *Phys. Rev. A* **15**, 2339.
- Plummer, E.W., B.P. Tonner, N. Holzwarth and A. Liebsch, 1980, *Phys. Rev. B* **21**, 4306.
- Polatoglu, H.M., M. Methfessel and M. Scheffler, 1993, *Phys. Rev. B* **48**, 1877.
- Puschmann, A., J. Maase, M.D. Crapper, C.E. Riley and D.P. Woodruff, 1985, *Phys. Rev. Lett.* **54**, 2250.
- Radzig, A.A. and B.M. Smirnov, 1985, *Reference Data on Atoms, Molecules and Ions*, Vol. 31, Springer Series in Chemical Physics. Springer-Verlag, Berlin.
- Ramsey, M.G., D. Steinmüller, F.P. Netzer, T. Schedel, A. Santaniello and D.R. Lloyd, 1991, *Surf. Sci.* **251/252**, 979.
- Rangelov, G., N. Memmel, E. Bertel and V. Dose, 1991, *Surf. Sci.* **251/252**, 965.
- Rettner, C.T., H.E. Pfnür and D.J. Auerbach, 1985, *J. Chem. Phys.* **84**, 4163.
- Richardson, N.V. and N.R. Palmer, 1982, *Surf. Sci.* **114**, L1.
- Rieger, D., R.D. Schnell and W. Steinmann, 1984, *Surf. Sci.* **143**, 157.
- Riffe, D.M., G.K. Wertheim, P.H. Citrin, 1990, *Phys. Rev. Lett.* **64**, 571.
- Saddei, D., H.-J. Freund and G. Hohlneicher, 1980, *Surf. Sci.* **95**, 257.
- Saiki, R.S., G.S. Herman, M. Yamada, J. Osterwalder and C.S. Fadley, 1989, *Phys. Rev. Lett.* **63**, 283.
- Salaneck, W.R., C.B. Duke, W. Eberhardt, E.W. Plummer and H.-J. Freund, 1980, *Phys. Rev. Lett.* **45**, 280.
- Sandell, A., 1993, Thesis, Uppsala University.
- Schichl, A., D. Menzel and N. Rösch, 1982, *Chem. Phys.* **65**, 225.
- Schichl, A., D. Menzel and N. Rösch, 1984, *Chem. Phys. Lett.* **105**, 285.
- Schmeisser, D., F. Greuter, E.W. Plummer and H.-J. Freund, 1985, *Phys. Rev. Lett.* **54**, 2095.
- Schneider, C., H.-P. Steinrück, P. Heimann, T. Pache, M. Glanz, K. Eberle, E. Umbach and D. Menzel, 1988, *Verhdl. DPG O-24.4*.
- Schneider, C., H.-P. Steinrück, T. Pache, P.A. Heimann, D.J. Coulman, E. Umbach and D. Menzel, 1990, *Vacuum* **41**, 730.
- Schönhammer, K. and O. Gunnarsson, 1978, *Solid State Commun.* **26**, 399.
- Seaburg, C.W., E.S. Jensen and T.N. Rhodin, 1981, *Solid State Commun.* **37**, 383.
- Seaburg, C.W., T.N. Rhodin, M. Traum, R. Benbow and Z. Hurych, 1980, *Surf. Sci.* **97**, 363.
- Sheppard, N., 1988, *Ann. Rev. Phys. Chem.* **39**, 589 and references therein.
- Shinn, N.D., 1986, *J. Vac. Sci. Technol. A* **4**, 1351.
- Shinn, N.D., 1990, *Phys. Rev. B* **41**, 9771.
- Shinn, N.D. and T.E. Madey, 1984, *Phys. Rev. Lett.* **53**, 2481.
- Shinn, N.D. and T.E. Madey, 1985, *J. Chem. Phys.* **83**, 5928.
- Shinn, N.D. and K.-L. Tsang, 1990, *J. Vac. Soc. Technol. A* **8**, 2449.
- Smith, R.J., J. Anderson and G.J. Lapeyre, 1976, *Phys. Rev. Lett.* **37**, 1081.
- Smith, R.J., J. Anderson and G.J. Lapeyre, 1980, *Phys. Rev. B* **22**, 632.
- Somorjai, G.A. and M.A. Van Hove, 1979, *Adsorbed Monolayers on Solid Surfaces*, Vol. 38, Structure and Bonding. Springer-Verlag, Berlin.
- Spanjaard, D. and M.C. Desjournes, 1990, in: *Interactions of Atoms and Molecules with Solid Surfaces*, eds. V. Bertolani, N.H. March and M.P. Tosi. Plenum, New York, p. 255.
- Sprunger, P.T. and E.W. Plummer, 1991, *Chem. Phys. Lett.* **187**, 559.
- Stampfl, C. and M. Scheffler, 1995, *Surf. Rev. Lett.* **2**, 317.
- Stampfl, C., 1996, *Surf. Rev. Lett.* **3**, 1567.
- Stampfl, C., J. Burchhardt, M. Nielsen, D.L. Adams, M. Scheffler, H. Over, W. Moritz, 1992, *Phys. Rev. Lett.* **69**, 1532.
- Starke, U., P.L. de Andres, D.K. Saldin, K. Heinz and J.B. Pendry, 1988, *Phys. Rev. B* **38**, 12277.
- Steinkilberg, M., 1977, Thesis, Technical University München.
- Steinrück, H.-P., W. Huber, T. Pache and D. Menzel, 1989, *Surf. Sci.* **218**, 293.
- Stroscio, J.A., S.R. Bare and W. Ho, 1984, *Surf. Sci.* **148**, 499.
- Surman, M., S.R. Bare, P. Hofmann and D.A. King, 1987, *Surf. Sci.* **179**, 243.
- Szeftel, J.M., S. Lehwald, H. Ibach, T.S. Rahman, J.E. Black and D.L. Mills, 1983, *Phys. Rev. Lett.* **51**, 268.
- Taylor, J.B., 1933, I. Langmuir, *Phys. Rev.* **44**, 423.
- Toennies, J.P., 1991, *Experimental Determination of Surface Phonons by Helium Atoms and Electron Energy Loss Spectroscopy*, Vol. 21, Springer Series in Surface Science. Springer-Verlag, Berlin, p. 111.

- Turner, D.W., C. Baker, A.D. Baker and C.R. Brundle, 1970, *Molecular Photoelectron. Spectroscopy*. Wiley, New York.
- Tüshaus, M., E. Schweizer, P. Hollins and A.M. Bradshaw, 1987, *J. Electron Spectrosc. Relat. Phenom.* **44**, 305.
- Uhlenbrock, S., private communication.
- Umbach, E., 1982, *Surf. Sci.* **117**, 482.
- Umbach, E., A. Schichl and D. Menzel, 1980, *Solid State Commun.* **36**, 93.
- Villars, D.S., 1931, I. Langmuir, *J. Am. Chem. Soc.* **53**, 486.
- Walsh, A.D., 1913, *J. Chem. Soc.* 2266.
- Wambach, J., G. Illing and H.-J. Freund, 1991, *Chem. Phys. Lett.* **184**, 239.
- Weast, R.C., 1973, *CRC Handbook of Chemistry and Physics*, The Chemical Rubber Comp., 54th edn.
- Weimer, J.J. and E. Umbach, 1984, *Phys. Rev. B* **30**, 4863.
- Weimer, J.J., E. Umbach and D. Menzel, 1985, *Surf. Sci.* **159**, 83.
- Weinelt, M., W. Huber, P. Zebisch, H.-P. Steinrück, M. Pabst and N. Rösch, 1992a, *Surf. Sci.* **271**, 539.
- Weinelt, M., W. Huber, P. Zebisch, H.-P. Steinrück, B. Reichert, U. Birkenheuer and N. Rösch, 1992b, *Phys. Rev. B* **46**, 1675.
- Wendin, G., 1981, *Structure and Bonding*, Vol. 45. Springer-Verlag, Berlin.
- Winterlin, J., R. Schuster, D.J. Coulman, G. Ertl and R.J. Behm, 1991, *J. Vac. Sci. Technol. B* **9**, 902.
- Woodruff, D.P., C.F. McConville, A.L.D. Kilcoyne, Th. Lindner, J. Somers, M. Surman, G. Paolucci and A.M. Bradshaw, 1988, *Surf. Sci.* **201**, 228.
- Wurth, W., J.J. Weimer, E. Hudeczek and E. Umbach, 1986, *Surf. Sci.* **173**, L619.
- Yu, R. and P.K. Lam, 1988, *Phys. Rev. B* **37**, 8730.
- Zaera, F., E. Kollin and J.L. Gland, 1985, *Chem. Phys. Lett.* **121**, 464.
- Zangwill, A., 1988, *Physics at Surfaces*. Cambridge University Press, Cambridge.